ADVANCED ENERGY MATERIALS
www.advenergymat.de

Tunable Photovoltaics: Adapting Solar Cell Technologies to Versatile Applications

Hosni Meddeb, Maximilian Götz-Köhler, Nils Neugebohrn, Udayan Banik, Norbert Osterthun, Oleg Sergeev, Dennis Berends, Colleen Lattyak, Kai Gehrke, and Martin Vehse*

Solar photovoltaics (PV) offer viable and sustainable solutions to satisfy the growing energy demand and to meet the pressing climate targets. The deployment of conventional PV technologies is one of the major contributors of the ongoing energy transition in electricity power sector. However, the diversity of PV paradigms can open different opportunities for supplying modern systems in a wide range of terrestrial, marine, and aerospace applications. Such ubiquitous and versatile applications necessitate the development of PV technologies with customized design capabilities. This involves multifunctional characteristics such as aesthetic appearance, visual comfort, and heat insulation. To enable on-demand adaptation to the requirements of distributed applications, tunable solar cells (SC) feature exceptional degrees of freedom in the manipulation of their intrinsic properties via adjusted materials engineering. The pertinent tuning abilities include but are not limited to bandgap energy, transparency, color, and thermal management. In this review, the main principles of different tuning approaches are specified and an overview of relevant concepts of tunable SC technologies is presented. Then, the recent integrations of cutting-edge tunable PV adapted to versatile applications are systematically summarized. In addition, current challenges and insightful perspectives into potential future opportunities for omnipresent tunable PV are discussed.

1. Introduction

Urged by the environmental risks due to the burning of fossil fuels, the reliance on non-renewable energy resources must dwindle toward a transition to long-term sustainability in the global energy systems.[1–4] This accelerates the progressive deployment of clean and renewable energy resources such as solar, wind, hydro, geothermal, and biomass, to enable a steady mitigation of greenhouse gas emissions, which are causing the planetary climate change and global warming.[5–7] Additionally, due to the economic development and the worldwide urbanization, a continuous rise of the global energy consumption across all key sectors, that is, power, heating, industry, and transport is occurring. This is expressed by an increase in the annual global electricity demand by 4.5% in 2021 corresponding to additional 1000 TWh.[4] Hence, strict criteria for the selection of competitive and abundant energy alternatives are imposed, requiring high yield at affordable prices.[8] The share of total renewables power generation excluding hydropower exceeded 3000 TWh in 2020, corresponding to almost 12% of the global electricity generation.[3] Considering an effective synergy between various sustainable energy candidates, solar photovoltaics (PV) have demonstrated great capabilities that can satisfy the requirements in the pathway towards 100% renewable electricity.[9–12] Owing to the research and development activities over the last decades, the power conversion efficiencies of solar cells (SC) have skyrocketed with a prolonged operation lifetime (>15 years) and a drastic plummeting in manufacturing costs (global average module selling price below $0.25 per W).[6,13–15] The rapid universal deployment of PV resulted in a contribution of about 3.4% in the worldwide electricity generation in 2020.[3] Presently, the global installed PV capacity is approaching 1 TW and it is envisioned to reach ≈10 TW by 2030 and 30 to 70 TW by 2050.[16] Interestingly, along with massive electricity production using conventional solar power plants and rooftop solar panels, ancillary concepts of PV offer new strategies for supplying modern systems in versatile applications.[17–19] Moreover, diverse functionalities beyond solar energy harvesting can be afforded by adaptive PV, including aesthetic appearance, visual comfort and thermal management.[17,18,20,21] The distributed nature and the ubiquitous accessibility of multifunctional PV products are substantial features of solar PV in contrast to other renewable energies. However, traditional SCs dominating the market impose intrinsic optoelectronic and thermomechanical limitations, that prohibit their multifunctional utilization. To overcome these drawbacks, novel functional materials and innovative device architecture

H. Meddeb, M. Götz-Köhler, N. Neugebohrn, U. Banik, N. Osterthun, O. Sergeev, D. Berends, C. Lattyak, K. Gehrke, M. Vehse
German Aerospace Center (DLR)- Institute of Networked Energy Systems
Urban and Residential Technologies
Oldenburg 26129, Germany
E-mail: Hosni.Meddeb@dlr.de

The ORCID identification number(s) for the author(s) of this article can be found under https://doi.org/10.1002/aenm.202200713.

DOI: 10.1002/aenm.202200713

designs are developed to provide customized solar PV with tunable properties in a controlled manner.

These tuning capabilities in adjustable SCs cover a multitude of aspects such as bandgap,[22] transparency,[17,20] color,[21] thermal management,[23–25] mechanical flexibility,[26–28] weight,[29] and size.[30–33] Tunable PV can be defined as SC technologies that present a manipulation of inherent properties through material design of the functional components and retrofits or via device architecture engineering. The primary aim is to enable suitable customization and adaptation to the specific requirements of a given application. Hence, conventional PV can be transformed into multifunctional power-harvesting devices adapted for the integration into different systems like building façades,[21,34] smart windows,[17,18,20,34] automobile skins,[35,36] greenhouses for agrivoltaics,[18,37] wireless sensors for the Internet of Things (IoT),[38–40] wearable electronics,[18,41] floating, and underwater equipment[42,43] as well as aerial vehicles and aerospace units.[19] In this way, depending on the technology readiness level (TRL), several PV technologies can possess their own niche market owing to their potential for customization and adaptation to integrated PV.[29,44–46] In particular, the tunability features can turn customized solar panels into one of the best contenders to power the nascent electrical vehicles and self-powered buildings.[4,21,35]

In this review, we provide a comprehensive overview of the recent progress for a broad range of tunable SC technologies in terms of materials engineering, design approaches, state-of-the-art SC devices and relevant technological applications. This paper is divided into three main sections. First, the main principles and general criteria of the tuning approaches in SCs are outlined. The focus is rather attributed to spectral-related tuning over a broad range of light wavelengths, controlled by different functional materials in SCs. This includes the bandgap tunability of photoactive materials, the optical modulation in terms of color and visibility as well as the photonic thermal management of either the intrinsic SC device or the extrinsic surrounding. In addition, the main approaches that turn a SC from colored to color-neutral or from opaque to transparent are presented. A major scope of this review is to discuss the static concepts with predefined material design and photonic management alongside the dynamic approaches with reversible modulation of the light transmission in response to external factors. Second, relevant tunable SC devices are presented. Special attention is given to the impact of bandgap tuning on the efficiency limits of ideal PV devices in opaque, colored and transparent SCs. Furthermore, the fundamentals and the technological importance of the bandgap tuning in single junction and multijunction SCs are highlighted. Then, representative examples of realized SC technologies with adjustable color and transparency are underlined. Switchable SC technologies featuring smart and dynamic control of light transmission or color perception are of particular interest. As a main thermal tuning ability, the implementation of optics-based approaches like passive radiative cooling and sub-bandgap reflection to reduce the operating temperature of PV is also briefly reviewed. Third, we focus on the applications that are enabled by tunable PV technologies. This covers the integration of multifunctional PV in building façades, windows, greenhouses, vehicles, indoor, floating, underwater, and aerospace applications. For each PV integration scenario, we point out how the relevant tuning aspects can adapt the SC device and ensure its compatibility with the corresponding application. A critical evaluation in the framework of a TRL approach is addressed to discuss the technical maturity across different PV technologies customized for specific integration schemes. Ultimately, we present some insightful opinions about the added value of PV customization considering technological challenges, future directions, potential industrialization, and market perspectives.

2. Main Principles and General Criteria of Tuning Approaches in Solar Cells

A typical photovoltaic cell directly converts photon energy of the incident solar radiation into electrical power. The conversion mechanism consists of a sequence including the optical absorption of photons in the photoactive region creating an electron–hole pair, followed by a thermal relaxation towards the corresponding valence band (V_b) for hole and conduction band (C_b) for electron. Then, photogenerated free charge carriers are electronically separated and collected in the selective transport regions toward both side terminals to dissipate energy in the external circuit.[47] (**Figure 1**a,b) The power conversion efficiency (PCE) is defined as the ratio of electrical energy output to input energy from the light source. This parameter depends on external conditions such as the spectrum and intensity of incident radiation and the temperature of the SC. On device level, the efficiency is linked to characteristic parameters, such as the short-circuit current (J_{sc}), the open-circuit voltage (V_{oc}), and the fill factor (FF) as follows

$$\mathrm{PCE} = \frac{\text{output enery}}{\text{input energy}} = \frac{J_{sc} \times V_{oc} \times \mathrm{FF}}{P_{in}} \tag{1}$$

Interestingly, the PV device is sensitive to the energy distribution of the solar spectrum AM 1.5G with a total spectral power density of about 1000 W m^{-2}. Within different ultraviolet (UV, 280–400 nm), visible (vis, 400–800 nm), and near-infrared (NIR; 800–1400 nm) regions, the distribution in terms of power densities is UV = 93.9, 496, and 353 W m^{-2}, respectively.[48] While the distribution of photon flux is about 5%, 43%, and 52% for each of UV, visible, and NIR, respectively.[49] It is noteworthy that the light source specifications in terms of intensity and/or spectral range can be different in some specific applications like indoor PV concentrated PV and space PV. Therefore, apart from the aim of superior PCE, the precise management of solar spectrum from near-ultraviolet to visible to mid-infrared offers diverse opportunities in terms of visual transparency, color appearance, and heat management (Figure 1a). Furthermore, holistic material design and device structure engineering enable extra degrees of manipulation in the optoelectronic properties, the thermo-mechanical characteristics, and the spatial dimensions. In the following, diverse tuning capabilities are described in respect with different SC device regions. The discussed components are based on a multitude of organic and inorganic materials that can be synthesized by a large variety of vacuum and/or solution-processable methods.

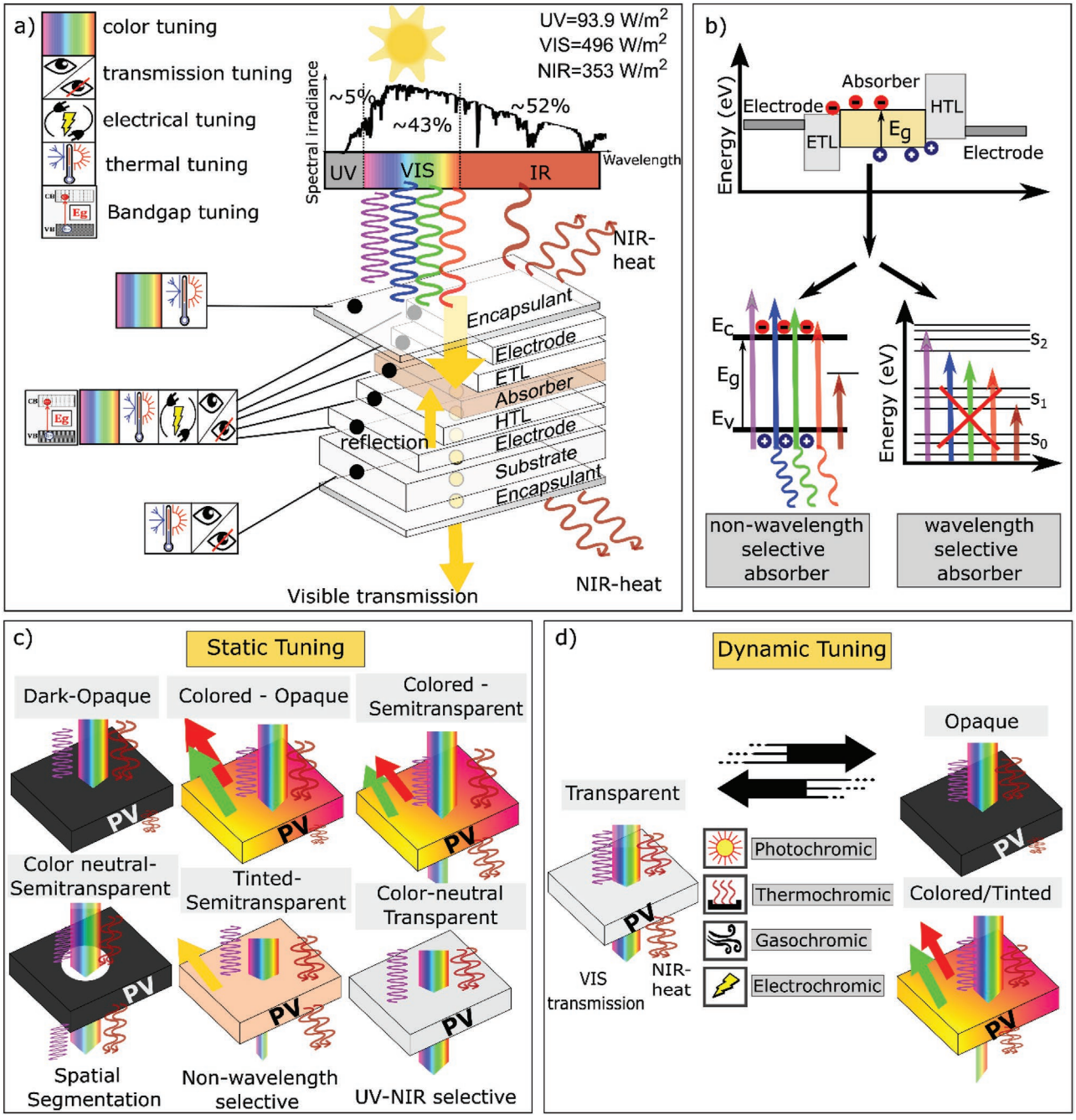

Figure 1. a) General schematic of a typical thin-film solar cell structure under sunlight spectrum and possible tuning aspects related to different functional components. b) Simplified energy band diagram and difference in the optoelectronic properties between non-selective and selective photoactive absorbers. c) Static approaches for optical tuning in opaque, semitransparent, transparent and colored PV. d) Dynamic approaches for optical tuning from transparent to opaque or tinted via photochromic, thermochromic, gasochromic, and electrochromic switching.

2.1. Tuning Capabilities Within the Solar Cell Device Components

In the following, we will outline the tuning capabilities in each functional component of a typical thin-film SC following the schematic in Figure 1a. A systematic analysis is addressed in photoactive materials, electrode layers, optical structures, substrates and encapsulants. It is noteworthy that the survey of tuning features will cover all the three generations of PV from conventional crystalline silicon (c-Si) wafer-based SCs to a wide variety of emerging organic and inorganic thin-film PV technologies.[50,51] Also, most of the adjustment abilities remain valid regardless the differences in architectures (substrate, superstrate, planar, mesoporous, etc.) or in structures (wafer-based, thin films, microstructured, and nanostructured quantum wells, nanowires, or dots).

2.1.1. Photoactive Materials

The photoactive material is the core of each SC and determines most of its electrical and optical characteristics. As illustrated in Figure 1b, we can distinguish two main types of photoactive materials according to the spectral absorption in visible range: non-wavelength-selective absorbers allowing photogeneration via continuous broadband absorption over the solar spectrum including visible wavelengths, and wavelength-selective absorbers allowing restricted photogeneration at specific wavelengths particularly in the UV (<435 nm) and/or NIR (>670 nm) range, but, transmit a fraction of visible light wavelengths.

Non-Wavelength Selective Broadband Absorbers: Within a photoactive semiconductor, the transition of electron from the valence band (E_v) to the conduction band (E_c) occurs by absorbing a photon of light with energy equal or higher than the forbidden bandgap ($h_v \geq E_g$). Hence, the optical bandgap of the non-wavelength selective photoactive material controls the absorption threshold of the SC device.[52] The wavelength-dependent absorption in a semiconductor material is determined by the intrinsic optical properties (refractive index n and extinction coefficient κ or absorption coefficient α), the dispersion relations and the thickness.[53] Tuning the bandgap, the optical properties, the thickness as well as the structural morphology of the photoabsorber can drastically alter the spectral response to the incident light. This can result in several optical characteristics ranging from high transparency, to selective reflection to near-unity absorption depending on the optical properties of the surrounding functional layers and electrodes.[17,20,53] On a practical level, the bandgap of the active materials in common single junction SC is ranged between ≈1 and ≈2.5 eV.[51] Interestingly, most of semiconductor absorbers are characterized by a significant bandgap tuning feature. The bandgap of the photoactive material is crucial in the determination of the output characteristics and the performance limit of the PV device.[50,54,55] Furthermore, the specifications of the absorber material is pivotal for the control of light transmission through corresponding SC device. To achieve an adequate degree of light transmission through a photoactive material different approaches can be adopted such as substantial thinning, designing the optical bandgap for adjustable absorption range or space segregation between the opaque parts of SC.[17,20,21,56] The latter method is possible even for the case of c-Si wafer absorber with opaque nature and very limited transparency potential at ultrathin level,[57,58] by punching micro-hole array to allow a systematic tuning of the light transmission with the adjustment of the filling fraction design.[57]

Moreover, the choice of the absorber material type and thickness will define a multitude of characteristics beyond the optoelectronic properties such as mechanical flexibility, thermal management, and weight magnitude.

Wavelength-Selective Absorbers: For UV-selective PV, continuous-band absorbing semiconductors with wide-bandgap above 2.85 eV (435 nm), such as metal oxides (ZnO, NiO,TiO_2), ABX_3 perovskites, quantum dots, and organic materials are used, allowing an absorption cutoff of the entire fraction of light spectrum above 435 nm.[59–63] In contrast, the requirements for NIR light harvesting can be satisfied in organic solar cell (OSC) featuring ultra-narrow bandgap of donor and acceptor materials in a bulk heterojunction.[64,65] To achieve selective absorption of both UV and NIR, excitonic materials with distinct absorption maxima and minima are employed such as low-bandgap polymer donors and non-fullerene small molecular acceptors.[17,64,65] Within these organic photoactive materials, the optical absorption mechanism is manifested in discrete molecular orbitals (S_1, S_2, ... S_n) from the ground state (S_0).[17] (Figure 1b) By engineering the molecular structure, the bandgap energy and the discontinuity of states can be tuned. This can enable a shift of the light harvesting beyond the visible band into the NIR range.[17] Hence, this impediment in absorption discontinuity turns out to be an advantage in controlling the spectral absorption outside the visible wavelengths range.

2.1.2. Carrier Transport Layers, Electrode Materials, and Optical Structures

Charge Carrier-Selective Contacts: In general, the electron (ETL) and hole (HTL) transport layers should be optically characterized by high transparency and low parasitic absorption to maximize the photogeneration in the inner absorber regions or to promote visible light transmission in the case of see-through PV. However, a color tunability can be obtained through the modification of ETL and/or HTL by thickness variation, or by integrating photonic crystal and post-tinting nanostructures.[53,66]

Electrode Materials: For opaque SCs, the common back electrodes are metal materials (Au, Ag, Al) thicker than 100 nm to ensure superior electrical conductivity and quasi-ideal internal reflection to the PV device for extended optical path and enhanced absorption.[67] However, for semitransparent and transparent PV, effective transparent front and bottom electrodes are desired, providing the best compromise between the electrical conductivity and optical transparency.[68,69] High transparency enables light penetration into the front side of PV device and light escape from the back side of PV device. Whereas, excellent conductivity allows the transfer of the photogenerated current to the outer electrical circuit. Also, good internal mechanical flexibility is desired for the integration in flexible PV technologies. A wide variety of front and back electrodes in transparent PV is presented in literature.[64,69–71] Most common materials are ultrathin metals,[68,72,73] transparent conductive oxides (TCO),[74] oxide/metal/oxide multilayers,[75] metal nanowires,[72,76] carbon nanotubes,[77,78] and transparent conducting polymer such as (PEDOT:PSS).[70]

Optical Structures: Spectral control and optical design are substantial approaches for light manipulation in PV applications.[79] In this regard, various optical structures are employed in PV technologies such as photonic crystals, distributed Bragg reflectors (DBRs), dielectric mirrors, optical cavity structures, and antireflection films. Most of these structures consist of thin multilayers with different refractive indices. One dimensional photonic crystal is based on reflection of light wavelengths lower than the photonic bandgap. Whereas, distributed Bragg reflector, dielectric mirror and optical cavity rely on the interference behavior that control the light reflection and transmission within the multilayer stack. Such concepts

rely on the manipulation of the thicknesses and the refractive indices (n) in the multilayers system. Interference effects arise from the coherent superposition of the reflected and transmitted electromagnetic fields. This is controlled by the refractive index change at several interfaces, altering the phase relationship between reflected light beams from the different interfaces. Further details on the working principles, materials and architectures of these optical structures integrated in PV devices can be found in many reports.[79–81] The above-mentioned optical structures can be used not only to enhance the light harvesting or to control the light propagation directions, but also to achieve selective reflection as well as multifunctional spectrum-sensitive features. This provides substantial tuning capabilities to meet the requirements of versatile applications in terms of aesthetic, coloration, heat-insulation and cooling.[23,82]

2.1.3. Substrates

Regarding the tunability features in thin film SCs, a large variety of substrates can be used depending on the desired device configuration and the target application.[27,28,83] Substrates are classified by material type into three main categories: metals, ceramics, and plastic polymers.[27,28,84] Hence, the availability of various substrates contributes to the tunability of thin-film PV devices in respect of optical properties, mechanical flexibility, stretchability, and weight.[26,28,83,85]

2.1.4. Encapsulants and Cover Glasses

It is possible to utilize the cover glass and the encapsulant for customized color perception and aesthetic appearance.[21] Moreover, encapsulants and cover glasses can play a significant role in the adjustment of thermal radiation management and heat transfer.[82,86,87] This is acquired when these components absorb and then emit infrared thermal radiation which exclude heat and enable SC cooling.[82,87] Also, the choice of the encapsulation scheme promote the mechanical tunability of flexible and lightweight PV.[88]

2.2. Optical Tuning Aspects

The tuning of transparency and colors are among the optical modulation capabilities of PV technologies. Hence, SCs can be adjusted from opaque to visibly transparent and also from colored to color-neutral. In the following sub-sections, both static, and dynamic optical tuning approaches to realize colored and transparent PV technologies are presented and relevant components that enable such customization are outlined.

2.2.1. Static Approaches for Optical Tuning

Typically, the optical appearance of a SC device in terms of transparency or color is pre-designed and fixed at the manufacturing stage and remains unchanged along its entire lifetime. Figure 1c illustrates different static approaches for optical modulation.

Static Color Tuning: The color of a SC is perceived based on a synergy between the light source specifications, the sensitivity of the human eyes and particularly the spectral reflectance of the PV device.[53]

In traditional opaque SCs, the main characteristics are thick and optically dense photoabsorbers. For absorber thicknesses below the absorption length, thick metal back reflectors block the transmission of incident light and enhance the absorption. Light management strategies such as front antireflection, scattering enhancement, resonant absorption and perfect back reflection are commonly used. These approaches enable further internal reflections and extension of the optical light path and passes inside the device.[67] Hence, the absorption in the photoactive region is maximized.[67,89] Therefore, opaque SCs are often adjusted for near-complete absorption of visible light and appear as monotone dark or even black.[90]

By manipulating the material design and the device architecture, colorful opaque and semitransparent SCs with a wide range of colors can be realized through internal or external spectral engineering approaches. The external strategies rely on the implementation of additional external coloring structures either on the front or on the back side of the basic PV device. Whereas, the internal strategies are applied within the functional components of the inner PV device from the photoactive layer to the electrodes.

Since the color appearance is mainly controlled by the spectral reflectance of the PV device, color tuning can be enabled through external design strategies by changing the reflection characteristics with additional structures to the primary device. On the front side of SCs, several optical structures can serve as coloring agents facing the incident light. These include antireflection coatings, reflective filters composed of multilayer films with alternating low- and high-index materials, luminophores,[91] printable colorful coating formed by a mixture of polymers and dyes,[92] pigments,[93] subwavelength plasmonic resonators,[94,95] and optical microcavities.[96,97]

The advantage of the external design strategies with reflective filter is the versatility and large degree of freedom in color manipulation for any type of underlying PV.[91]

On the encapsulant and cover glass level, several practices of dielectric mirrors or colorful coatings can be applied separately from the PV module fabrication and then easily transferred.[21] Nearly-perfect colors can be produced by coating the inner glass surface with photonic structural reflectors,[98] painting technologies of cover glass,[99] or etching treatment of the outer glass surface.[100] Bragg reflectors with a resonance peak at a specific wavelength within visible range, applied on internal cover glass surfaces is one of the common coloring approaches.

In the internal color design strategy, the photoactive materials themselves can yield a color tuning via the change of thickness,[101] chemical composition,[102,103] optical bandgap,[104,105] or structure morphology.[106,107] Regarding the carrier transport layers, the creation of color can be obtained by tinting coatings,[107] thickness change or integration of patterned nanostructures and precisely designed photonic crystals.[66,108] As for the coloration through the transparent electrode region, the widely used method is the spectral engineering of the

optical interference in microcavities composed of metal-dielectric-metal.[109] The variation of the dielectric thickness corresponding to the cavity length leads to different resonance conditions enabling color tuning.[110,111]

Similar to the opaque coloring technologies, semi-transparent SCs can also be tuned to show vivid coloration in both reflection and transmission modes. Hereby, the coloration effect can be a result of optical resonances in the complete layers stack of the PV device, or in single layers, as well as a result of pigment molecules. Also, semitransparent dielectric mirrors can be applied as optical color filter structures owing to their selective reflection.

More details on the different coloration approaches in opaque and transparent PV can be found elsewhere.[21,91]

All the above-mentioned internal and external approaches differ in terms of the ability to generate vivid and distinctive color, the color tunability and the angle sensitivity.[53]

The quantitative parameters for assessing the color quality of SCs, like the color coordinates in the chromaticity diagram, the color rendering index (CRI) and the correlated color temperature (CCT), are explained in Section S1, Supporting Information.

Static Transparency Tuning: With regard to transparency modulation in SC technologies, the primary aim is to enable a transmission of a fraction of the incident light over the spectral sensitivity of the human eye in the visible region.[20] The transmission of the visible light is influenced by the spectral absorption of the photoactive materials in the SC.[17] Accordingly, along this manuscript, we refer to transparent PV (TPV) as SC technologies with UV–NIR wavelength selective absorbers and semitransparent PV (ST-PV) using non-wavelength-selective photoactive materials. The main adopted approaches for TPV and ST-PV are

1) The partial absorption and transmission of light in the visible spectrum can be enabled through thinned or wide-bandgap broadband absorbing materials, according to Beer-Lambert law. Typically, ST-PV with thinned absorber tend to exhibit a tinted color appearance.
2) The spatial segmentation approach consists of local removal of a fraction from the photoactive area in SC device. This enables a color neutrality aspect with higher degree of optical transmission as the spacing area increases, but, accompanied with a drop in the photocurrent and efficiency level due to the reduction of the photoactive area.
3) Luminescent solar concentrators (LSC) use luminophores to guide light in glass or polymeric media via total internal reflections towards PV devices placed at the edge.[17,20,21] Interestingly, omitting light blocking components such as interconnection schemes over the solar harvesting area, allows outstanding levels of transparency and color fidelity in LSC.[112]

The main figures of merit to characterize transparent SCs are elucidated in the supplementary section S2. This includes optical parameters such as the average visible transmission (AVT) and parameters combining power conversion and transparency like light utilization efficiency (LUE).

Due to the major differences in the specifications of ST-PV and TPV technologies as well as the large possible adjustment capabilities, wide range of PCE, AVT, LUE, and CRI outputs can be obtained.[51] It is worthy to mention that the bifaciality attribute enabling the illumination from both sides is inherent in transparent PV, desired for the aesthetic of semi-transparent colored PV[111,113] and beneficial for opaque SCs.[114,115]

All the previously presented approaches for static color and transparency tuning are predefined in the fabrication process and then the optical characteristics remain unchangeable over time once the PV device is in operation.

2.2.2. Dynamic Approaches for Color and Transparency Tuning

Unlike, static optical tuning approaches with predefined material design and photonic management beforehand, dynamic optical tuning approaches rely on a smart and reversible modulation of light transmission in response to external factors. Figure 1d, showcases the main dynamic reversible strategies for optical modulation. According to stimuli type, the optical switching mechanisms are categorized as electrochromic, gasochromic, photochromic, and thermochromic, related to voltage, gas, light, and temperature factors, respectively.

Electrochromic Switching: Electrochromic switching is mostly based on the movement of ions between electrochromic materials (such as inorganic metal oxides WO_3, NiO, MoO_3...) and an ion reservoir (e.g., H^+ or Li^+).[116,117] The combination of PV and electrochromic layers results in photoelectrochromic windows, which combine the benefits of energy generation and optical response by external stimuli.[118–121] The electrochromic layers are attached to an electrode of the ST-PV. Most studies use the supplied energy by the SC to self-power an electrochromic redox reaction and change the transparency or the color of the full SC device.

Gasochromic Switching: Gasochromic switching involves the interaction of oxidizing or reducing gases, like oxygen and hydrogen, with transition metal oxides such as tungsten oxide (WO_3), or metals like magnesium and titanium.[122,123] Due to the absorption of gaseous molecules, the responsive materials undergo a phase change such as a transition from metallic to a metal hydride dielectric state upon hydrogenation.[124] This leads to a dramatic change in the optical response.[125] Depending on the thickness and the material type of the gasochromic structure, the phase change can induce a transition from a reflective/absorptive to a transparent state.[122,123,126] Since the gasochromic mechanism requires a direct interaction with a gas, the responsive material is commonly exposed to the surrounding environment and therefore placed in the external electrode of the switchable SC.[122,123,126] A careful consideration for the thickness of the gasochromic layer is required to allow sufficient transmittance of visible light. For instance, the thickness can be above 100 nm for the case of WO_3 but, it is restricted to way below 100 nm for Mg due to the high opacity level.[123]

Photochromic Switching: As for the photochromic mechanism, it typically consists of a reversible transition between a colorless state in the dark and colored state during illumination.[127] In PV, this switching dynamic mechanism has been exploited mainly in dye-sensitized solar cells (DSSCs) that allow a change in color and self-adjustment of the visible light

transmission when irradiated upon.[128] Moreover, the combination of a photo-responsive liquid-crystal layer with a transparent SC can allow an optical tuning from a transparent, energy-harvesting mode under incident light to an opaque, idle mode in the dark.[129]

Thermochromic Switching: Another category of switching technologies in PV are thermochromic devices where the light regulation occurs passively in response to the environmental temperature in continuous change. Typically, vanadium oxide (VO_2) and perovskite can be applied as thermal-responsive materials.[34,130–135] that enable the tuning of the absorbance intensity or shifting the absorbance band through a phase transition process.[127] In particular, the structural phase transitions in perovskite can undergo thermally-induced reversible transitions with tunable color and transparency in the visible range.[133,136,137] The required heating to trigger the thermochromic switching can be realized reversibly by means of a photothermal process upon illumination, leading to a transition from absorbing and colored PV to a transparent state.[136]

All the above-mentioned dynamic switching technologies have been established for smart windows,[127,137,138] and have recently attracted particular interest in the PV field.[133,139] For solar devices, by integrating one of the dynamic switching mechanisms, an on-demand customization or self-adjustment of the entire optical properties including transmission, absorption, and reflection can be provided.[128] The stimulus-responsive element is then a part of the functional materials composing the SC and can be inserted in different regions from the inner absorber to the external electrode.[123,126,133,139] Hence, similar to smart window technologies, switchable PV can allow a reversible and dynamic optical modulation with a drastic change from transparent to opaque or colored states due to either chemical composition or structural changes.

The implementation of the aforementioned switching technologies into SCs can take place at different component levels of the PV device. In the gasochromic and electrochromic concepts, a direct interaction between the responsive material and the stimuli agent is required. Therefore, the corresponding functional switchable layers that change their reflectivity and transparency should be implemented as external electrodes in SCs.[126,140] Whereas the photochromic or thermochromic mechanisms can be inherently implemented within the photoabsorber regions in switchable dye-sensitized and perovskite switchable SCs.[133]

2.3. Optoelectronic Tailoring of Bandgap Energy in Photoactive Materials

Most of the photoactive materials employed in PV have a tunable bandgap, which is a key parameter that determines the optoelectronic properties. The bandgap energy can be modulated via various strategies such as chemical composition,[141–144] doping, alloying,[145] strain engineering, lattice constant manipulation,[146] quantum confinement,[147,148] and many other methods.[145,149–151] In the following, we present some of the well-known examples of photoactive materials in PV featuring bandgap tuning via composition change or via quantum confinement (QC) effects.

2.3.1. Composition-Tunable Bandgaps

One of the most common examples of composition-tunable bandgaps are thin films based on group IV semiconductors (Si, Ge, C) and their compounds. Their bandgap values can vary from below 1 eV to beyond 2.5 eV by alloying with each other or with oxygen and nitrogen or also by varying the deposition process parameters. These variations can affect the crystallinity as well as the microstructure including the interatomic spacing, bond angles and degree of atomic coordination.[152] As shown in **Figure 2**a (pink data points), I-III chalcopyrite Cu(In,Ga,Al)$(Se,S)_2$ systems can be formed by various multinary alloys, enabling the bandgap tailoring from narrow-bandgap regime ($CuInSe_2$-1.04 eV) to wide-bandgap regime 3.5 eV ($CuAlS_2$) and hence, covering a wide range of solar spectrum.[153] For II–VI binary bivalent metal chalcogenides $M^{2+}Ch^{2-}$ (Ch = S, Se, Te), containing metal cations from group II (Zn, Mg, Mn, Cd....) typically in wurtzite or zincblende structure (Figure 2a black graph), the band gaps of these isostructural A_xB_{1-x} alloys can be estimated using Vegard's law.[153] For III–V compound semiconductors, the bandgap tuning is accessible via lattice matching and high-quality epitaxial growth forming III–V alloys with multiple lattice constants. In general, larger tolerance to mismatch on the same substrate can enable wider range of bandgaps.[145] The bandgap tailoring in III–V-based PV can be effective in quantum well and multijunction SC technologies.[146,154]

The bandgaps of organic semiconductors can also be manipulated. Typically, in a bulk-heterojunction OSC, the molecule-based absorber layer comprises electron donor (D) in conjunction with acceptor (A).[155] To underline the bandgap tunability in organic photoactive materials, a representative list of non-fullerene acceptors and polymer donors and their corresponding energy levels is depicted in Figure 2b. In particular, selective IR absorption requires a reduction of the bandgap E_g to below 1.5 eV.[64,156] This implies that to harvest photons in the near-IR region, the bandgap of both donor and acceptor materials in the bulk heterojunction must be smaller than the energy range of visible wavelengths (380–780 nm).[65] In this context, a schematic diagram of the energy levels showing the band gap narrowing mechanism of a D–A type polymer is illustrated in Figure 2c. This can be generally enabled by minimizing the bond length alternation (BLA) as the average of length difference between carbon-carbon bonds in the chain.[64,157] In this respect, different adopted chemical engineering strategies are explained in relevant literature.[64,156,158] To realize low-bandgap polymer donors, the main utilized strategies are the molecular design of donor-acceptor (D–A) and stabilization of structure by quinoidal resonance along the conjugated backbone.[18] Further technical specifications and scientific background of these strategies can be found elsewhere.[18,64,65,158] In the case of small-molecular acceptors, in spite of the high performance of fullerene-based materials, they are characterized by restricted bandgap tunability due to the closed-cage structure. Hence, extra chemical design is required to further shift the absorption in the NIR range. This favors the synthesis of non-fullerene small molecules with fused ring-based acceptor or electron-withdrawing moieties.[64] Interestingly, all these narrow-bandgap organic NIR-photoabsorbers are relevant for

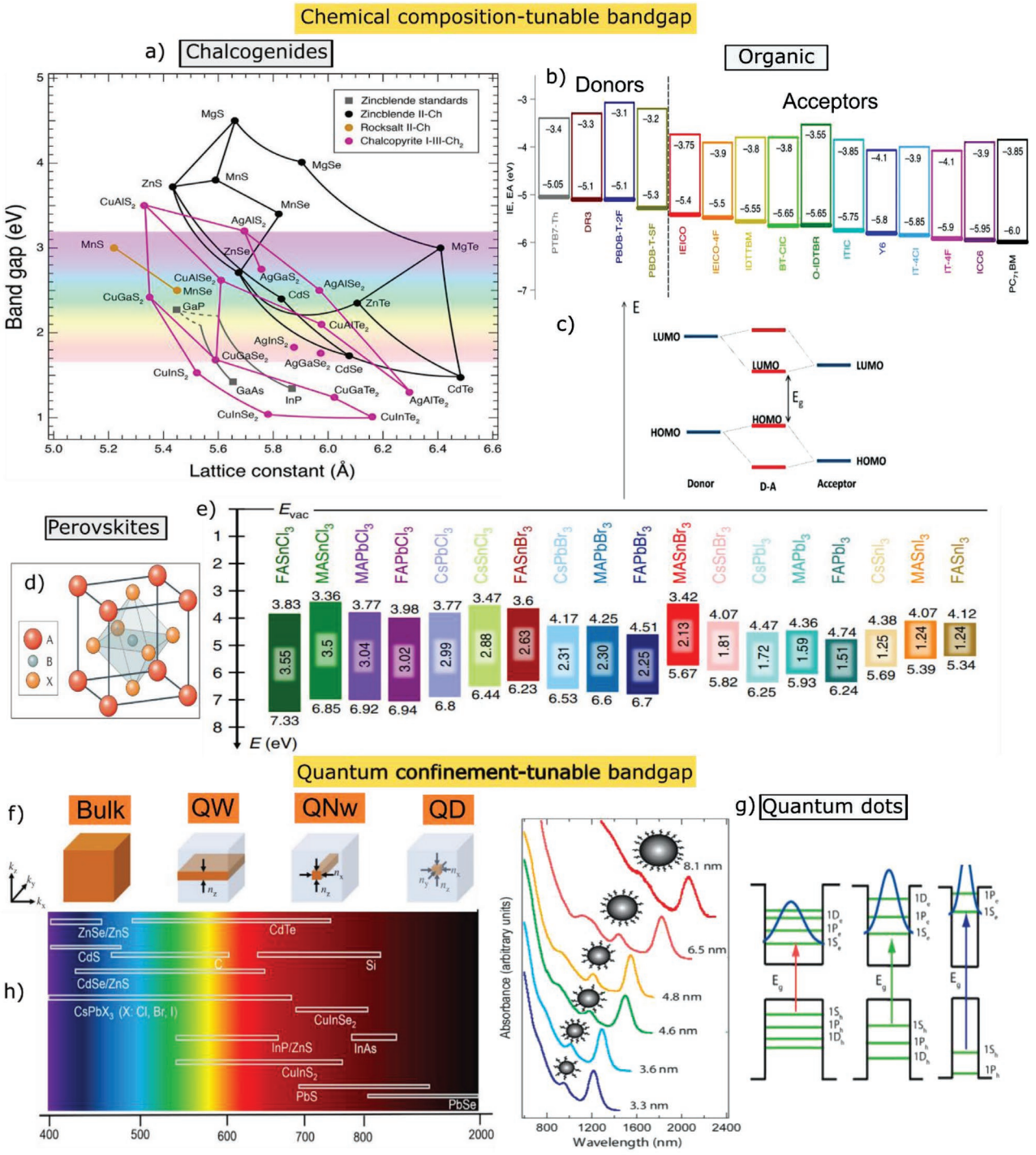

Figure 2. a) Room-temperature band gaps of different chalcogenide materials such as zincblende II–VI alloys, rocksalt II–VI alloys, ternary I–III–VI_2 chalcopyrite chalcogenides and some standard binary zincblende III-V compounds. Reproduced with permission.[153] Copyright 2020, American Chemical Society. b) Electron affinity (EA) and ionization energy (IE) levels of some representative non-fullerene acceptors and polymer donors. Adapted with permission.[165] Copyright 2021, Springer Nature. c) Band gap narrowing mechanism of a D–A copolymer in molecular orbital theory between the lowest energy unoccupied molecular orbital (LUMO) and the highest-energy occupied molecular orbital (HOMO). Reproduced with permission.[166] Copyright 2015, American Chemical Society. d) Illustration of ABX_3 perovskite lattice structure. Reproduced with permission.[142] Copyright 2017, Springer Nature. e) Schematic energy level diagram of different metal halide perovskites with the corresponding ionization energy, electron affinity and optical gaps values (all in eV). Reproduced under the terms of the CC BY license.[141] Copyright 2019, the Authors. Published by Springer Nature. f) Schematic illustration of 1D, 2D, and 3D quantum-confined nano structures compared to bulk material. Reproduced under the terms of the CC BY license.[163] Copyright 2018, the Authors. Published by the Royal Society. g) Quantum-size shifted absorption, discrete excitonic transitions and bandgap dependence on PbSe QD size. Reproduced with permission.[167] Copyright 2012, Elsevier. h) The emission range of representative QDs with different elemental composition and tunable particle sizes. Reproduced with permission.[164] Copyright 2017, Elsevier.

color-neutral transparent PV device with maximized light transmission in the visible spectrum.

One of the most striking paradigms of bandgap tunability by compositional engineering are perovskite materials.[142,159,160] In PV, halide perovskite photoabsorbers are 3D ABX_3 structures with corner-sharing metal halide octahedra, where, A is a small organic of inorganic cation (charged +1), B is a metal cation (charged +2), and X is a halide anion (charged –1) (Figure 2d). Typically, A components can consist of Cs, formamidinium $(CH(NH_2)_2^+$ (FA) or methylammonium $(CH_3–NH_3)^+$ (MA), B elements can be Sn, Pb, or Ge, while, X atoms can represent Cl, Br or I. Importantly, the substitution of A, B, and X ions enables the broad tuning of the bandgap energy from ≈1 to 3.55 eV.[141,142] (Figure 2e) Typically, a gradual increase of the energy bandgap is induced by going from I to Br to Cl or by substituting Sn with Pb or also by replacing the MA^+ cation by FA^+ or Cs^+ ions.[142,159] This is due to the changes in the density of states, chemical compositions and bond angles and lengths by including different cations and anions.[142] Owing to the change of chemical composition, the absolute energy levels are altered by the effective atomic energy levels of the metal cations and halide anions, their hybridization strength, as well as structural variations including size and distortion of the crystal lattice.[141] Further details about the physical mechanisms governing the variation of the bandgap and the absolute energy levels in perovskites can be found elsewhere.[141,142] One of the important applications of these attributes are UV-harvesting transparent PV based on perovskite photoactive materials.

Overall, the bandgap tuning via compositional engineering is a key design strategy not only for the improvement of PV performance but also for the realization of spectrum-sensitive functionalities such as visible transparency and selective absorption.

2.3.2. Quantum Confinement-Tunable Bandgaps

Unlike composition-tunable bandgaps, quantum confinement-tunable bandgaps are manifested via size tailoring in semiconductor materials. Generally, by reducing the size of semiconductor nanostructures down to a comparable level with its exciton Bohr radius (R_B), a restriction of the degrees of freedom and phase space for the charge carriers occurs and quantum confinement effects arise.[147,161,162] Thus, semiconductor materials with larger exciton size and Bohr radius are more susceptible to QC effects. Higher degrees of quantum confinement are manifested by going from quantum well (QW) with confinement in only one dimension (two degrees of freedom) to quantum nanowire (QNw) with confinement in 2D (one degrees of freedom) to quantum dot (QD) with confinement from all the three dimensions (zero degrees of freedom). (Figure 2f) It follows that a persistent localization of exciton via quantum-size effect is compensated by an increase of momentum and kinetic energy. This is accompanied by a discretization of the energy level and an increase of the energy bandgap in low-dimensional nanostructures compared to the bulk material with constant bandgap and continuous energy spectrum.[147,163] Hence, quantum confinement effects imply size-dependent tuning in the optoelectronic properties of semiconductor nanostructures, including the bandgap energy, band edge positions, the density of states and the absorption transition probability.[163] Such phenomena can be observed in Figure 2g, showing QC effects on shifted absorption, discrete excitonic transitions and bandgap as a function of PbSe QD sizes. The fundamental implications of QC on the DOS and the energy are briefly introduced in the Section S3, Supporting Information. It is noteworthy that for a given semiconductor, QC effects are more pronounced as the degree and the dimensions of confinement are higher, namely, higher in QD than in QNw and QW.[147] In colloidal quantum dots with different elemental composition, including II–VI (e.g., CdX, X = S, Se, Te), III–V (e.g., InP, InAs, GaAs), IV–VI (e.g., PbX, X = S, Se, Te), and group IV (C, Si, and Ge), wide bandgap tunability from UV to NIR range can be achieved due to the synergy between quantum-size effects and chemical composition.[164] (Figure 2h)

2D semiconductor materials in the form of few-layers and monolayers can also be potential photoabsorbers, known for their thickness-dependent optoelectronic properties and significant QC effects. These materials exhibit highly tunable and precisely controllable bandgaps.[149]

Overall, QC-tunable bandgaps in low-dimensional semiconductors could enable distinct features and practical applications in SC technologies based on QW, QNw, and QD nanostructures.

2.4. Thermal Tuning Aspects

2.4.1. For the Intrinsic Solar Cell Devices

Unlike under standard test conditions (AM1.5), that is, one sun illumination at a temperature of 25 °C, solar modules in the field operate at temperatures of about 20—40 °C higher than ambient. This happens since about 80% of the incoming sunlight is converted to heat, leading to a drop rate of efficiency typically between –0.1% K^{-1} and –0.5% K^{-1} depending on the environment.[168–170] To reduce the operating temperature of PV, a reduction of the generated heat in the device and/or an increase of released heat to the surrounding environment is desired.[87] This can be tailored through photonic management and spectral engineering approaches.[82,169]

On one hand, among causes for excess heat excess generation in PV modules (e.g., thermalization, recombination, ohmic losses, entropy generation),[171,172] sub-bandgap parasitic absorption can be prevented by introducing spectrally selective optical filters. This reflects away sub-bandgap photons with insufficient energy for photocurrent generation from the SC.[173–175] Moreover, selective filtering by reflecting the high energy UV photons which contribute to thermalization can be useful in some PV configurations.[82,169,171] A more effective way to minimize the heat generation through thermalization would be to increase the cell efficiency or to implement multijunction design.[171,176]

Simultaneously, the PV module cooling by the rejection of waste heat to the surrounding environment occurs through three heat transfer mechanisms, namely. conduction, convection and radiation.[177,178] In particular, passive radiative cooling ability in SCs can be realized by spectral tuning the PV devices for high emissivity (ε) in the atmospheric transparency window

-also called sky window- (wavelength band $\lambda \approx 8$–13 μm) to benefit from the coldness of the universe ($T \approx 3$ K).[170,179,180] The analytical expressions of different power components governing the energy balance are presented in Section S4, Supporting Information. Detailed fundamental principles of passive radiative cooling for SCs can be found in several relevant papers.[169,181–183]

The above mentioned optical tuning strategies like subbandgap reflection methods and passive radiative cooling concepts are beneficial for the appropriate thermal management of PV devices.[184–187]

2.4.2. For the Extrinsic Surrounding in Interior Building Spaces

Apart from power generation, SCs with tunable transmittance integrated in windows can also reduce the amount of light entering the room. This ensures heat insulation function and thereby minimize the energy requirements for cooling building spaces. The heat dissipation in smart windows can be achieved by strongly reflecting the near-infrared radiation which are not utilized in the power generation.[23,25] The main thermal metrics for PV window are introduced in Section S5, Supporting Information. This includes the infrared–rejection rate (IRR) and solar heat gain coefficient (SHGC). Thus, the integration of tunable ST-PV and TPV with static or dynamic approaches into solar windows can play a key role in the thermal management and heat insulation of building interiors or vehicle spaces.

2.5. Further Tuning Capabilities Beyond Spectrum-Sensitive Aspects

Although the focus in this review is rather devoted to spectrum-sensitive tunability aspect, nevertheless we briefly mention here further capabilities that are implicitly considered and are definitely essential for various applications.

Considering mechanical properties of SCs, it can be tuned from rigid to flexible to stretchable.[85,188] A wide variety of flexible and stretchable SC technologies can be found in many relevant reviews.[26–28,83,85,188,189] Flexible SC devices offer the ability to apply a mechanical deformation such as bending or stretching without failure and preferably in a reversible and recoverable way.[26,28,83] To realize a flexible thin-film SC, proper choice of the entire device components and compatible fabrication processes are essential.[27,28,72] Since ceramics and thick glass are considered as non-ductile and brittle,[28] only ultrathin flexible glass, metal foils, polymers and papers can be possible candidates as substrate for flexible thin film PV,[27,83,190]

Unlike thin-film PV, in c-Si wafer-based PV, the conventional substrates are rigid and brittle. However, by thinning down c-Si below 50 μm, a mechanical bending occurs and the bendability and the flexibility increases as the thickness of the c-Si is further reduced.[58,191,192]

Typically, the flexibility and the bendability of the functional materials and the SC devices are characterized and quantified by relevant mechanical parameters such as bending curvature radius, Young's modulus and elongation yield strength and elastic or total elongation.[26–28,83,193] For stretchable SC, fibershaped or intrinsically stretchable structures are employed due to their multidirectional stretching ability, their resistance against tensile fracture and their accommodation to strains.[26,85] This allows to achieve the required properties in regard of the crack-onset strain, the elastic modulus and the durability after multiple cycles.[85,188]

The power-per-weight is controlled by the design of functional components and retrofits of SC.[29,83,194,195] The adjustment of the PV weight can be from massive to lightweight and ultra-lightweight. Massive and non-ductile PV technologies are mainly deployed in solar power plants and rooftop panels. Lightweight and flexible PVs are mostly vital for integration scheme with weight restrictions and curved surfaces such as in vehicles, greenhouses, wearable electronics and aerospace applications.[19,29,196–202] While, stretchable SCs are relevant for wearable textile and portable devices.[41,203–205] Furthermore, the size of PV devices can be adapted from upscaled integrated systems to miniature micro-cells.[30,32,206] In this way, on one hand, large-area solar PV can meet the size requirements of applications like buildings, vehicles, agrivoltaics. On the other hand, small size SCs are suitable for integration in skin-mountable electronic devices.[30,207] Another tuning aspect is the possibility to change from static fixed to movable solar panels equipped with sun tracker systems for adjustable tilt angles. This dynamicity is beneficial for power production and shading control in windows and agrivoltaics.[208–210]

3. State of the Art of Tunable Solar Cell Technologies

3.1. Synergetic Impact of Bandgap and Optical Tuning on Efficiency Levels: From Opaque to Colored to Transparent PVs

3.1.1. Opaque PV with Near-Complete Absorption

The fundamental thermodynamic limit defining the maximum theoretical efficiency of a single-junction SC as a function of the absorber bandgap is determined by the Shockley–Queisser (S–Q) detailed-balance model.[211] Within the SQ formalism, a balance between photogeneration process and radiative recombination as unique loss mechanism is considered, where all photons with energies above the photoactive material bandgap (E_g) create free electrons and holes. This results in one electron per absorbed photon to contribute to the electrical current. Accordingly, single-junction SCs with an optimum $E_g \approx 1.34$ eV are be capable of reaching a PCE around 33% under standard solar spectrum and intensity conditions (**Figure 3**a). However, in practical reality, the throughput of a SC is affected by an interplay between the light photons absorption, the transport and collection of free charge carrier towards the contacts and the recombination of electrons and holes being the major loss mechanism.[212,213] These physical mechanisms are linked to the key properties of the photoactive material, such as the absorption coefficient α, the charge-carrier mobility μ, and the charge-carrier lifetime τ.[212,213] Thus, the combination of the optical and electrical losses affects the output characteristics that is, V_{oc}, J_{sc}, and FF. This leads to further disparity between the theoretical limit and the experimental efficiency that varies

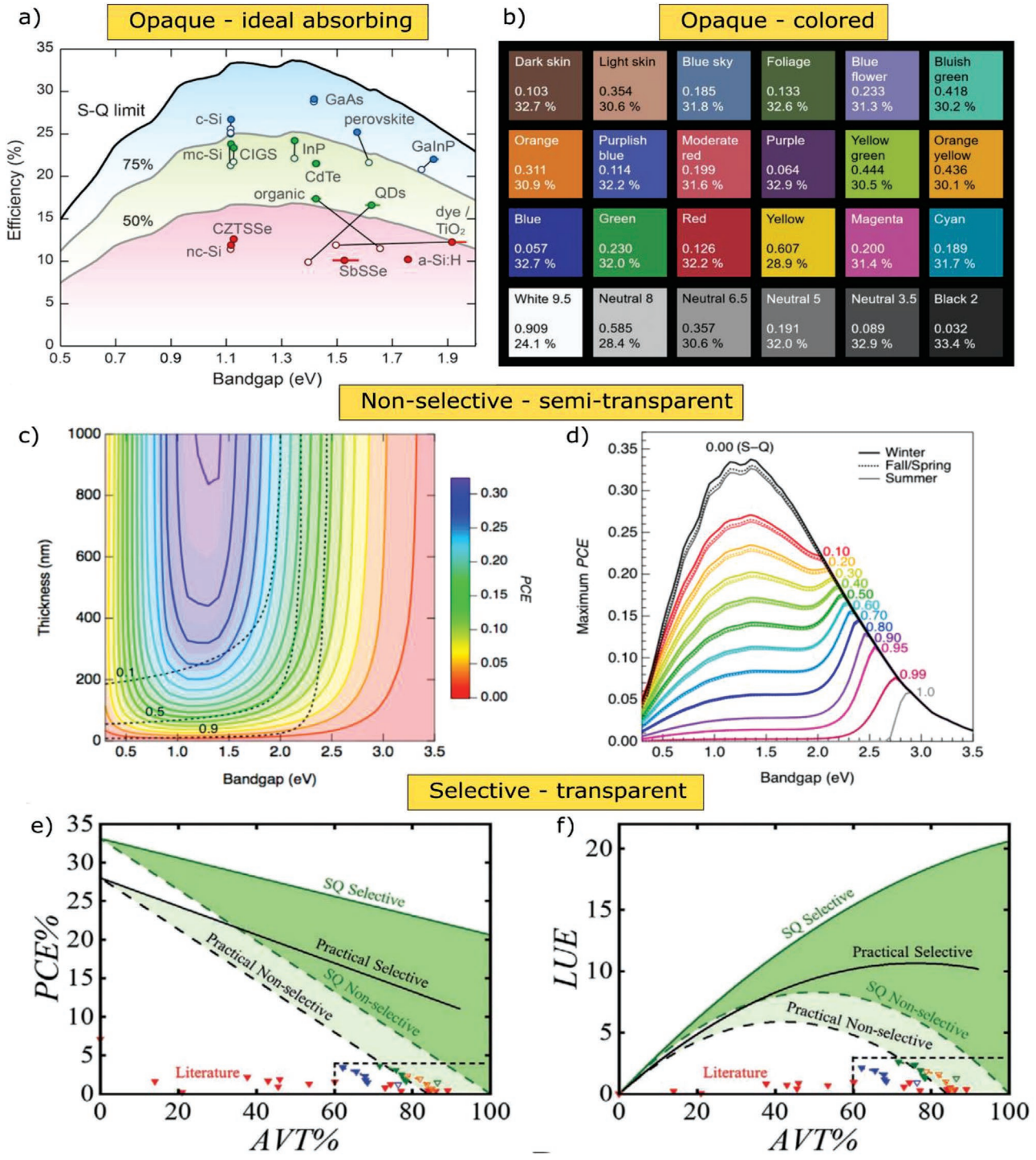

Figure 3. a) Best experimental efficiencies for opaque single junction solar cells from different PV technologies as a function of the effective absorber bandgap. The solid, dashed, and dotted lines indicate 100%, 75%, and 50% of the theoretical thermodynamic efficiency limit. Reproduced with permission.[214] Copyright 2020, American Chemical Society. b) Theoretical efficiency limits for each colored opaque PV, with specific Y coordinate in the CIE chromaticity diagram. Reproduced with permission.[219] Copyright 2019, The Royal Society of Chemistry. c) Contour plot of PCE as a function of absorber thickness and bandgap. The dashed black curves are lines of constant AVT = 0.1, 0.5, and 0.9 where the absorber thickness was optimized for maximum PCE, d) Maximum PCE versus bandgap for different AVT values. The set of black curves assumes an optically dense film approximated to the S–Q limit for each season. Each set of colored curves at constant AVT is indicated by the corresponding value. Reproduced with permission.[55] Copyright 2019, American Chemical Society. e) PCE versus AVT, f) LUE = PCE × AVT versus AVT. Different lines present a comparison between non-wavelength-selective ST-PV with partial visible transmittance and wavelength-selective TPV in ideal and practical limit scenarios. Reproduced with permission.[221] Copyright 2021, Wiley-VCH.

significantly between different for SC technologies, as shown in Figure 3a.[214] Hence, the selection of materials, design and the device structure engineering in PV technologies would determine the potential performance and the generated power yield.[50,54,213] PV devices can be categorized according to their performances as low-cost low-efficiency and high-cost high-efficiency systems.[13,51,215] Importantly, such tunability aspect is decisive in the selection of target applications. High-efficiency SC technologies (PCE > 20%) including III-V, c-Si, perovskite, CIGS and CdTe are potential real-world candidates for specific applications with limited installation area like residential sector, vehicle-powering as well as aerospace applications. Other thin film SCs and emerging PVs like dye-sensitized, amorphous silicon, kesterite, inorganic, organic, and others, yield low efficiency levels.[216,217] Hence, such SC technologies are more suitable for ancillary types of energy conversion like building-integrated PV (BIPV) and indoor PV. However, in colored, semitransparent or visibly transparent SCs, the alteration of the light transmission and reflection inevitably diminishes the energy harvesting capability in the PV device and results in a drop of the power throughput level.[17,55,218–220]

3.1.2. Opaque Colored PV

Halme and Mäkinen established a reference point for the theoretical efficiency limits of ideal colored opaque photovoltaics.[219] The implications of the optical losses on the power conversion efficiency due to the production of color by reflecting of a fraction from the visible light were quantitatively determined compared to ideal black SC. As can be noticed from Figure 3b, most of the colored opaque SCs can yield a theoretical efficiency limit above 29% corresponding to a performance loss below 14% relative to an ideal black SC with 33% efficiency.[219] When different colors were compared, yellow-green SCs outperforms the blue, red, and purple counterparts. It was also found that for the majority of colored SCs, the optimal bandgap is around 1.1 eV, in correlation with c-Si. Furthermore, the ideal efficiency decreased monotonically with increasing relative luminosity.[219] Typically, color-induced losses can be minimized by utilizing narrow and sharp peaks in the reflection spectrum to produce the desired color.[222]

3.1.3. Non-Wavelength-Selective Semitransparent PV

In the context of semitransparent PV with non-wavelength-selective absorbers, Wheeler et al. adapted a modified S-Q detailed balance model for the integration of PV windows in different seasons considering the average visible transmission (AVT) besides the efficiency (PCE).[55] They established the dependence of PCE on the trade-off between the absorber thickness and bandgap (Figure 3c). Moreover, the decrease of the PCE with increasing AVT was quantitatively determined. The ideal efficiency dropped gradually from 33% for optically dense (S–Q limit) absorbers at a bandgap of 1.35 eV to 5% for wide-bandgap (≈3 eV) UV-harvesting transparent PV (Figure 3d). They also deduced that the ideal bandgap range for maximum efficiency level can be altered compared to the common S–Q as it is strongly dependent on the transmission level. Mainly, for a low AVT level ≤ 0.3, the optimum bandgap ≈1.35 eV remained in agreement with the standard S–Q model. This regime is valid for thin-film technology with photoactive thinning approach and partial absorption.[55] However, when the AVT exceeded 0.3, the ideal bandgap shifts progressively from 2 to 3 eV, as the AVT increased.[55]

Brabec and co-workers determined the efficiency limits of colored semitransparent organic OSCs. By examining the interplay between efficiency, transmitted color, and band gap, they concluded that high efficiencies can be achieved for a wide range of colors, whereas, optimized bandgap, and absorption spectrum were required, especially for high AVT exceeding 40%.[223]

3.1.4. Wavelength-Selective Transparent PV

For UV–NIR wavelength-selective transparent photovoltaics, a theoretical model for the performance potential limits was established by Lunt and co-workers.[17,218] As shown in Figure 3e, the thermodynamic efficiency limit of a single junction TPV could reach around 20% even with an average visible transmission of 100%, considering a photogeneration in UV (<435 nm) and NIR (>670 nm) wavelengths range. This is due to the large fraction of the solar photon flux in the infrared region, whereas, the PCE limit for an opaque PV with an AVT of 0% is 33%.[218] Considering only UV-selective PV with wide bandgap photoactive materials (E_g > 2.85 eV), the estimated detailed balance limit is restricted below 7% .[59] Regarding the bandgap aspect, the ideal value corresponding to the highest efficiency changed from 1.36 eV (910 nm) in opaque cell to 1.12 eV (1100 nm) for visibly transparent cell.[17] While broadband absorbing ST-PV technologies suffered from a drastic decay in efficiency at high transmission degree (down to PCE ≈ 0% when AVT exceed 90%) which was expressed by a steep slope in the thermodynamic limit evolution, the UV–NIR selective absorber could preserve high PCE performance even at the highest transmission (Figure 3e). This is an exceptional feature for UV–NIR wavelength selective TPV in high transmission regime compared to broadband absorber counterparts[17,218] It was estimated that a realistic limit of 13% PCE can be expected for UV–NIR selective TPV considering all the inevitable optoelectronic losses, while still ensuring a high level of visible transparency.[17]

As can be seen in Figure 3f, the fundamental limits of LUE as a function of AVT differ drastically according to the spectral absorption in the visible range between non-wavelength selective ST-PV and UV–NIR wavelength selective TPV solar technologies.[17,218] The disparity is more pronounced at high AVT levels. For non-wavelength selective PV, the distribution of ideal LUE is parabolic-like with and an optimum LUT ≈ 8% around AVT = 50% and 0 at the extreme values of AVT, that is, 0% and 100%. For UV–NIR wavelength selective PV, the increase of AVT leads to a continuous rise of LUE up to 20.6% for corresponding AVT of 100%.[17] The determination of LUE enables the evaluation of the experimental performance in terms of both visible transparency and power conversion simultaneously

compared to the theoretical limit.[17,224] It can also act as an metric for assessment of the progress of a designated semi-transparent and transparent technology among reported others in the field.[17,51]

3.1.5. Implications of the PCE-AVT Trade-Off on the Target Applications

According to the combination of power throughput, transparency level, and aesthetic quality, integrated PV technologies can satisfy the requirement of multifunctional distributed applications. Opaque-colored SCs with minimal losses compared to completely opaque counterpart is desired for power generation and appearance in building façade. Highly transparent color-neutral PV (AVT > 50%) with efficiency in the range of 5–10% can be suitable for power generating window and heat insulation. Whereas, colored semitransparent PV with similar PCE can be employed in semi-transparent greenhouse and tinted glass façades. Lower efficiency level (PCE ≈2–5%) may be sufficient for self-powered low-power electronics or smart windows.[17]

3.2. Bandgap Tuning in Single Junction and Multijunction Solar Cells

3.2.1. Bandgap Tuning in Single Junction SC Technologies

Here, we survey several single junction SCs in which the capability of bandgap tuning has marked their development and their progress. The focus is devoted to PV technologies featuring tunable bandgaps either by chemical composition or under quantum confinement effects, as already introduced in Section 2.3. The impact of bandgap tuning on transparency and coloration will be addressed in separate sections.

Representative SC Technologies with Chemical Composition-Tunable Bandgap: Since their discovery, perovskite-based solar cells (PSC) have revolutionized the PV field and have offered tremendous advantages in terms of bandgap and absorption onset tuning.[22,225] In the first published paper on PSC, Miyasaka's group pointed out the chemical management capabilities to realize different energy gaps with a series of organic-inorganic perovskite materials enabling high photovoltage levels.[226] Subsequently, Seok and co-workers presented a breakthrough that contributed to the success story of perovskite PV and attracted the attention towards their bandgap tunability features (**Figure 4**a).[102] Through halide substitution of iodine by bromine in $MAPb(I_{1-x}\ Br_x)_3$, the chemical management enabled an exquisite bandgap tuning over almost the entire visible spectrum. The band gaps of $MAPbI_3$ and $MAPbBr_3$ were reported as 1.5 and 2.3 eV, respectively. When the biggest halide I^- was substituted by a smaller Br^-, the absorption thresholds of PSCs were gradually blue-shifted.

These findings have triggered tremendous research and development activities and material engineering efforts to further extend the bandgap tuning capabilities and improve the PV devices performance (Figure 4b).[22,225,227] Nowadays, myriads of PSC are reported with widely different ABX_3 perovskite compositions and corresponding bandgaps.[227] Considering the recent breaking record efficiencies exceeding 25% with ≈80% of the bandgap-related thermodynamic limit,[228,229] halide perovskite-based SCs are well-positioned as game-changer in the PV performance race. In addition to the established high throughput, cost-effective, and industrial-compatible fabrication processes of PSCs have enabled the advancement of the technology from research and development at lab-scale level to large-scale industrial level.[230–232] This progress has sparked the foundation of several specialized manufacturers in perovskite-based PV such as Oxford PV, Saule Technologies, and Swift Solar.

Another example of bandgap tuning by chemical composition are OSC technologies. The introduction of donor:acceptor bulk heterojunction in the active layer have been a successful way to upgrade the efficiency (Figure 4c).[238,239] The boost in efficiency levels around 1% to over 9% was attributed to the development of novel organic materials with lower optical gaps, such as polymer:fullerene combinations having higher charge separated state energies.[240] The evolution of organic PV field was traced in several related papers.[155,166,240,241] Recently, a growing interest has been attributed to next-generation organic PV based on non-fullerene acceptors at the expense of traditional fullerene counterparts.[233,242,243] A step ahead is the ternary strategy which consists of introducing a third component into the binary host system to further improve the energy level alignment in the photoactive layer, and hence, the PV performance.[244,245] In general, the bandgap tuning of donor and acceptor leads to an adjustable effective bandgap which is a crucial parameter to determine the OSC efficiency. Also, the reduction of the energy-level offset between donor and acceptor molecular states is beneficial for improving the photovoltaic performance.[165,246,247] To point out this fact, Scharber, Brabec, and co-workers established the design rules as a function of the bandgap and the energy levels in bulk donor:acceptor heterojunction, assuming the state-of-art materials and device architectures at that time (Figure 4c).[155,248] It was concluded that for a specific acceptor, an optimum organic donor-acceptor bandgap of 1.45 eV and a minimum LUMO offset of 0.3 eV to enable efficient charge transfer were recommended to maximizing the efficiency. These findings underline the importance of bandgap tuning of donors and acceptors in bulk heterojunction OSC. Recently, along with the materials development, the optimization of the level alignment in the photoactive layers of bulk heterojunction OSC featuring efficient charge carrier splitting and transport enabled a record-breaking PCEs > 18%.[249] These demonstrated performances have enabled the expansion of organic PV technologies as one of most potential contenders for deployment in distributed niche applications. In addition, the compatibility of the fabrication process with affordable roll-to-roll manufacturing have facilitated the lab-to-fab translation,[250] and therefore, have stimulated the establishment of many producers of organic solar panels like Heliatek and ASCA.

In CIGS-based absorbers, the bandgap can be tailored by changing the lattice parameter due to different bond strengths. This can be achieved by controlling the chemical composition during the synthesis process. It follows that E_g can typically be tuned from 1.04 to 1.7 eV by varying the Ga/In ratio with

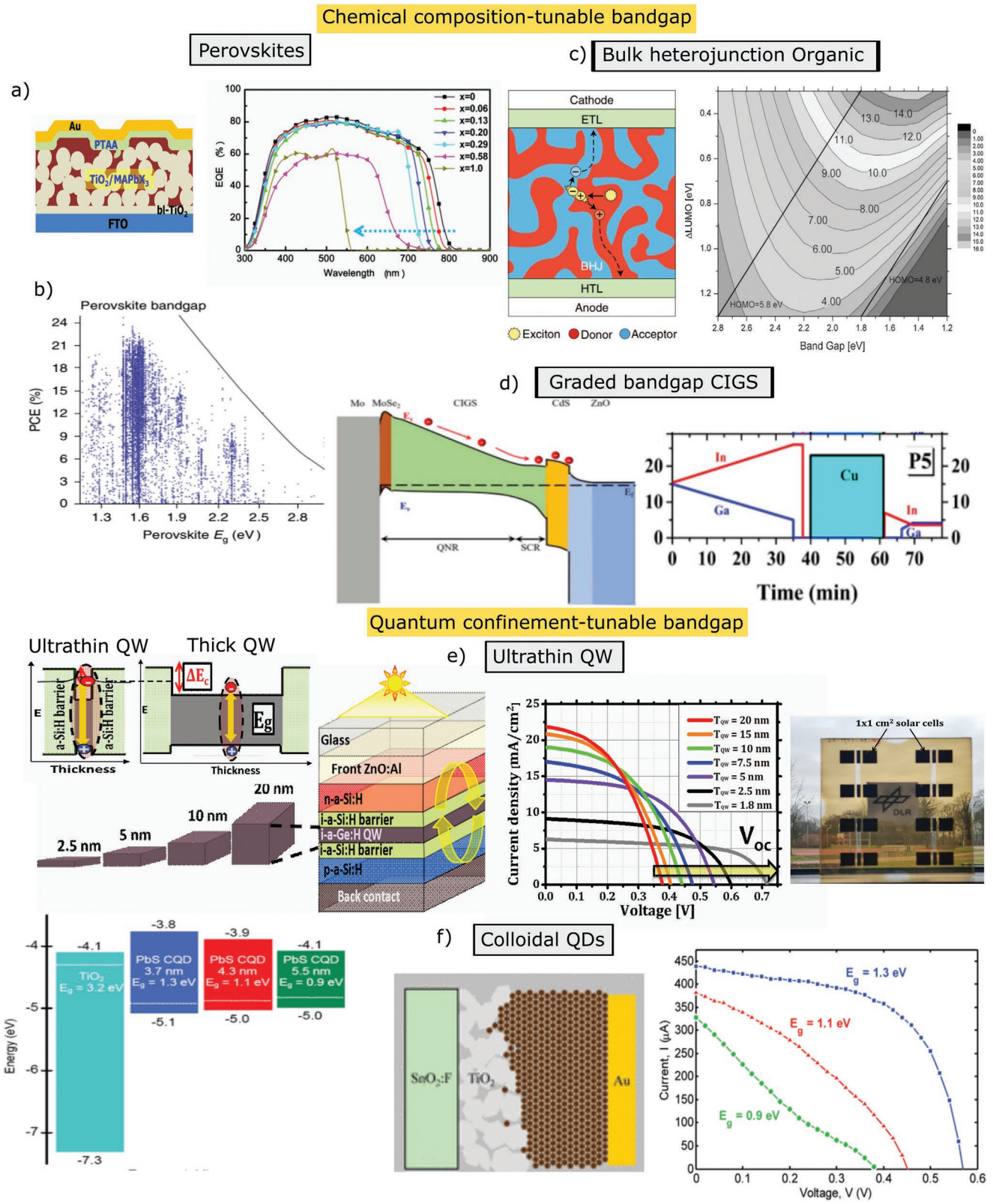

Figure 4. Perovskite-based PV. a) Device structure of $TiO_2/MAPbX_3$ hybrid heterojunction (left) External quantum efficiency (EQE) spectra of $MAPb(I_{1-x}Br_x)_3$ heterojunction SCs (right). Reproduced with permission.[102] Copyright 2013, American Chemical Society. b) PCE versus Eg for perovskite SCs in the global open-access database. The Shockley–Queisser limit is given as a solid line. Reproduced under the terms of the CC BY license.[227] Copyright 2021, the Authors. Published by Springer Nature. c) Organic bulk heterojunction SC structure (left) Reproduced with permission.[233] Copyright

continuous substitution of indium by gallium.[251] This tunability feature is exploited in the graded bandgap CIGS concept by controlling the position of the conduction band minimum to enable better electrons collection.[143] Following the first seminal report by Conteras et al.[252] and the introduction of three-stage co-evaporation method,[253] the active control of Ga grading within the absorber has contributed in the efficiency enhancement of CIGS-based PV.[143,254] Commonly, a double-graded conduction band profile with V-shape is used, which is characterized by a narrow bandgap notch point closer to the absorber front surface and wide bandgap at both edges. This improves the optical absorption of long wavelengths and the electrical properties of the junctions.[143,251]

Apart from the common V-shape, Gong et al. explored different shapes of Ga grading with different graded bandgap profiles using time-dependent Ga and In deposition rates.[234] The best profile, depicted in Figure 4d, reached a PCE of 20.3% without post-treatment. Considering a record efficiency exceeding 23%,[255] the scientific and technological progress in CIGS-based PV has been accompanied by an evolution at the industrialization level with several manufacturers of mass production CIGS solar panels on the market such as Ascent Solar, Flisom, and Avancis.

Representative SC Technologies with Quantum Confinement-Tunable Bandgap: As for quantum-confined nanostructures, quantum well solar cells (QWSC) are the most widely developed and commercially successful PV device relying on quantum effects. Since its discovery by Barnham et al.,[256] this technology has attracted considerable attention in the PV community. The relevant architecture is based on a low-bandgap semiconductor QW region inserted between two high-bandgap barrier semiconductors. Taking advantage of QC effects, QWSC can present distinguished features such as the size-tunable optoelectronic properties, the ability of bandgap engineering, the minimization of radiative recombination, the utilization of excitonic absorption and the enhancement of photocurrent with minimized voltage losses.[154,257] In particular, QWSC technologies based on epitaxial crystalline III–V semiconductors made great progress owing to bandgap engineering and the development of advanced materials and device architectures[154] enabling PCE > 26%.[258] Recently, a growing interest has been attributed to perovskite QWSCs as experimental proof-of-concepts at research level.[259,260] Liang et al. demonstrated that the control of QC effect with the fine regulation of QWs in graded structures was beneficial for the improvement of the efficiency (PCE > 20%) and the stability of SC device.[259] Sargent and coworkers showed that QC-tunable heterostructures in reduced-dimensional perovskite QW enabled a 23.91%-efficient SC device.[260]

An exciting example for the significant impact of QC-tunable bandgap was proposed by Meddeb et al., who realized a proof-of-concept for one of thinnest QWSC device using a hydrogenated amorphous silicon/germanium materials system (Figure 4e).[235] When the thickness of the a-Ge:H nanoabsorber was reduced from 20 nm down below 2 nm, an upward shift of the conduction band occurred, resulting in a bandgap tuning from below 1 eV up to 1.56 eV. This leads to a trade-off between different PV characteristics, while maintaining a comparable power conversion level (PCE ≈ 4%). The photocurrent drop due to the thickness reduction was mainly compensated by an increase in both V_{oc} and FF. This was manifested due to the influence of the band gap widening and the band offset reduction at the QW/barrier heterojunction. The substitution of single QW by multiple QW configuration was proved to further boost the PCE level beyond 5%.[261]

As can be seen in Figure 4e, showing a photograph of a-Ge QWSC with a 2 nm-thick QW, quasi-total absorption was achieved in the opaque mode, owing to the enhanced absorption under photonic confinement.[262] Whereas, the thickness reduction promoted the light transmission through the areas without back contact. This would be beneficial for semitransparent devices.[263] The proof-of-concept for ultrathin SC technology based on a-Ge QW is still at lab-scale and upscaling activities for the development of large-area modules are on-going.[264]

In a more general context, the features of QWSCs are typically not only restricted to technological advancement, but can also open a path for interesting physical mechanisms which can be governed by bandgap tuning like hot carriers concept.[265,266]

For colloidal QD PV technologies, it is often stated that the most attractive characteristic is the tunable band gap, which is easily achievable by adjusting the QD sizes.[267,268] One of the seminal works in this regard was presented by Sargent and coworkers, demonstrating quantum-size based optimization of heterojunction colloidal QD SCs (Figure 4f).[237] The change of the QD size from 5.5 to 3.7 nm leads to an increase of the bandgap from 0.9 to 1.3 eV. This enabled a boost in the power conversion efficiency. Owing to the unexpansive fabrication processes, the upscaling techniques and the gained maturity over the last decade, it is believed that colloidal QD PV technology is moving forward toward commercialization.[269,270]

Broader Context of the Bandgap Tuning in Single Junction SC: From a universal perspective, Peters and Buonassisi established a correlation between lab-measured efficiencies and energy yield based on satellite data for various single junction PV technologies with different bandgaps.[271] It was found that the bandgap noticeably influenced the energy yield. The variation in harvesting efficiency with location was more pronounced for smaller bandgaps. For a similar efficiency, different bandgaps resulted in distinct behaviors under the influence of water vapor and temperature. It was concluded that an optimum band-gap for maximizing energy yield was 1.35 eV.[271]

2018, Springer Nature. Contour plot showing the power conversion efficiency of a bulk heterojunction solar cell with PCBM as acceptor material (LUMO level 4.3 eV). Reproduced under the terms of the CC BY license.[155] Copyright 2013, the Authors. Published by Elsevier. d) Band diagram for graded bandgap CIGS PV (left) and corresponding deposition rate profile for graded absorber (right). Reproduced with permission.[234] Copyright 2019, Elsevier. e) Ultrathin a-Ge:H QW PV structure and energy level for thin and thick QW (left) *J–V* curves for different QW thicknesses (middle). Reproduced with permission.[235] Copyright 2020, Elsevier. Photograph of ultrathin QW SC devices (right). Reproduced with permission.[236] Copyright 2020, IEEE. f) Colloidal QDs PV. Energy bands of QDs with different sizes (left) Colloidal QDs SC structure (middle) *I–V* curve of with different QD size and corresponding bandgap (right). Reproduced with permission.[237] Copyright 2010, American Chemical Society.

To this end, the band tuning capabilities have not only marked the history of many PV technologies, but also contributed to the progress and evolution of their performance from lab-scale to industry level to global energy yield. This is not only restricted to single junction SCs, but can be extended to multijunction devices.

3.2.2. Bandgap Tuning in Multijunction SC Technologies with Tandem Configuration

Principles of Bandgap Tuning in Multijunction SC: To date, among the so-called third-generation PV concepts, multijunction devices are the unique technologies that have practically surpassed the corresponding detailed-balance limit of single-junction SC. **Figure 5**a illustrates a stack of sub-cells in a tandem configuration where high-energetic photons are absorbed in a wide-bandgap region, while the absorption of low-energetic photons take place in the narrow bandgap semiconductor. This results in a broader spectral absorbance range and can potentially enable energy harvesting across the full solar spectrum (Figure 5b).[272] As depicted in Figure 5c, the sequence of the bandgaps across the energy diagram follows a descending order from higher values at the side of the device facing the light source, toward lower values at the adjacent region to the back reflective contact. Each photoactive material selectively absorbs a specific portion of light wavelengths with energy higher than its bandgap and transmits photons with lower energy to the subsequent subcell. Thus, both thermalization losses for high-energy photons and below-bandgap losses for low-energy photons, are reduced.[172] Obviously, the power throughput increase incrementally with the number of junctions.[273] Importantly, the multijunction SCs approach is sensitive to bandgap combinations and requires spectral engineering and precise tuning of the absorbers bandgaps in the subcell system.[273–277] Bremner et al. performed a study on the optimum band gap combinations for multijunction PV and determined the theoretical maximum efficiency for a band gap value as part of a multijunction stack from two up to six sub cells, as shown in Figure 5d.

Importance of Bandgap Tuning in the State of the Art of Tandem SCs: Experimentally, one of the most striking achievements showcasing the effectiveness of bandgap tuning in multijunction configuration, was the realization of six multijunction SC with a PCE of 39.2% under one-sun and 47.1% under 143 Suns concentration.[146] Unlike traditional multijunction devices (typically encompassing GaInP, GaAs, and Ge) with sub-optimal bandgap combinations, inverted metamorphic multijunction benefit from the leverage of ideal bandgap tuning to the solar spectrum (Figure 5e). The optimal bandgap sequence is achieved by combining both lattice-matched (high bandgaps) and lattice-mismatched (low bandgaps) sub-cells using III–V alloys with multiple lattices. Hence, the first three high-bandgap junctions are formed by $Al_{0.18}Ga_{0.33}$ $In_{0.49}$ P, $Al_{0.23}Ga_{0.77}$ As, and GaAs layers, then, bottom lower-bandgap junctions use $Ga_{0.84}In_{0.16}As$, $Ga_{0.66}In_{0.34}$ As, and $Ga_{0.42}$ $In_{0.58}$, as alloys with low threading dislocation density (Figure 5f).[146]

Practically, the restriction of the number of junctions to two-junction SC devices could enable benefits in terms of minimized technological complexity, high-efficiency, and low-cost potentials.[278]

As illustrated in Figure 5g, a wide range of material combinations have been developed in two junctions tandem PV technologies such as III–Vs,[146] III–V/Si[279–281] (PCE_{best} = 35,9%),[280] perovskite/Si[282–284] (PCE_{best} = 29.8%),[13] chalcogenide/Si,[278] perovskite/perovskite[285–287] (PCE_{best} = 26,4%),[288] perovskite/CIGS[289–291] (PCE_{best} = 25%),[290] perovskite/organic[292,293] (PCE_{best} = 24%),[294] organic/organic[295,296] (PCE_{best} = 20.2%),[297] a-Si/organic (PCE_{best} = 15.1%),[298] and many others.[51] Several research works addressed a generalized guide for the theoretical maximum PCE of two-junction tandem configuration as a function of top and bottom sub-cell bandgaps with both 2-terminal and 4-terminal architectures.[142,274,276,299] As depicted in Figure 5h, the best combinations to achieve the highest efficiency of two-junction tandem cell encompass a top cell with a bandgap of 1.7–1.9 eV and a bottom cell with a bandgap of 0.9–1.2 eV. Most of these successful practical achievements were made possible owing to the bandgap tuning capabilities.

One of the most outstanding paradigms of the effectiveness of bandgap tunability in tandem technologies is the integration of perovskite materials.[159,299,300]

In all-perovskite tandem SC, a general strategy is to combine mixed bromide/iodide wide-bandgap (≈1.8 eV) front subcell and a mixed lead–tin narrow-bandgap (≈1.2 eV) back subcell.[285] Eperon et al. made a breakthrough in an all-perovskite tandem PV (PCE > 20%) with ideally matched bandgaps, by combining a rear infrared absorbing (1.2 eV bandgap) $FA_{0.75}Cs_{0.25}Sn_{0.5}Pb_{0.5}I_3$ perovskite with a top wider bandgap $FA_{0.83}$ $Cs_{0.17}$ $Pb(I_{0.5}$ $Br_{0.5})_3$.[285] The bandgap control was achieved by means of Br:I ratio tuning and using a mixture of FA and Cs cations. Palmstrom et al. demonstrated a band-gap tuning strategy based on mixing large and small A-site cations to enable a wide bandgap of 1.7 eV leading to PCE = 21.3% for all-perovskite flexible tandem SC as one of the most efficient flexible thin-film PVs.[301] Recently, the efficiency all-perovskite tandem SC (PCE = 26.4%) exceeded that of the best-performing single-junction PSC (PCE = 25.5%).[288]

Considering the common low-cost fabrication processes, the combination of perovskite and organic semiconductors in tandem SC is an attractive strategy. A new milestone for perovskite–organic tandems was set by reaching an efficiency of 24%. The corresponding system combined a wide-gap (1.85 eV) perovskite $FA_{0.8}Cs_{0.2}Pb(I_{0.5}Br_{0.5})_3$ subcell with narrow-gap (1.33 eV) PM6:Y6 organic subcell featuring non-fullerene acceptors.[294] Impressively, tandem organic technology enabled a breakthrough in the field of OSC by entering the era of 20% efficiency.

Among tandem technologies, silicon-based tandem SCs are considered as one the most attractive option owing to the well-established industrial manufacturing and the dominance of the mainstream c-Si single junction technologies in PV market.[278,302,303] In terms of performance, this is also stimulated by the achievement of high efficiencies on large area c-Si PV reported by several companies such as JinkoSolar, Longi, Trina Solar, Panasonic, SunPower, and Kaneka.[304] Owing to the low bandgap ($E_g \approx 1.1$ eV) and the superior material

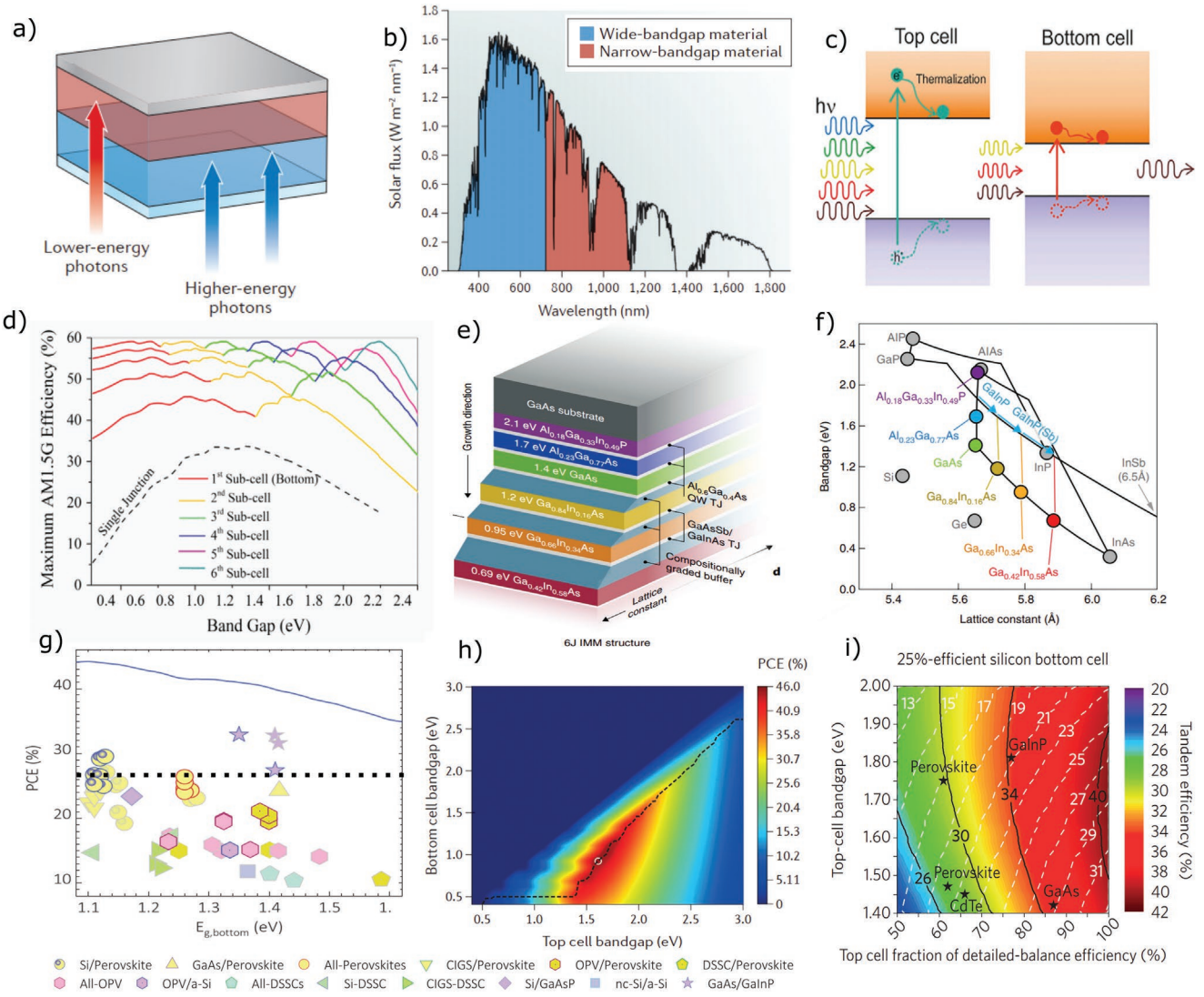

Figure 5. a) Simplified schematic of two-junction tandem solar cell with wide-bandgap subcell for short-wavelengths absorption (in blue) and narrower-bandgap subcell for long-wavelengths absorption (in red). b) Corresponding range of spectral absorption for top and bottom cells in the solar irradiance spectrum. Adapted with permission.[142] Copyright 2017, Springer Nature. c) Basic energy diagram for a double-junction tandem solar cell. Reproduced with permission.[159] Copyright 2017, Elsevier. d) Maximum efficiency for a band gap value as part of a multi-junction stack from two up to six sub cells. Reproduced with permission.[273] Copyright 2016, Elsevier. e) Simplified schematic of inverted metamorphic multijunction (IMM) structure with III-V-based 6 junctions and f) corresponding bandgap as a function of lattice constant for the 6-Junction IMM semiconductor design. Reproduced with permission.[146] Copyright 2020, Springer Nature. g) Highest efficiencies for best performing two-junctions tandem research solar cells as a function of bottom junction absorber bandgap energy from different PV technologies Adapted with permission.[51] Copyright Copyright 2021, Wiley-VCH. Dashed black line indicates the highest efficiency for c-Si heterojunction SC with PCE = 26.7%. h) Theoretical maximum power conversion efficiency PCE as a function of front (top) and rear sub-cell bandgap in 2 terminals architectures. Reproduced with permission.[142] Copyright 2017, Springer Nature. i) Estimation of the maximum possible efficiency for a tandem device with 25%- efficient c-Si as bottom cell as a function of the top-cell bandgap and efficiency. Black contour lines mark the tandem efficiency, and the dashed white contour lines point out the efficiency of the top cell separately. Reproduced with permission.[275] Copyright 2016, Springer Nature.

properties of c-Si, it presents a good candidate as a bottom cell in a tandem configuration with two multi-junctions.[275] Since the bandgap tuning of III–V semiconductor alloys is controlled via the change of lattice constant by employing epitaxial growth processes, the combination of c-Si, having a fixed lattice constant with III–V, will induce technological and cost constraints, albeit their expected high level efficiencies.[146,278] Thus, it is desired to designate further adequate candidates as top cell partners in c-Si-based tandem SCs. It is demonstrated that such selection process should be performed based on the concept of spectral efficiency η (λ), wavelength-resolved efficiency.[262] In order to realize a tandem combination with significant boost in performance compared to single junction c-Si, both, appropriate bandgap of the top cell and high efficiency conditions are desired. The maximum efficiency of a tandem configuration is determined as a sum of the integrated subcell spectral efficiencies weighted by the corresponding spectrum range and normalized to the incident photon power[275]

$$\eta_{\text{tandem}} = \frac{\int \eta_{\text{top}}(\lambda) I(\lambda) d\lambda \dfrac{\phi_{\text{top}}(\lambda)}{\phi_{\text{incident}}(\lambda)}}{\int I(\lambda) d\lambda} + \frac{\int \eta_{\text{buttom}}(\lambda) I(\lambda) d\lambda \dfrac{\phi_{\text{buttom}}(\lambda)}{\phi_{\text{incident}}(\lambda)}}{\int I(\lambda) d\lambda} \quad (2)$$

where ϕ is the photon flux, $I(\lambda)$ the spectral irradiance (in W m^{-2} nm^{-1}), λ the wavelength. The efficiency limit, given in Equation (2), is assumed without considering the possible optical and electrical losses. Depending on the bandgap tunability of the top sub cell absorber materials, a prediction of the tandem efficiency with a 25% efficient baseline c-Si bottom cell as a function of the bandgap and the efficiency of the top cell can be compiled, as shown in Figure 5i. The fraction of the detailed-balance limit related to the corresponding bandgap is considered as an analogy to the efficiency value. Modeling under real-world conditions predicts PCE above 32% with optimized perovskite bandgaps between 1.65 and 1.74 eV.[305]

So far, only Perovskite/Si, III–V/Si and III–V-based tandems could exceed the highest efficiency of single junction c-Si SC with PCE = 26.7%. Practically, many groups published perovskite/Si tandem cells with top cell bandgaps ranging from 1.64 to 1.75 eV and efficiencies above 25%.[282,284,290,306,307] An outstanding representative example is the demonstration of 29.15%-efficient monolithic perovskite/Si tandem with $Cs_{0.05}(FA_{0.77}\ MA_{0.23})_{0.95}\ Pb(I_{0.77}\ Br_{0.23})_3$ absorber having a bandgap of 1.68 eV.[282] The bandgap adjustment was enabled by controlling the Br/I ratio with 23% Br. Considering the most recent record in perovskite single junction SC with PCE ≈ 25.2% (corresponding to ≈80% of the bandgap-related thermodynamic limit),[228,229] a tremendous boost of perovskite/Si tandem performance can be expected in the near future aiming to surpass the single junction S–Q limit.

Moreover, the bandgap tuning is even relevant for industry-compatible perovskite/Si integration. For instance, a bandgap enlargement by 0.02 eV is needed when using industrially-relevant 100 µm-thick Czochralski (CZ) textured c-Si instead of typical 280 µm-thick planarized float-zone (FZ) c-Si.[308]

Challenges and Prospects of Tandem SC Technologies: The above-mentioned progress status and demonstrated potential of bandgap tuning capabilities in multijunction PV can further promote the technology readiness toward the industrial manufacturing.

In the PV community, the choice of the most advantageous multijunction SC technology is still under debate.[278] Nevertheless, it is speculated that the demonstrated performances of III–V/Si perovskite/Si and perovskite/perovskite multi-junction SC technologies would valorize their expediency as potential candidates for industrialization.[278,286,302] A general requirement for all tandem PV technologies is the upscaling from cell fabrication to module integration. Hence, depending on the number of terminals and the tandem design, special attention should be devoted to the selection of the upscaling approach that ensures the appropriate interconnection between tandem cells in strings and modules with minimal optical and resistive losses.[302] Since multijunction technologies can cause more complications in the fabrication process and rising costs, it is important that their delivered power throughputs exceed those of their single junction counterparts. From an industrial and commercial point of view, tandem PV can be uniquely more advantageous than conventional single junction technologies, if the disproportion in levelized cost of electricity (LCOE) is further reduced.[309–311] This can only be achieved by reaching even higher efficiencies and power densities in W m^{-2} than state-of-the-art single junctions PV while sustaining cheaper costs of materials and processes in \$ W^{-1}.[278,309] Currently, this is one of the major obstacles for the integration of tandem PV technologies in urban and residential applications.[302] However, novel developed materials and concept innovations are expected to further reduce the fabrication cost and promote the economic competitiveness of tandem technologies, with regard to conventional single junction counterparts.[310,312] To reach an acceptable commercial deployment standards, tandem technology should retain around 80% of the initial efficiency after 25 years.[302,313] Therefore, further outdoor and long-term reliability testing, as well as lifetime energy yield assessments are required to justify the economic viability.[313]

To tackle this challenge, research work has been devoted to investigate the stability of tandem PV technologies. Especially perovskite/Si are known to suffer from degradation issues.[313,314] As an example for the stability assessment, it was demonstrated that 26.7%-efficient perovskite/Si tandem SC with a top bandgap of ≈1.7 eV preserves more than 80% of its initial PCE after 1000 h of continuous illumination.[307] According to the estimation of Blakers and co-workers on perovskite/Si tandem SC, a top cell degradation between 0.9% and 1.3% can be allowed in a realistic degradation scenario to retain 80% of the initial power in a tandem module after 25 years.[313] De Wolf and co-workers investigated the outdoor performance of a stable perovskite/silicon tandem SCs for a week in a hot and sunny climate, where the PV device temperature exceeded 60 °C under direct sunlight.[315] This induced an opposite trend in the evolution of bandgap as a function of temperature for both subcell with a narrowing of c-Si and broadening of the perovskite. Then, the optimal bandgap of the perovskite top cell is altered in a range below 1.68 eV for field performance at operational temperatures.[315]

One can deduct from all the research progress and technological development in the field of multijunction PV that the bandgap tunability is a key factor in defining the solar-to-electricity conversion efficiencies as well as the outdoor performance at high temperatures.

Given the above-described status and progress in the field of tandem PV, it is projected that these features are not only attractive for the common space and concentrator applications, but also suitable for the integration into utility scale installations, residential applications and PV-powered vehicles. This would further raise the solar electricity capacity as one of the world's major energy sources.

3.3. Static Color Tuning in Opaque and Semitransparent Solar Cells

In this section, the focus is devoted to static color tuning capabilities for different opaque and semitransparent SCs technologies in reflection and transmission modes. A broad overview on different colorful opaque and semitransparent PV technologies is beyond the scope of this work, however, in this regard the reader can refer to further relevant reviews.[21,53,91]

3.3.1. Opaque Colored Solar Cell Technologies

As presented in Section 2.2.1, different external and internal modification strategies are relevant for coloring opaque SCs.

External Design Strategies: Bläsi et al. introduced an industrial-compatible photonic color concept inspired from the Morpho-butterfly on a cover glass of 1 m^2 modules. They achieved saturated blue, green and red colors with homogeneous appearance for all angles of incidence (**Figure 6**a). The power performance of test PV module was >94% power compared to a black reference one.[316] Guo and co-workers presented a five-layered trans-reflective color filter on the top of c-Si solar panel (Figure 6b).[317] This approach resulted in vivid colors due to distinctive narrowband reflection (≈60% peak reflection) with an angle-invariant appearance up to ±60°. The transmitted light was utilized in the SCs and could yield a high PCE of ≈13.9% corresponding to a decrease of only ≈3.9% compared to the initial c-Si panel.[317] Although it seems counterintuitive from a PV perspective, even white-colored modules can be realized. Interferential selective filters on a textured glass allow diffused reflection of the complete visible spectrum. The remaining infrared light is transmitted to silicon heterojunction SCs for power conversion. This concept yielded efficiencies above 10% corresponding to about 40% power loss compared to the standard counterpart.[318] Jolissaint et al. reported on so-called Kromatix solar modules following a similar approach with ≈7% power loss.[100]

Colored and white solar glass technologies with photonic multilayer coatings deposited by vacuum techniques are widely used and commercially available by different BIPV companies such as ISSOL,[319] Solaxess,[320] SwissINSO.[321]

Multilayer dielectric mirrors are also exploited in the coloring of thin film PV. As an example, exploiting a nonperiodic SiO_2/TiO_2 multi-nanolayer filter, Yoo et al. showed colorful PSCs with PCE up to 18.9%.[322] Colored thin-film CIGS PV modules with high aesthetic standards were also developed by AVANCIS using homogeneous structural color filter on glass surfaces.[323] In spite of the complex process and elevated cost, dielectric filters can achieve pure colors with angular insensitivity, glare suppression and high long-term durability. To enable more than a single color, it is possible to customize the appearance of SCs by implementing an interlayer with printed predefined pattern between the glass cover and SCs.[324–326] Similar customized design schemes with multi-colored patterns are already available and provided by PV compagnies like Kameleon Solar.[327]

On the use of pigments or dyes for painting the glass cover or interlayer encapsulation sheet, Slooff et al. showed a wide range of colors. Furthermore, they demonstrated the possibility of customized patterns by print technology with minimized power efficiency drop.[325] The printing technology is simple and relatively inexpensive. However, long-term degradation in real environment is still questionable.[21,325] Recently, Bae et al. demonstrated colored PSCs using liquid cholesteric helicoidal superstructures.[328] This approach allows easy color tuning through the modulation of the chiral dopant content, birefringence of the host liquid and the optical design respectively. An example of the compatibility of painting technology at industrialization level is colored PV using ceramic screen printing provided by Onyx Solar.[329]

Kutter et al. reported a comparative study between colored encapsulants, ceramic printed glass covers and spectral-selective photonic structures in terms of power loss, color appearance, and cost.[333] They pointed out that structural filters provide stronger color saturation and better electrical performance (–3% to –7%) than colored encapsulants (–6% to –31%). Furthermore, they showed, that the manufacturing prices of decorated BIPV modules (74–163 € m^{-2}) are in a similar range with standard cladding materials, such as bricks (60–100 € m^{-2}).[333]

Another external coloration approach that can be easily integrated and is particularly compatible with traditional c-Si is via antireflection coating (ARC). These dielectric thin films (oxide, nitride, sulfide, and others) are directly applied on the surface of c-Si SC. They are generally designed to eliminate the reflectance in the range between 600 and 700 nm leading to intrinsic black or dark blue color.[21] However, by tuning the thickness and the refractive index of the thin films in the ARC, various colors can be achieved due to the manipulation of the spectral reflectance. Many successful demonstrations of stable and low-loss colored c-Si PV modules by means of ARC have been rep orted.[91,330,334,335] On research level, Ding et al. showed tunable high-saturated colors throughout the visual spectrum with coordinate positions near the edges of the chromaticity diagram (Figure 6c). They employed MgF_2/ZnS ARC with different thicknesses on graphene/c-Si heterojunction SC.[330] Different colored SC devices yielded PCE values in the range 10.7–13.2%. Also, such stylish coloring approach is adopted by some PV companies like LOF Solar Corp.[336]

Internal Design Strategies: Regarding the internal design strategies, different functional components within SC device can also enable coloring. Primarily, the photoactive materials themselves can allow color tuning via structural morphology control or bandgap change. One of the representative works in this regard was reported by Ding et al. utilizing a nanostructured perovskite photoactive layer as a reflection grating (Figure 6d).[106] Such transformation was made possible by utilizing a combination of a hundred-micrometer sized large domain structure and a concentric ring photonic nanostructures. The cells with PCE of about 12% displayed a heterogeneous mixture of iridescent colors with a wide distribution of reflective hues instead of single pure color. A representative example of color adjustment via bandgap tuning in perovskite was shown by Cui et al. through the control of chemical composition from $MAPbI_3$ (dark brown), $MAPbBrI_2$ (dark red), $MAPbBr_2I$ (red), to $MAPbBr_3$ (orange). The corresponding efficiencies are 12.76%, 6.84%, 4.12%, and 3.53% respectively.[337]

Within the carrier transport layers, the creation of color can be obtained by the integration of post-tinting nanostructures and precisely designed photonic crystals.[66,108,338] In this context, Snaith and co-workers unveiled the first exploration of colorful PSCs employing a porous photonic crystal scaffold TiO_2/SiO_2 with alternating layers (Figure 6e).[66] This yielded PCE values ranging from 4.5% to 8.8% and tunable structural colors across the visible spectrum. However, it imposed additional fabrication steps.

For the coloration through the transparent electrode, the widely used method is the spectral engineering of the optical interference in microcavities composed of metal-dielectric-metal.[109] The variation of the dielectric thickness

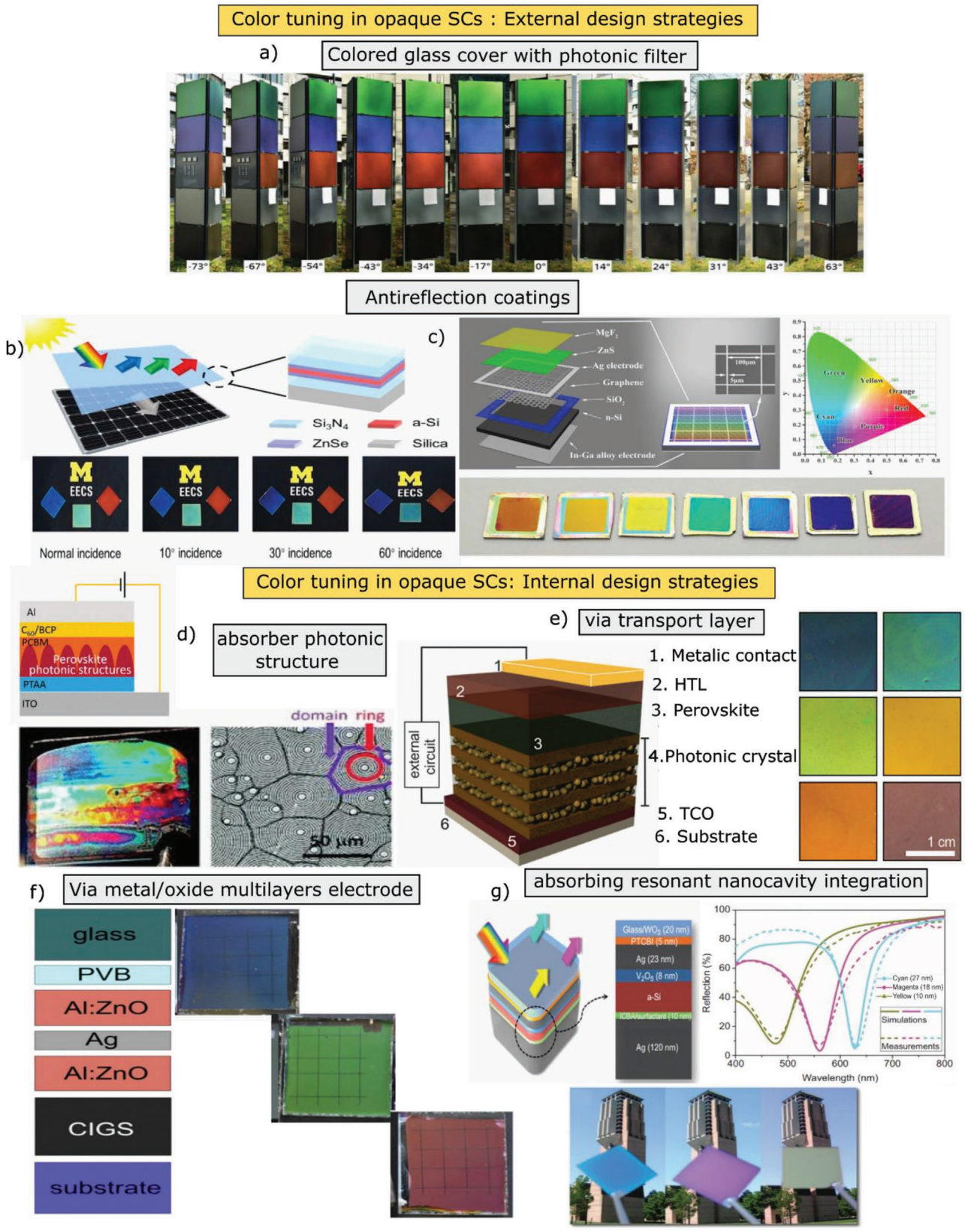

Figure 6. a) Series of photographs of colored demonstrator modules, taken from 12 different azimuth angles (73° left to 63° right). Reproduced under terms of the CC-BY license.[316] Copyright 2021, The Authors. Published by IEEE. b) Schematic diagram of colored SCs via angular-robust trans-reflective filter atop consisting of five layers with high index a-Si sandwiched between two stacks of dielectrics (top) Photos of fabricated RGB colored

corresponding to the cavity length leads to different resonance conditions enabling color tuning.[110,111] As a representative example, Neugebohrn et al. suggested a substitution of standard transparent front TCO in CIGS modules with an oxide/metal/oxide (OMO) multilayer. The OMO acted as both an electrode and as a coloring layer. (Figure 6f).[331] The color tuning is achieved by simply varying the thickness of the oxide layers which alter the reflected spectrum and hence the color of PV modules. An improved electrode with the implementation of a wetting layer enabled a PCE of about 13%.[339] Stimulated by the pioneering work of Kats, Capasso and co-workers on strong interference effects in highly lossy media,[80,340] many relevant demonstrations of decorative PV based on optical absorbing resonant nanocavity have been realized. Lee et al. showed a colored ultrathin PV with subwavelength a-Si absorber below 30 nm embedded between two reflective metal electrodes (Figure 6g).[332] Tunable colors with high angular stability were generated by varying a-Si thickness due different resonance conditions. Although the advantage of ultrathin layers and lower material consumption, such a concept still suffer from low efficiency level about only 3%.

Challenges and Prospects: A general point to consider for all color tuning strategies is that the human eye is more sensitive to some specific colors than others. For instance, this means that in practice for a green SC a less intense reflection is needed compared to a red cell with equal luminosity.[222] All the above-mentioned internal and external approaches differ in terms of the ability to generate vivid and distinctive color, the color tunability, the angle sensitivity, the induced PCE losses, the scalability, and the process fabrication complexity.[53]

To this end, despite the multitude of coloring solutions provided by scientific research, only cost-effective and industry-compatible engineered optical structures are sufficiently competitive to reach a commercialization level. This is the case for the established market of external colored solar glass technology with high versatility for traditional PV as well as ARC coloring for Si PV. We believe that structural color filter technologies compatible with the fabrication process of SCs can have a potential niche market, especially for decorative emerging thin film PV like perovskite. Moreover, each company usually offers a unique color palette and different set of techniques. Therefore, the establishment of standard solutions would further contribute to a more widespread application of colorful PV modules. This will promote their aesthetic integration in the underutilized exterior elements of buildings and vehicles.

3.3.2. Semitransparent Colored Solar Cell Technologies

Similar to the opaque coloring technologies, semi-transparent SCs can also be tuned to show vivid coloration. Again, both external and internal design strategies can be applied to achieve coloration.

External Design Strategies: The two main concepts to achieve external coloration are multilayer dielectric mirrors and LSC technologies. By incorporating dielectric mirrors, Quiroz et al. developed colorful semitransparent PSCs.[341] As the coloring structure and the cell device are mechanically stacked and electrically decoupled, a multitude of combinations can be easily realized. For different colored ST-PSC, a variation of PCE between 4% and 4.3%, and AVT between 12% and 28% was achieved, relative to a pristine cell with a PCE = 3.6% and AVT = 46%. Lee et al. presented a semitransparent PSC with dielectric multilayer mirror on the back side consisting of alternating TiO_2 and SiO_2 layers (**Figure 7**a).[97] The coloring was controlled with the number of dielectric layers. However, the color appearance was also dependent on the angle of incidence and the observer's angle. Overall, an efficiency of 10% was achieved.

Another well-established technique to reach coloration while maintaining high transparency are LSCs, due to the ability of absorption and reemission at longer wavelengths in luminophores. (Figure 7b). This allows for a high variability in coloration and design methods, which are described in detail in other reviews.[342,343] Meinardi et al. discussed the control of color with different type and amount of chromophores embedded in the waveguide.[344] Several research works presented semitransparent colored LSC based on QDs and conjugated polymers, for coupling with PV.[91,345–349]

Internal Design Strategies: The thickness of the transparent electrodes can be adjusted to achieve colorful semitransparent SCs. Jiang et al. showed that changing the thickness of a PEDOT:PSS electrode between 48 and 160 nm allowed a wide range of color in semitransparent PSC (Figure 7c).[350] The thickness of the electrode layer influenced also the electric performance, where thinner layers resulted in lower FF. Overall, efficiencies between 11.6% for a 48 nm PEDOT:PSS layer and 15.4% for a 160 nm-thick layer were achieved. Wang et al. presented a bifacial semitransparent PSC with color tunability due to thickness variations of the ITO electrode (40–320 nm) and the copper thicyanate hole-transport layer (20–220 nm). They showed that the change of color resulted in a variation of efficiency between 10.6% and 13.3%. Li and co-workers

samples under ambient light illumination taken with a black background at four different viewing angles (bottom) Reproduced with permission.[317] Copyright 2019, The Royal Society of Chemistry. c) Schematic illustration of colored Gr/Si heterojunction SCs with MgF_2/ZnS double ARC layer. Inset shows the SEM image of the Ag grid mesh (left). Photographs of Gr/Si heterojunction solar cells (device area: 1 cm^2) with different colors. (bottom) Coordinates of seven colors in CIE chromaticity.(right) Reproduced with permission.[330] Copyright 2018, Elsevier. d) Illustration of colorful perovskite SC device structure (top). Photographs of colorful device with a front aluminum electrode under 1-sun illumination (left). Plane view SEM image of colorful perovskite film showing the polygon domains and concentric ring structure in each domain (right). Reproduced with permission.[106] Copyright 2015, The Royal Society of Chemistry. e) Schematic of photonic-crystal-based perovskite solar cell. (left) Colors from blue to red displayed by devices integrating different photonic-crystals. (right) Adapted with permission.[66] Copyright 2015, American Chemical Society. f) Schematic CIGS with oxide/metal/oxide multilayers electrode (left). Photographs of blue, green and red colored CIGS solar cells. (right) Adapted with permission.[331] Copyright 2019, Elsevier. g) Device structure of ultrathin a-Si/organic hybrid solar cells with decorative colors (top left). Reflection spectra of colored devices with varied a-Si thicknesses (cyan-27 nm), (Magenta-18 nm) yellow-10 nm) at normal incidence. (top-right) Photograph of solar cell devices reflecting colors (bottom). Reproduced with permission.[332] Copyright 2014, Springer Nature.

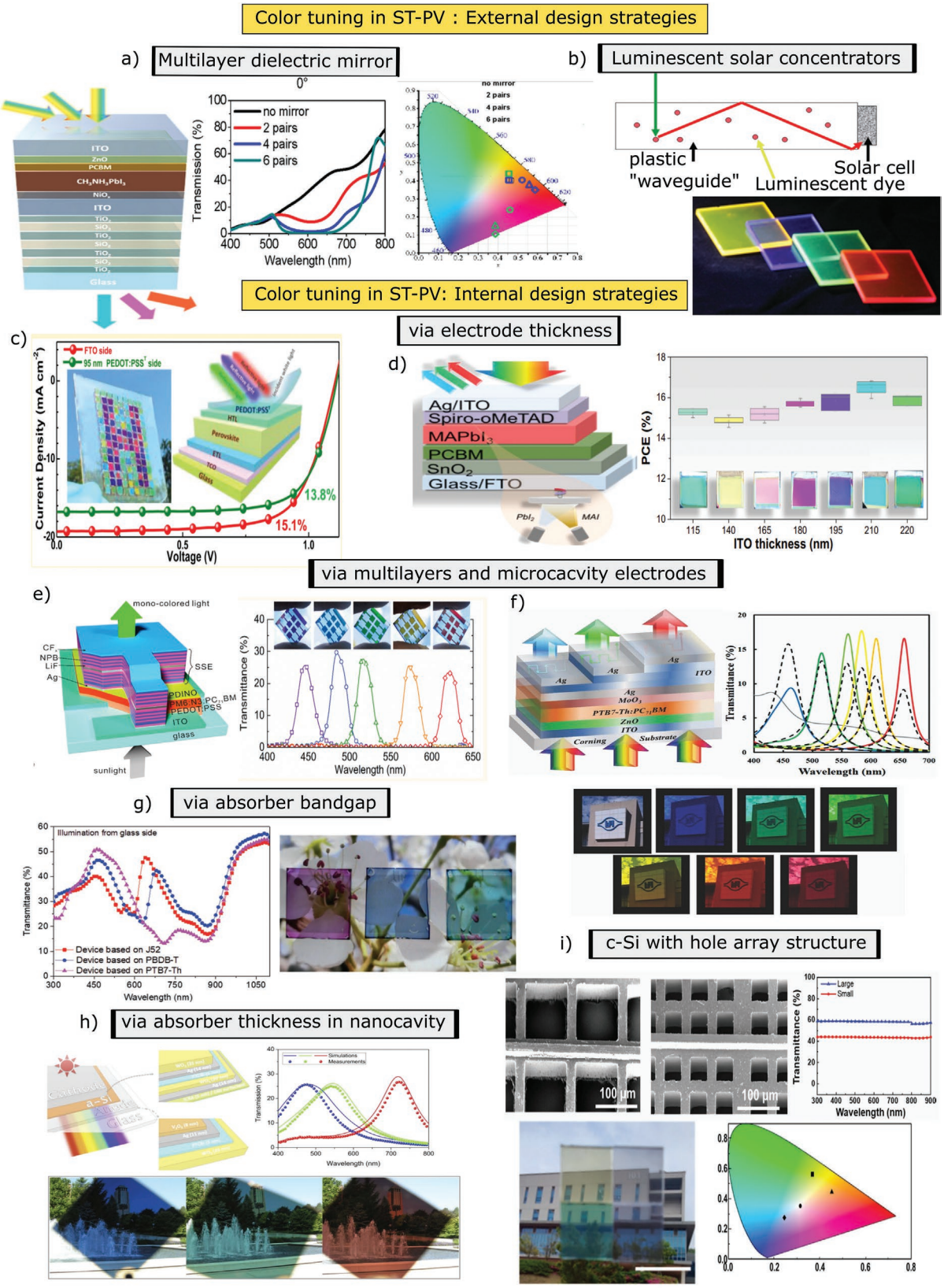

Figure 7. a) Schematic of semitransparent colored perovskite SC with multilayer dielectric mirror. (left) Transmission spectra of devices with different numbers of multilayer pairs at incidence angle (middle). Color coordinates in the chromaticity diagram for different colored SCs. Reproduced with permission.[97] Copyright 2017, The Royal Society of Chemistry. b) Illustration of light incidence (green arrow) and reemission at longer wavelength

also tuned the ITO thickness in semitransparent PSC and showed different colors with efficiencies between 15% and 17% (Figure 7d).[110] To further refine the coloration, more complex structures such a multilayers and microcavities can be implemented as electrodes. This allows for a broader range of colors with high purity. Wang et al demonstrated a complex multilayer structure consisting as back spectrally selective electrode. This resulted in tunable narrow transmission peaks at selected wavelengths from violet to red, with high color purity close to 100% (Figure 7e).[351] The semitransparent OSCs achieved efficiencies between 14% and 15%, and peak transmittance between 23% and 30%. A microcavity concept consisting of ITO sandwiched between metallic silver layers was developed by Lu et al. as electrode material for semitransparent OSCs (Figure 7f).[352] The obtained PCE were ranged between 8.2% for yellow-green and 7.2% for red colored semitransparent SCs, compared to 9%-efficient opaque SC. While, the peak transmittance levels at specific color were between 14% and 18%.

Besides the electrode layers, the absorber layer can also be varied in order to achieve a color appearance of transmitted light. Cui et al. demonstrated that the organic photoactive material of a semitransparent OSC can be blended with different polymer donors which result in a strong coloration of the system (Figure 7g).[353] The different donors changed the resulting absorption spectra and thereby altered the spectrum of transmitted light. PCEs between 3% and 7% were obtained with high AVT of above 30%. Lee et al. demonstrated semitransparent colored ultrathin a-Si/organic hybrid SC incorporated as an optical absorbing nanocavity (Figure 7h).[354] The variation of the a-Si nanoabsorber thickness between 6 and 31 nm resulted in controlled transmitted colors with low angular sensitivity up to angles of 70°. Such concept yielded peak transmittance around 30%, but, suffered from low PCE of about 3%. Similarly, color tuning can be realized by optimizing the multilayer interferences in colloidal QD semitransparent SC.[356]

Recently, Kang et al. demonstrated perforated semitransparent c-Si SC with periodic hole structure, yielding high AVT between 45% and 60% (Figure 7i).[355] The color of the SCs was tuned between blue, green, and yellow, by adding different organic dyes into the PDMS matrix on top of the device. The resulting efficiencies for different colors were around 7%.

Challenges and Prospects: Colored semitransparent SCs can be realized by a multitude of external and internal design strategies. The main technical evaluation criteria include color tunability, purity, visible transparency, and PV performance. Most of the adopted coloring method are well-established at research level, with high aesthetic quality. However, simple, cost-effective, and fabrication-compatible approaches are desired for large-scale integrations. In this context, among the different coloration approaches, color tuning by changing the transparent electrode thickness is estimated to be the most suitable and straightforward method without requiring additional fabrication steps. In particular, organic and perovskite-based thin-film SCs technologies are prominent candidates for colored transparent PV, featuring outstanding efficiencies, excellent visible transparency and vivid colors. Overall, the upscaling of colored semitransparent PV technologies would promote their application in urban façades with architectural design.

3.4. Static Transparency Tuning in Semitransparent and Transparent Solar Cells

In this section, state-of-the ST-PV and TPV technologies are presented and the main technical specifications of transparency tuning are discussed.

3.4.1. Non-Wavelength-Semitransparent PV

Color Neutrality Bottleneck in ST-PV: In practice, non-wavelength selective PV with thinned absorbers often characterized by unfavorable brownish or yellowish tint depending on the spectral absorption. Wheeler et al. analyzed the color appearance of ST-PV with continuous spectral absorption.[55] It was concluded that for all AVT values with varying the thickness and the bandgap (E_g = 0.3 − 4 eV) of a thin-film absorbers, the occupation in the CIE chromaticity diagram was located between yellow, orange, and red.[55] Hence, the coordinates for neutral grey (x, y) = (0.33, 0.34) known as a popular choice for architectural aesthetic are never reached for thinned absorber PV technologies (**Figure 8**a).[55] Moreover, the bandgap variation changes the x and y components and hence affects the coloration for different AVT levels. For AVT < 30%, ideal-bandgap absorbers, corresponding to maximum PCE for each visible

(red arrow) in luminescent solar concentrator. (top) Photograph of different colored semitransparent luminescent solar concentrators illuminated by ultraviolet light. (bottom) Reproduced with permission.[342] Copyright 2012, Wiley-VCH. c) Device architecture of colored cells with PEDOT:PSST as the top spectrally selective electrode. Photograph of a colored schematic "H" assembled by colorful perovskite SC. *J–V* curves of the blue-colored cell illuminated from both side glass (PCE = 15.1%) and electrode sides (PCE = 13.8%). Reproduced with permission.[350] Copyright 2016, American Chemical Society. d) Schematic of semitransparent colored perovskite SC architecture. (left) PCE of different semitransparent colored SCs as a function of the ITO electrode thickness, determining the color appearance. (right) In the inset, photographs of the ST-PSCs in the corresponding position of ITO thickness. Reproduced with permission.[110] Copyright 2020, Elsevier. e) Device architecture schemeatic of semitransparent colored organic SC with spectrally selective electrode. (left) corresponding digital photographs and transmission spectra of various colored devices (right) Reproduced with permission.[351] Copyright 2020, American Chemical Society. f) Schematic representation of the microcavity-based organic SC. (left) Transmittance spectra of different SC devices. (right) Digital images of colorful semitransparent SC devices from blue to red. (bottom) Reproduced with permission.[352] Copyright 2018, Wiley-VCH. g) Transmission spectra and photograph of semitransparent colored organic SCs with three different polymer donors. Reproduced with permission.[353] Copyright 2017, Wiley. h) Schematic device structure, transmission spectra and photographs of colored ultrathin hybrid a-Si/organic featuring absorbing nanocavity. The colors correspond to different a-Si thicknesses (blue-6 nm), (green-11 nm), and (red-31 nm). Reproduced with permission.[354] Copyright 2014, Springer Nature. i) SEM picture of Si solar cell with hole structures for 60% and 45% transparency (top left) Corresponding transmittance spectra (top right) Photos of yellow, green and blue PDMS-encapsulated semitransparent colored Si SCs and corresponding color coordinates (bottom). Reproduced with permission.[355] Copyright 2021, Wiley-VCH.

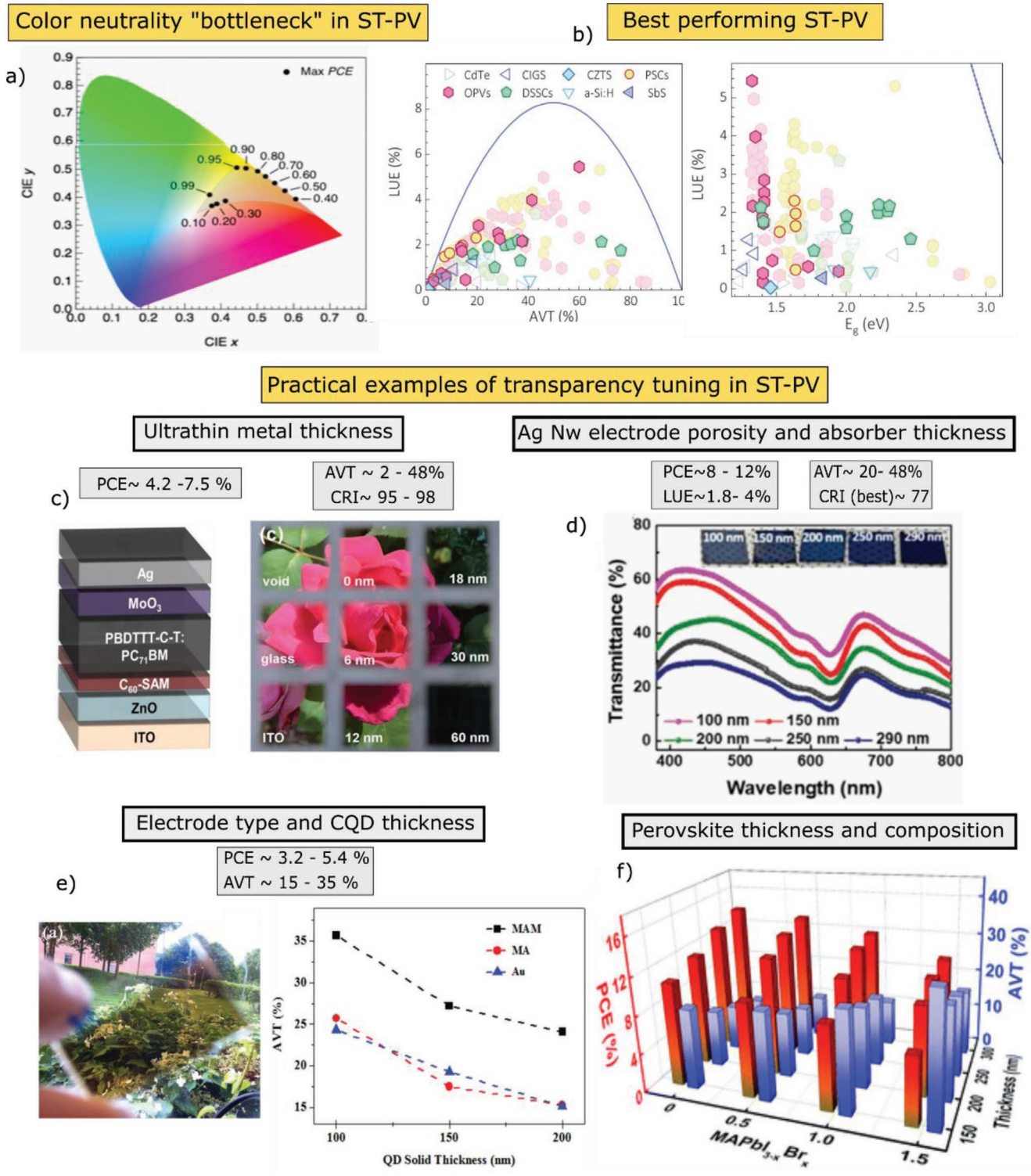

Figure 8. a) CIE Chromaticity plot of achievable color range by ST-PV with thinned absorber. Reproduced with permission.[55] Copyright 2019, American Chemical Society. b) Experimental results of best performing ST-PV in terms of AVT vs LUE (left) and LUE vs E_g (right). Continuous lines correspond to the theoretical limit of LUE. Reproduced with permission.[51] Copyright 2021 Wiley-VCH. c) Structure ST-PV device based on organic absorber. (left) Photograph of devices with different Ag electrode thicknesses. Reproduced with permission.[68] Copyright 2012, The Royal Society of Chemistry. d) Dependence of transmission spectra on the absorber thickness in ST-OSC with Ag nanowire-based electrode. Reproduced with permission.[360] Copyright 2021 Wiley-VCH. e) Photograph of ST-PV with colloidal quantum dot absorber and oxide/metal/oxide electrode. (left) Dependence of AVT on the thickness of CQD solid for different types of back electrodes. (right) Reproduced with permission.[363] Copyright 2016, Wiley-VCH. f) 3D histogram plot of PCE and AVT variation as a function of perovskite composition and thickness. Reproduced with permission.[104] Copyright 2018, The Royal Society of Chemistry.

light transmittance (VLT) are less sensitive to coloration. However, as the bandgap exceeds the ideal value, hues of orange and red are expected to appear. When the AVT is higher than 30%, the x and y components of ideal-bandgap absorbers are away from the neutral-color coordinates and hence prone to high coloration aspect from orange to yellow as AVT increases.

State-of-the-Art ST-PV with Tunable Transparency: In Figure 8b, the state-of-art efficiencies for different organic and inorganic PV technologies are shown. The reported AVT values for ST-PV are ranged from ≈5% for different thin-film PV technologies to above 85% for a near-infrared luminescent concentrator architecture.[51,357] However, in the case of ST-PV, the light transmission is inherently promoted at the expense of the photogenerated current, hence, the drop in the PCE is inevitable.[20,55]

In practice, the interplay between AVT and PCE give rises to LUE values that the lowest are around 0% for different thin-film PV technologies and the highest exceed >5% for perovskite and organic PV technologies.[51,358,359] Regarding the bandgap dependency, it is noticed that low-bandgap photoactive materials result in higher LUE levels, especially for organic and perovskite PV technologies with superior performance compared to other counterparts. While higher bandgaps yield lower LUE values due to poor PCE.

In the following, several outstanding examples for ST-PV using different approaches to tune the transparency are presented. Chen et al. demonstrated an organic ST-PV with high color rendering index and efficiencies between 4.2% and 7.5%.[68] The high CRI value between 95 and 98 were achieved by the optical shaping of the transmitted spectra with ultra-thin Ag layers (Figure 8c). The thickness change of the Ag layer allowed to adjust the AVT of the ST-PV between 48% and 2%. Jeong et al. combined organic ST-PV with Ag nanowire electrodes to reach high transparency and electrical conductivity (Figure 8d).[360] By varying the porosity of Ag Nw from 10% to 60%, PCE was changed from 4.2% to 9.7% with AVT values around 43%. Whereas, the variation of the thickness of organic absorber layers yielded more significant tuning capabilities, with adjusted PC from 8% to 12% and AVT between 20% and 48%. The best achieved CRI was about 77 (Figure 8d). Baran and co-workers demonstrated a record ST-PV cell based on organic absorbers with a PCE of 8.8% and an AVT value of 58% resulting in an outstanding LUE of 5.26%.[358] ST-PV based on ultrathin a-Si absorber enabled PCE about 6% with low AVT around 20% and red-brown tint.[361] Shin et al. tuned the transparency of CIGS-based semitransparent SC, by adjusting the absorber thickness between 300 and 900 nm.[362] Using the thinnest absorber, low AVT of 9% and a PCE of 9.78% was achieved. The transmission spectrum was dominated by the absorption edge of the CIGS layer, leading to characteristic coloration. Zhang et al. investigated the interplay of the colloidal QD solid thickness and the electrode type on the PCE and AVT outputs (Figure 8e).[363] The increase of the QD thickness from 100 nm to 200 nm resulted in a reduction of AVT by almost 10% for different electrodes i.e metal, metal/oxide and oxide/metal/oxide. This was accompanied by an increase of the PCE from 3% to >5%. In a similar concept, the introduction of TeO_2 antireflection capping layer in semitransparent colloidal QD SC enabled an efficiency of 7.3% with AVT of 20.4%.[364] Lee et al. employed different thin metal top electrodes using Ag and Cu for ST-PSC. The brown-tinted devices were characterized by PCE high than 11% and AVT of ≈20%[365] Yuan et al. established a general trade-off between AVT and PCE as a function of the thickness and composition of $MAPbI_{3-x}Br_x$ perovskite absorber (Figure 8f).[104] For a fixed thickness, an increase of Br content with wider bandgaps leads to higher AVT, but slightly lower PCE. The combination of moderate absorber thickness (≈200 nm) with wide bandgap conditions perovskite absorber are more advantageous for ST–PSC, reaching an AVT ≈20% and PCE of about 8%.

Roy et al. analyzed the color comfort and degradation of semitransparent DSSC after 2 years of ambient exposure by evaluating CRI and CCT parameters. It was found that while AVT slightly dropped, the visual comfort was enhanced by ≈30% which promotes the possible utilization of such technology for low-power building integration in hot weathers.[366]

Challenges and Prospects: The most common practices for light transmission tuning mainly involve the change of the absorber and the electrode thicknesses. Among different thin-film ST-PV, perovskite, and organic-based SC technologies yield better trade-off between AVT and PCE, and hence, higher LUE. A balance between high efficiency, long-term stability, and cost-effective manufacturing is demanded to ensure the feasibility for real-world applications.[367]

Besides the suitability of organic materials for semitransparent PV,[368] further progress in the development of inexpensive upscaling methods,[369,370] the improvement of device lifetime[44,371] is still required for reliable lab-to-fab transfer. Similarly, for perovskite-based ST-PV, the transition from lab-scale SC devices to module scale impose the employment of deposition techniques such as blade coating, slot-die coating, roll-to-toll methods and printing.[231] In addition, large-scale modularization without sacrificing performance[372] and appropriate stability assessment[373] should be ensured. Currently, several semitransparent PV technologies are under development by industrial manufacturers, such as semitransparent organic PV with transparent mesh electrodes from ASCA[374] and semitransparent perovskite PV from Saule technologies.[375]

The presented examples of ST-PV show that color neutrality can be assumed as a bottleneck for ST-PV that prone to unfavorable tint. To overcome this issue, spatial segmentation and wavelength-selective photosensitivity are rather the alternative solutions. For practical purposes, most of the light-transmitting structure like skylight or windows in buildings and vehicles require the highest AVT alongside color-neutrality aspect. Hence, ST-PV are more likely to find application in most of the building skin and façade areas for aesthetic appearance purpose.

3.4.2. Wavelength-Selective and Neutral-Colored Transparent PV

Wavelength-Selective Transparent PV: As shown in Section 2, well-defined optical material properties and spectral engineering are prerequisite for the realization of wavelength-selective TPV. In this section, the progress, strategies and potentials of UV and NIR-selective transparent PV technologies are reported. For UV-selective PV, the blue-shifting of the absorption edge outside of

the visible spectrum to maximize AVT and CRI is typically performed exploiting wide-bandgap semiconductors such as metal oxides (NiO, ZnO...), QDs, organic or perovskite photoactive materials. In metal oxide-based UV-selective PV, typically with p-type NiO/n-type ZnO heterojunction configuration deposited by physical vacuum deposition techniques, the bandgap range can be varied between 2.7 eV (≈460 nm) and above 3.2 eV (≈387 nm). Upon illumination with AM1.5G spectrum, PCEs below 0.5% and AVT values between ≈50% and 70% are obtained.[60,61] For TPV based on TiO_2/NiO heterojunction, an optimum TiO_2 thickness of 100 nm was found to give the best trade-off between optical transparency and electrical performance.[376] Using such metal oxide materials system, the bandgap control is crucial to preserve high CRI and AVT for the case of absorption limit above 440 nm, as well as, preventing the photocurrent and performance deterioration for absorption onset below 430 nm.[59] The incorporation of ultrathin a-Si between p-NiO and n-ZnO could improve the carrier collection and light utilization efficiency at specific wavelengths.[379] But, lower AVT about 40% and PCE below 0.5% were obtained on a PV device with a size of 25 cm^2.[380] UV-selective TPV was also realized using green carbon QDs, reaching only a PCE of about 0.6% and an AVT of 37%.[63] Additionally, near-ultraviolet SCs based on wide-bandgap polyaromatic hydrocarbons organic pairs yields a V_{oc} exceeding 1.6 V and PCE between 1.3% and 1.5% with an AVT above 60%, supplying sufficient power for electrochromic smart window.[62] Lunt and co-workers initiated the exploration of halide perovskite in selective UV-harvesting TPV devices in 2018, by precisely adjusting the absorption onset between 410 and 440 nm.[59] This bandgap widening is enabled via compositional control of $MAPbCl_{3-x}$ Br_x replacing the big halide with small ones (I > Br > Cl). The demonstrated TPV devices deliver a PCE up to 0.52% with an AVT of 73% and an outstanding CRI over 93%.[59] A step forward for this lead halide-based TPV technology was achieved by further optimizing the thickness and the composition and tuning the bandgap via chlorine and bromine doping. The devices reach efficiencies over 1% with AVT above 70%.and CRI above 90, while retaining 80% of the initial performance after 150 h and over 60% after 500.[377] (**Figure 9**a) Selective ultraviolet (UV)-harvesting visibly transparent photovoltaics can be also realized using $CsPbCl_3$ with an absorption edge of ≈420 nm, resulting in an efficiency of 1.19%, and a CRI of 91, but, suffer from moderate AVT of 53.1%.[381]

Another approach to realize colorless TPV is the adoption of concepts with NIR-harvesting from the long-wavelength side of the solar spectrum using low-bandgap polymer donors and small molecular acceptors as organic photoactive materials.[64,65] A proof-of-concept of NIR-selective organic TPV was realized in 2011, featuring peak absorption beyond 650 nm. Combined with near-infrared mirror ensuring optical-interference, the device enables a PCE of 1.3% and AVT above 65%.[382] Then, subsequent research works have been developed, aiming for IR absorption by narrowing the bandgap between LUMO and HOMO from above 1.4 to <1.1 eV, then, further take advantage of the large fraction (≈52%) of the solar photon flux in the infrared. The reported results give rise to peak absorptions between 700 and 900 nm, cutoff absorption range 780–1100 nm, PCE 2.6% and 5.3%, wide span of AVT range between 25% and 63% with a clear PCE-AVT trade-off while CRI could reach extremely high values up to 97%.[64] As a representative example of this TPV category is the realization of semitransparent SC based on Thienylbenzodithiophene-Diketopyrrolopyrrole PBDTT-DPP (donor):PCBM (acceptor) heterojunction absorber embedded between two transparent electrodes. Such device yields a PCE of 4% and a high AVT of 64%.[383] The incorporation of incorporating large size selenium in PBDTT-DPP polymer donor photoactive material to form PBDTT-SeDPP which strengthen the interchain interaction and reduce the bandgap. The TPV devices with AgNW-based composite electrode result in a peak absorption at 810 nm a cutoff at 900 nm yielding a PCE of 4.6% and an average light transmission of 63%.[384]

For the case of small molecular acceptors, multiple small bandgap photoactive materials can meet the requirements for NIR-absorbing TPV.[64] However, non-fullerene small-molecular acceptors are preferred compared to fullerene counterparts to further narrow the bandgap.[65] Such enhancement of NIR-harvesting by combining both narrow-bandgap polymer donors and non-fullerene small molecular acceptors as organic photoactive materials boosts the performance level of organic TPV with efficiencies exceeding 7%. One of the first examples in this category was the incorporation of chlorine atoms in the electron-donating benzodithiophene (BT) to form BT-CIC. This reduces the bandgap below 1.3 eV and sets the absorption cutoff to 950 nm due to improvement of the intramolecular charge transfer and interactions. Using ultrathin Ag back contact, the semitransparent SCs achieve a PCE of about 7%, AVT of 43%, and CRI of 91.[385] Subsequently, many successful demonstrations of highly performing organic TPV based on non-fullerene small-molecular acceptors have been reported. For example, the integration of fused octacylic electron acceptor (FOIC) based on fused tris(thienothiophene) (3TT) in semitransparent SC leads to an absorption range between 600 and 950 nm with a peak at 836 nm, a low bandgap of 1.32 eV, a PCEs of up to 10.3%. Using transparent ITO as electrode for NIR-absorbing narrow bandgap nonfullerene acceptor enabled device output parameters as follow: PCE ≈ 8%, AVT ≈ 43%, LUE ≈ 3.5% and CRI of 86%. While the same device using ultrathin metal electrode yielded a slightly green-tinted ST-PV with PCE ≈ 10.8%, AVT ≈ 45%, and LUE ≈ 5%.[386] This points out the importance of the electrode selection in defining the optoelectronic trade-off. For NIR-DSSC, Sauvage and co-workers reported a relevant device having a PCE of 3.1% power conversion efficiency, an AVT up to 76%, and a CRI of 92.1%.[387]

One of the highest color-fidelity CRI in organic TPV approaching 100% was achieved on a neutral-color semitransparent SC with IHIC non-fullerene acceptor with strong NIR absorption assigned to an optical band gap of 1.38 eV, reaching a PCE of 9.3% and an AVT 21% (Figure 9b).[388] Outdoor testing of vertically positioned NIR- non-fullerene acceptor based organic semitransparent SC featuring 1D nanophotonic structure reveals a PCE of 9.7% and an AVT of 50% over a wide range of incidence angle up to 50°.[378]

Interestingly, it is possible to design a semitransparent PV featuring tandem structure with a combination of both UV and NIR selective photoactive materials. Such approach was realized by Zuo et al. using large-bandgap perovskite film ($FAPbBr_{2.43}Cl_{0.57}$, E_g ≈ 2.36 eV) as UV-selective absorber in the

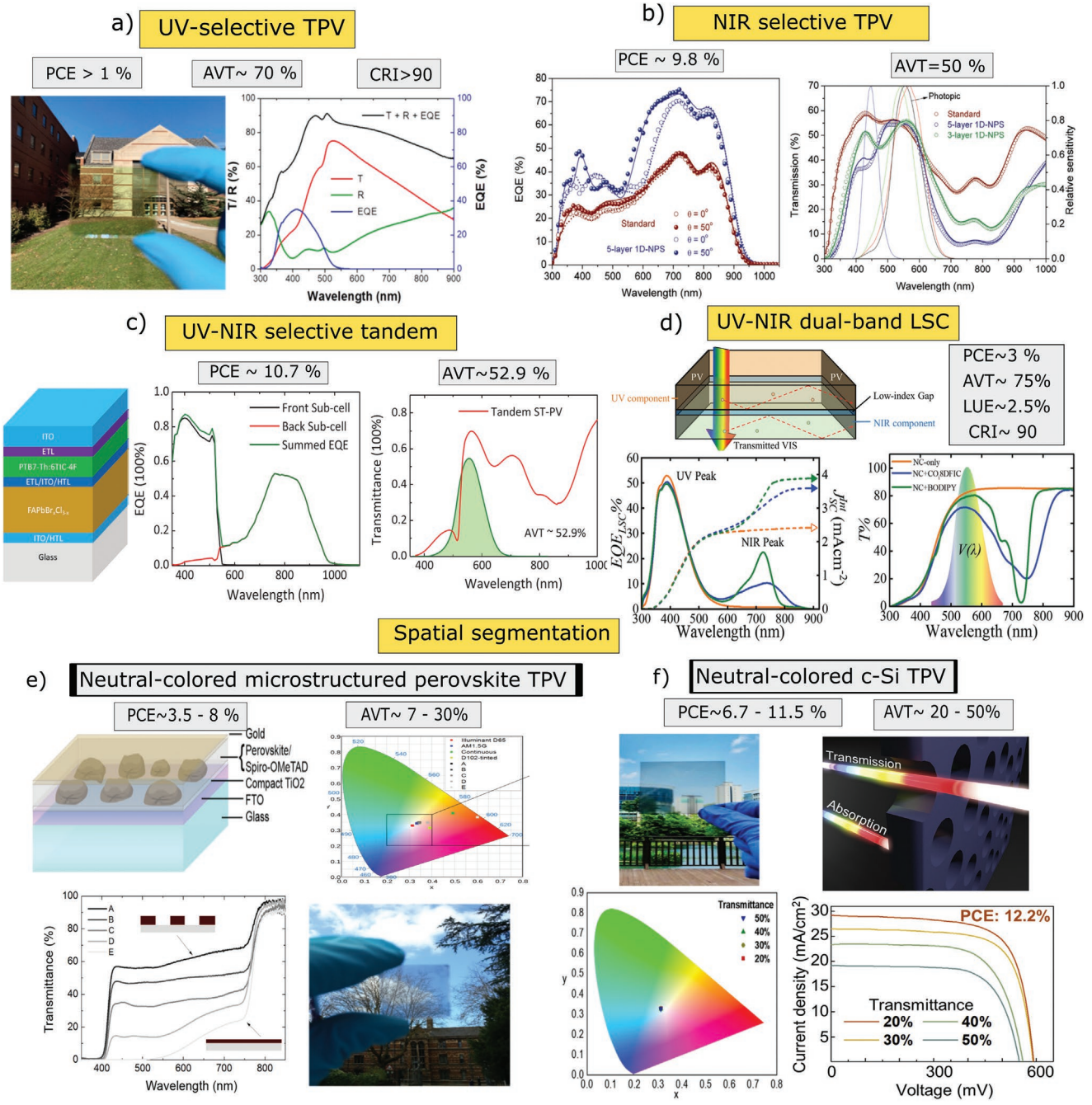

Figure 9. a) Photograph of fully assembled lead halide TPV device and corresponding transmission (T), reflection (R), and external quantum efficiency (EQE) spectra. Reproduced with permission.[377] Copyright 2019, American Chemical Society. b) Experimental and simulated EQE spectra of ST-OSC cells with and without nanophotonic structures at normal and at 50° incidence (left). Experimental and simulated light transmission spectra of ST-OSC cells with and without nanophotonic structures at normal incidence (right). The photopic curves are also depicted. Reproduced with permission.[378] Copyright 2020, Wiley-VCH. c) Design structure, EQE and transmission spectra of tandem ST-PV with selective absorption. Reproduced with permission.[359] Copyright 2019, Wiley-VCH. d) Schematic of dual-band selective harvesting transparent LSC. (top) Average EQE(λ) spectra of different transparent LSCs and the corresponding integrated short-circuit current density ($J_{SC\,Int}$) (bottom left) Transmittance spectra ($T(\lambda)$) of different transparent LSCs. Normalized photopic response of the human eye ($V(\lambda)$) is visualized for comparison. (bottom right) Reproduced with permission.[221] Copyright 2021, Wiley-VCH. e) Schematic of dewed planar perovskite heterojunction SC (top left) Transmittance spectra from a selection of dewed perovskite devices. Illustration of the most and least transparent films are shown as inset. (top right) Color coordinates of perovskite films with different transmittance level under AM1.5 illumination, on the CIE *xy* 1931 chromaticity diagram (bottom left) Photograph of semitransparent neutral-colored perovskite. (bottom right) Reproduced with permission.[107] Copyright 2014, American Chemical Society. f) Illustration of the neutral-colored transparent c-Si substrate showing light transmission (in all wavelength ranges) through the hole-shaped window and light harvesting in the absorption region (top) Color coordinates of the transparent c-Si SCs with different transmittances on the CIE 1931 chromaticity diagram. (bottom left) Illuminated *J*–*V* characteristics of the transparent c-Si SCs with different transmittance levels (bottom right) Reproduced with permission.[57] Copyright 2020, Elsevier.

top cell and low-bandgap (PTB7-Th:6TIV–4F, $E_g \approx 1.27$ eV) as NIR-selective absorber in the bottom subcell (Figure 9c).[359] Such concept provides a PCE of 10.7% and AVT of ≈53%, as one of the highest LUE in wavelength-selective TPV, pointing out the great potentials of tandem UV/NIR selective SC technology. Based on this brief overview about UV and NIR selective transparent PV, it is obvious that an impressive progress is fulfilled in terms of photoactive materials and device performance. This should be pursued along with the development of advanced transparent electrodes and light management schemes as well as the minimization of the visible absorption to preserve ultrahigh color neutrality. To this end, one can conclude that UV- and NIR-selective TPV are effective technologies not only for power generation in smart windows into buildings and vehicles, but also for the protection from UV and NIR radiations.[389]

Luminescent Solar Concentrator: A promising approach for see-through applications is the utilization of luminescent solar concentrators. Different LSC technologies based on various materials such organic or QDs were reported in literature.[112,221,390,391] Meinardi et al. reported the first example of LSC based on indirect-bandgap Si QDs with an area of 144 cm^2 reaching a PCE of 2.85% and 70% transmittance over the visible spectrum.[112] Klimov and co-workers proposed a large-area (>230 cm^2) tandem LSC based on two types of engineered colloidal QDs fluorophores. Owing to the exceptional spectral tunability, an optimum spectrum splitting is achieved, allowing a PCE of 3.1%.[391] By integrating NIR-emitting $CuInS_2$/ZnS QDs into 10 cm × 10 cm laminated glass LSC device, Bergren et al realized a PCE between 2.2% and 2.9% with a transmission of ≈44% for visible light. Recently, an outstanding achievement was reported by Lunt's group combining massive-downshifting phosphorescent nanoclusters as UV-luminophore and fluorescent organic molecules as NIR-luminophores into a dual-band selective-absorbing transparent LSC (Figure 9d).[221] This concept allowed a well-defined spectral selectivity and efficient harvesting of invisible light fractions. The device outputs reached PCE over 3%, AVT beyond 75%, and CRI of about 90%. It was reported that these achieved results are the highest for transparent LSC technologies up-to-date that surpass the practical limit of non-wavelength selective counterparts.[221]

LSC technology can provide good aesthetic and optical characteristics. However, several issues are still facing their widespread integration. The low efficiency and the performance drop at large-scale are among the main drawbacks.[91] Moreover, the reabsorption losses of reemitted light during waveguide mode are detrimental for the light concentration and the power generation.[392] Hence, the development of new materials with high quantum yield and large Stokes shift (the difference between the absorption and emission peaks of the luminophore), is required to minimize the reabsorption losses.[17] It was estimated that an increase of the Stokes shift >100 nm could enable LSC sizes in the range of 1 m^2, which is a target scale for the integration in versatile applications.[393] The key materials and the technological challenges facing the development and the industrialization of LSC were summarized elsewhere.[220] For a reliable assessment of LSC-PV performance, standardized characterization protocols should be adopted.[394] To this end, the demonstrated potential of visibly transparent LSC technologies in terms of power throughput, aesthetic standards and unique spectral tuning promote their seamless customization for window industry. The achieved progress in the field of LSC would enable further adaptation to multifunctional deployment in diverse applications.[343] This will be accelerated with the progress at industrial level, providing commercially available PV products such as QD-based LSC from UbiQD and ClearVue PV.

Spatial Segmentation: Another strategy to achieve color-neutral transparency is via spatial segmentation. The state-of-art of this technology has been thoroughly presented in several related reviews.[17,20,21] Spatial segmentation method can be applied to a large variety of PV technologies including c-Si based SCs and thin-film PVs. On the latter category, this strategy is typically applied for conventional second-generation thin-film PV including a-Si, CIGS, and CdTe.[17,20,21] This is due to the compatibility of relevant perforation process by laser ablation with the interconnexion scheme at the modularization level. For different kind of materials like perovskite and organic, the spatial segmentation can be achieved during the growth process at microscale. One of the most distinguished examples in perovskite field was the realization of color-neutral ST-PV based on microstructured perovskite material via morphological control.[107] Due to the spontaneous dewetting perovskite islands are formed enabling considerable light transmission in between spaces (Figure 9e). The color neutrality is ensured by the synergy between the complete absorption and transmission for different AVT levels as can be noticed in the chromaticity diagram. Whereas, the transparency can be tuned through the modification of the surface coverage. This leads to a modulation of AVT between 3.5% and 8% attributed to PCE between 7 and 30%.[107] Adopting similar approach and replacing methylammonium lead iodide perovskite with formamidinium lead iodide a 5.2%-efficient neutral-colored PV device with an AVT of 28% was reported.[395] This kind of spatial segmentation via morphological control could be a potential alternative with material consumption and simply feasibility features.

Typically, spatial segmentation of c-Si is performed by means of mechanical or laser cutting.[20,21] The use of thick standard c-Si substrate and the complexity of the removal processes are technological and economical drawbacks of this method, albeit their good performance. An array of thinner, miniaturized and spaced c-Si cells would be more techno-economically viable in this regard.[396]

An impressive spatial segmentation approach to achieve colorless transparent c-Si PV was reported by Lee et al. through precisely-designed microhole-shaped light transmission window array(Figure 9f).[57] By defining the filling fraction design a systematic tuning of the light transmission is enabled. A controlled modulation of AVT from 20% to 50% yields a progressive increment in PCE from 6.7% to 11.5%. Despite the outstanding throughput relative to others thin-film PV technologies, the use of a combination of photolithography and dry etching processes impose cost and compatibility issues for the industrialization of this technology.

Overall, the multitude of demonstrated high-efficient and neutral-colored PV technologies offer a wide choice of integration schemes into PV windows for both electricity generation and visual comfort purposes. We believe that LSC-PV

and UV–NIR selective TPV technologies with cost-effective and scalable fabrication methods are closest to the large-scale manufacturing and commercialization level, provided they meet the requirements of the involved stakeholders and customers' acceptance.

3.5. Dynamic Tuning of Transparency and Colors in Switchable Solar Cells

The transmission and color appearance of SCs can also be modulated dynamically in a reversible way using several techniques. It was described in Section 2.2.3 that the implementation of switching mechanisms at different positions inside and outside of the SC can lead to switchable PV with adjustable transparency or tinting. In this section, the technological approaches to stat-of-the art dynamically switchable SCs are presented.

3.5.1. Electrochromic Switching

The first realized devices share an electrode between a dye-sensitized SC and an electrochromic component to initiate optical switching on the absorption of light.[397] These so-called photoelectrochromic windows only convert enough solar energy to power the switchable device. Hereby, a reversible change of color was achieved due to electrochromic WO_3. More than ten years later, other publications presented photovoltachromic devices which were able to generated more electricity than required for switching.[398] Cannavale et al. studied for the first time photovoltachromic devices with semitransparent perovskite layers.[119] They achieved an average visible transmittance of 26% in transparent state and of 16% in colored state. The PCE was switched between 3.7% and 5.5%. The same group later also presented a switchable DSSC with micropatterned electrode. The power conversion efficiency of the photoelectrochromic device with DSSC was 1.84% for 1 sun illumination but the transmittance at 650 nm wavelength could be switched between 21% and 52%. The combination of a UV-harvesting OSC with an electrochromic switching mechanism was presented by Davy et al.[62] A photograph of the switching between colored and bleached states of electrochromic window powered by UV-selective OSC can be seen in **Figure 10**a. The transparency was switched between 10% and 55% at a wavelength of 650 nm. The switching was powered by a 1.3–1.5% PCE solar cell. Dyer et al. presented a vertically integrated electrochromic layer sandwiched between two polymer SCs.[399] While bleaching of the device was reached under forward bias conditions, the switchable window was colored under reverse bias. The device is also a net positive energy device, meaning that besides the optical modulation of the transparency additional electricity can be generated. The change in transmittance at 550 nm was 20% under illumination of 1 sun, while the PCE remained below 1%. Switching was initiated by selectively connecting the electrodes in the device.

Besides the combination of PV with electrochromic devices, liquid crystal systems were also studied. Hereby the polarization dependent switching of scattering and transmission of chiral nematic liquid crystals under different potentials is used. Xia et al. presented the combination of a semi-transparent PSC with a liquid crystal/polymer composite.[400] The roll-to-roll process compatible device achieved a switchable AVT of 11% and a PCE up to 16.6%. Previously presented self-powered switchable SCs with liquid crystal technology used the diffusive scattering of electrically tunable polymer dispersed liquid crystals coupled at the back electrode to enhance the absorption in an ultra-thin a-Si SC.[140] This allows a transition from transmissive to diffusive tinted states. The device showed a switchable transmittance at 650 nm between 40% and 70%, while the power conversion efficiency varied between 1.9% and 3.2%. The switching required a power of 0.8 mW cm^{-2} (Figure 10b). Kwon et al. analyzed the influence of the position of optically switchable photo-responsive chiral nematic liquid crystals on the efficiency and transparency of a DSSC.[129] They were able to achieve a maximum PCE of 7.9%, when the switchable liquid crystals were deposited below the bottom electrode of the device.

All the mentioned technologies partially used the electricity generated by the photovoltaic layers to change the transmission of the switchable SC. This means that for all of these devices, the switching capability depends on sufficient irradiation of the sun. Several other studies try to decouple the change of transparency from the illumination of the photoactive layers. One possible route to achieve this purpose is the use of gasochromic layers.

3.5.2. Gasochromic Switching

Yao et al. show that the combination of a semi-transparent polymer SC with a 120 nm-thick gasochromic WO_3 layer as a back reflector created a smart window with adjustable coloration and transparency.[122] The power conversion efficiency in blue-colored state is 10.2% with an average visible transmittance of 25.4 %. In bleached/transparent state, the efficiency decreases to 9.1% and the transmittance increases to 33.8%. A similar approach was demonstrated with a semi-transparent a-Ge:H SC featuring a switchable Mg back electrode of below 30 nm (Figure 10c,d).[126] The SC device reached 2.4 % efficiency in opaque state with 1% transmittance. The average visible transmittance was increased to 23.6% after the absorption of hydrogen.[401] Since the Mg layer in this approach is not only used as switchable layer but also as back electrode, switching influences the electrical performance, and turned the SC "off" during hydrogen absorption.

3.5.3. Photochromic Switching

A completely different approach of switchable SCs depending on the exterior illumination was proposed by Huaulmé et al. using photochromic organic absorber molecules (Figure 10e).[128] They created transparent DSSC with a photochromic diphenyl-naphthopyran unit inserted between donor and acceptor which turned into a deeply colored state upon illumination.[128] They were able to achieve an efficiency of 4.17%. The average visible transparency changed from 59%

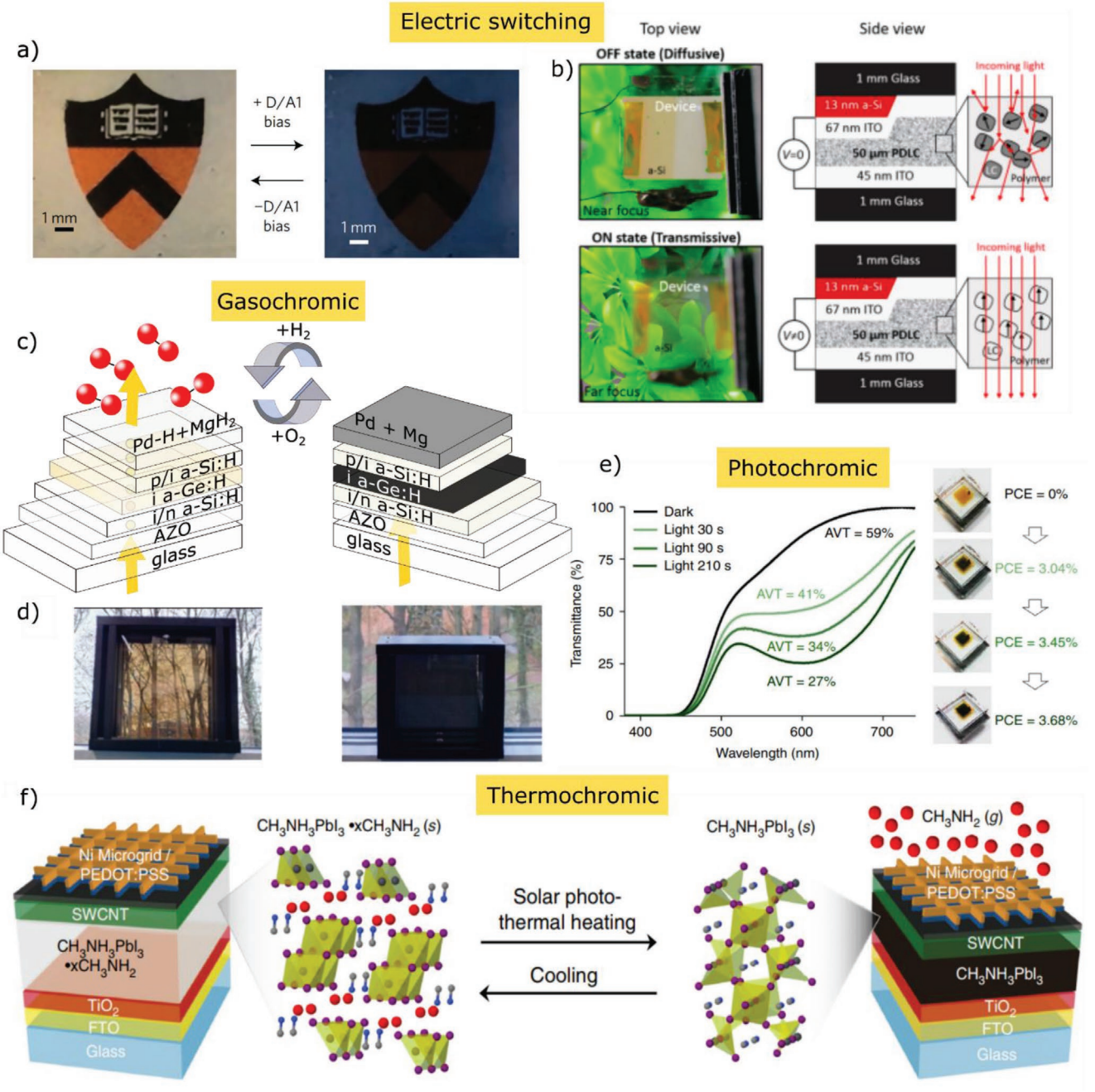

Figure 10. a) Photograph of the colored and bleached states of the electrochromic window powered by a UV-selective organic solar cell. Reproduced with permission[62] Copyright 2017, Springer Nature. b) Ultra-thin semi-transparent a-Si solar cell with liquid crystal switchable back contact. Photograph in opaque and transparent states (left), layer stack with a-Si and liquid crystals (right). Reproduced with permission.[140] Copyright 2017, American Chemical Society. c) Dynamic optical switching based on gasochromic Mg back electrode in ultrathin a-Ge:H solar cell. Adapted with permission.[123] Copyright 2020, American Chemical Society. d) Photograph of gasochromic solar cell in transparent state (left) and in opaque state (right). Reproduced with permission.[24] Copyright 2022, Elsevier. e) Photochromic switching: transmission spectrum and photograph of photochromic solar cells under different illumination conditions. Reproduced with permission.[128] Copyright 2020, Springer Nature. f) Schematic structure of thermochromic halide perovskite solar cell and illustration of complex dissociation in perovskite material. Reproduced under terms of the CC-BY license.[139] Copyright 2020, The Authors. Published by Springer Nature.

before illumination to 27% after illumination. It is important to mention that this technology integrates the switching mechanism directly into the absorber layer, opposed to the previous mentioned approaches, where the tuning functionality was achieved by additional layers or by functional electrodes.

3.5.4. Thermochromic Switching

Currently, one of the most active researched subgroup of switchable PV windows is thermochromic devices. These solar cells use the photothermal dissociation of halide perovskites as

a way to change the absorptivity of the photoactive layer and with it, the transparency. Lin et al. showed that the reversible transition of inorganic halide perovskite layers between a transparent non-perovskite phase and a colored perovskite phase can be used to create a smart photovoltaic window.[133] The required temperature to initiate the phase transition is 105 °C. At low temperatures the device reaches a visible transparency of 81.7%, while in colored state after reaching the high temperature, the visible transparency is decreased to 35.4%. The efficiency of the SC in colored state is 5.57%.

Wheeler et al. used a similar approach, shown in Figure 10f, where photothermal heating under illumination by the sun triggers the dissociation of methylamine to switch a SC from a transparent state with 68 % visible transmittance to a colored state with <3% transmittance. The power conversion efficiency in colored state is 11.3%. The change of the perovskite structure and the resulting change in optical properties was also used to create opaque SCs with changeable coloration.[136] Hereby, any transparency is omitted and the color impression results from the reflection and absorption of light.

3.5.5. Challenges and Outlooks of Dynamically Switchable SCs

All of the presented technologies aim to overcome the disadvantages of static SCs by dynamically adjusting the transparency of the window to the exterior conditions. While in early devices the SC only generated electricity to promote self-powered switching of an electrochromic layer, the latest generation of switchable photovoltaics is able to generate a surplus in electricity. Furthermore, switching technologies evolved to photochromic, thermochromic and gasochromic layers allowing for a more flexible application of the photovoltaic windows. An important issue for all switching technologies is the degradation of the device after several switching cycles. For switchable SCs, this degradation can be seen in the reduction of the maximum possible transmitted light, or in the reduction of power conversion efficiency or even both. This is a result of the switching processes not being fully reversible. While for gasochromic SC only up to 15 cycles of switching were shown without significant degradation,[122] electrochromic devices reach several thousand switching cycles without degradation.[402] Thermochromic perovskite layers have shown to withstand several hundreds of switching cycles.[139] This shows that further development and optimization is still necessary for all switchable SCs to become a replacement for current windows. Besides the degradation of the SCs, the implementation of the device in a building is also still difficult to realize. Gasochromic switching systems might require an external gas source to initiate the switching, which would also require gas pipes in the façade. Thermochromic SCs need high temperatures to change their transparency, which can be problematic in colder climatic regions, or when heat load should be avoided in the glazing elements. The color neutrality of switchable solar windows is also crucial for widespread acceptance of the technology. Hereby, especially the PSC with a red tint and the switching layers incorporating WO_3 require further improvement. The color portfolio is rather limited in dynamic tuning schemes compared to static tuning approaches. Furthermore, for all technologies the switching time is a crucial factor which has to be considered, since slow switching can have a detrimental effect on the acceptance of this technology. In conclusion, SCs with switchable transparency can be a valuable replacement of conventional windows but still need more research to fulfill their promise. Based on the presented potential of switching approaches, it is estimated that the integration of dynamic and reversible optical tuning in photovoltaic windows can allow an exceptional control over the power generation, the lightening, the heat regulation and the energy savings for buildings and vehicles.

3.6. Thermal Tuning and Temperature Regulation in Solar Cells

3.6.1. Optics-Based Thermal Tuning Approaches of PV

As stated in Section 2.4.1, multispectral thermal management of PV can be fulfilled by the implementation of UV and sub-bandgap reflection (SBR) methods to reduce the generation of waste heat and passive radiative cooling (PRC) concepts to boost the rejection of waste heat. The implication of each of these approaches is manifested in different wavelength ranges, that is, in the solar spectrum band from 0.3 to 2.5 μm for the UV and sub-bandgap reflection, and in the atmospheric transmittance window from 8–13 μm for PRC (**Figure 11**a). The theoretical maximum reduction of temperature is attributed to an ideal filter with cutoff at the absorber bandgap E_g for spectrally selective coolers and unity IR emissivity for radiative cooler.[169]

Herein, we survey the effectiveness of these two main spectral tuning approaches for the reduction of the operating temperature and the energy yield enhancement of SC. This would allow a better adaptation for PV integration in multiple applications and environments. Sun et al. suggested that appropriate design of selective-spectral cooling, combining both the exclusion of parasitic absorption via SBR and efficient radiative cooling via improved thermal emission, can reduce the temperature of terrestrial solar modules by up to 10 °C. This corresponds to ≈2.7% improvement of the short-term electricity output and 0.5% absolute increase in the efficiency of solar modules. Since SBR and PRC approaches tackle different self-heating sources, their simultaneous integration is expected to yield a superposed temperature reduction for all PV technologies.[169] Detailed quantitative evaluations and comparisons of both SBR and PRC heat mitigation strategies were addressed in literature.[87,171] In practice, spectral-selective cooling via SBR can be achieved by adding specifically designed photonic structures or quarter-wave stacks as infrared optical filters on the top of SCs. Such selective mirrors serve as short-pass filters that only permit the penetration of photons with energies above the absorber bandgap.[82,169]

3.6.2. Sub-Bandgap Reflection in PV

In a comprehensive photonic approach for SC cooling, Fan and co-workers proposed a photonic cooler made of multilayer dielectric stack of SiO_2, SiN_x, Al_2O_3, and TiO_2 films.[82] This 1D photonic structure can simultaneously allow strong heat

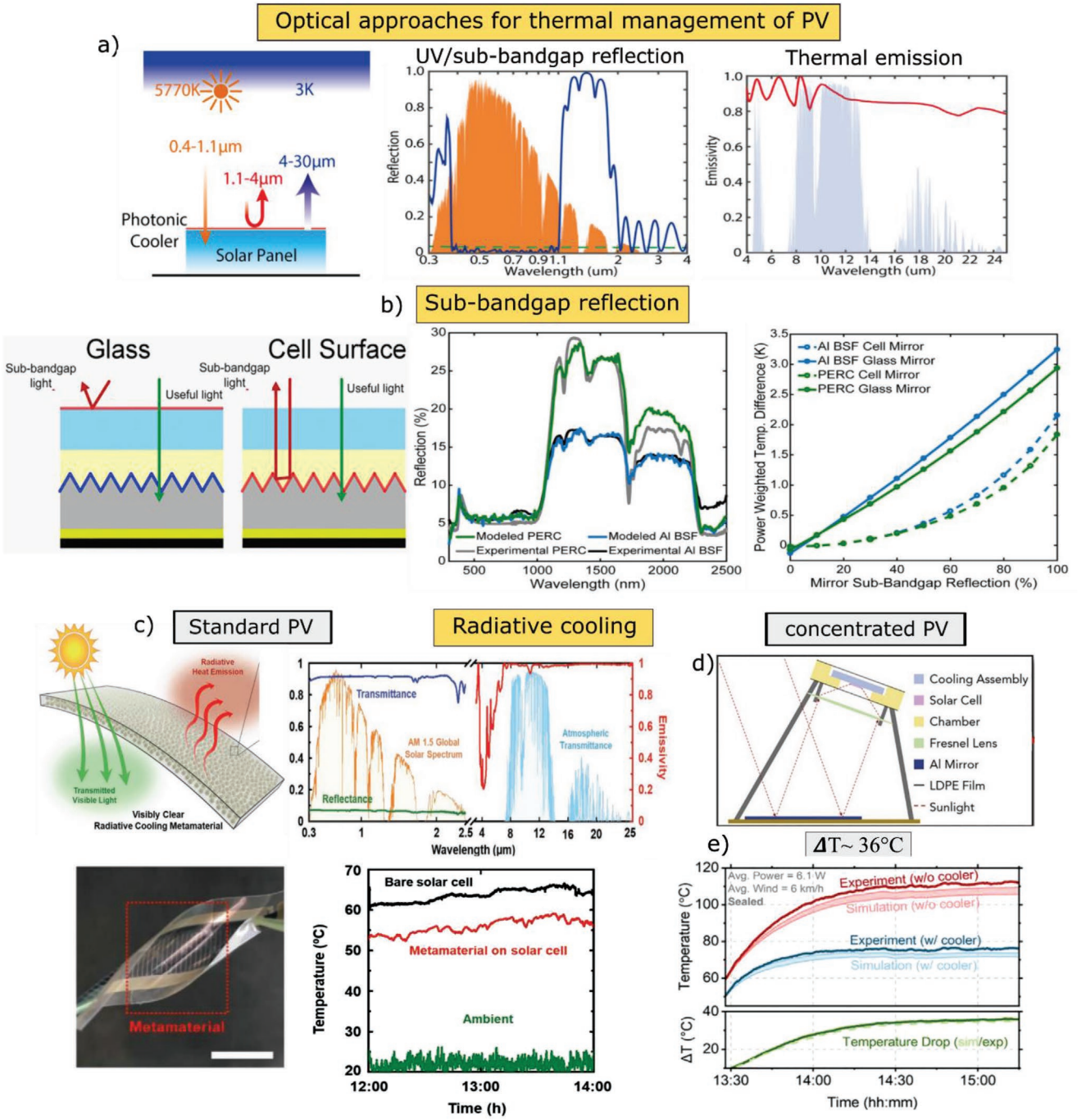

Figure 11. a) Schematic of solar absorption and thermal radiation properties with a photonic cooler coated on top of solar panel (left) Reflection spectrum of photonic cooler (middle) Emissivity spectra of the photonic cooler over IR wavelengths (right) Reproduced with permission.[82] Copyright 2017, American Chemical Society. b) Spectrally selective mirrors placed at the outer glass or at the cell surface. (left) Experimental and modeled spectral reflection for considered PV technologies. (right) Power-weighted average module operating temperature difference from the baseline case including spectrally selective mirrors at the glass or at the cell surface.(right) Reproduced with permission.[175] Copyright 2021, Elsevier. c) Radiative cooling for standard PV. Schematic illustration and working principle of visibly clear metamaterials for radiative cooling. (top left) Photographs showing the metamaterials with visible clarity and mechanical flexibilities attached on a flexible organic SC (bottom left) Measured transmittance and reflectance in the AM1.5 Global (1.5G) solar spectrum and emissivity in the atmospheric transmittance window for radiative cooler metamaterial. (top right) Temperature variations for ambient, metamaterial on a solar cell, and a control bare solar cell in outdoor conditions under solar irradiation (bottom right). Reproduced with permission.[403] Copyright 2021, Wiley-VCH. d) Illustration of concentrated PV system with Fresnel lens concentrators and an enclosure. The radiative cooler can be added to the heat spreader underneath the solar cell. Reproduced with permission.[404] Copyright 2020, Elsevier. e) Experimental and simulated temperature results with and without cooler for the evaluation of daytime passive radiative cooling performance. Reproduced with permission.[404] Copyright 2020, Elsevier.

radiation by mid-IR thermal emission and effectively reflect the UV and sub-bandgap wavelengths (Figure 11a). In particular, to achieve large solar reflection over the sub-band-gap wavelength range, constituent materials with large index contrast were employed. In order to simplify the complexity of spectrally selective mirrors, Ferry's group performed several design optimizations of a series of multilayer photonic sub-bandgap mirrors based on various materials including SiO_2, SiN_x, TiO_2, ZrO_2, and MgF_2.[173,174] A special interest was devoted to the angular dependence and geographical location. By integrating sub-bandgap photonic reflector on the outside of the glass cover, an enhancement in the annual energy output over 3.7% can be achieved compared to the baseline without a photonic mirror.[173] To assess effectiveness of parasitic light reflection method as a function of different PV module technologies, Silverman et al. compared the dependence of temperature reduction between c-Si and GaAs modules.[87] It was found that c-Si module achieved an annual irradiance-weighted temperature reduction of 3.8 K, while GaAs PV operated at 12 K cooler temperature level under the same conditions. This is influenced by the difference in sub-bandgap reflectivity, temperature coefficient and efficiency.[87] Slauch et al. established a comprehensive guide on the optical approach based on the rejection of incident sub-band-gap light for thermal management.[175] By including various reflectors and stutterers at different interfaces within PV modules, the practical limits of temperature reduction in operation under outdoor conditions are determined as a function of sub-bandgap reflectivity and reflective interface (Figure 11b). It was found that integrated sub-bandgap reflective mirrors on the outer glass or rear side are the most effective. For instance, a reduction of about 3.3 K annual power-weighted average temperature can be achieved by means of spectrally selective mirror at the top glass surface of c-Si module if the sub-bandgap reflection reaches 100%.[175] It is also important to consider the difference in the bandgap decrease evolution as a function of temperature between different absorbers, expressed by different temperature coefficients. Hence, the cut-off of spectrally selective filters needs to be designed according to the temperature dependence of the bandgap, especially for concentrated PV.[169]

3.6.3. Passive Radiative Cooling of PV

The other main approach for heat mitigation of SCs is passive radiative cooling. The emergence of PRC concepts has stimulated numerous reports to present overview about the integration of this technology in PV.[177,181,185,405,406] It is important to mention that different antireflection coatings on bare silicon SCs, and, in particular, glass covers with large amount of silica in standard solar panels already possess a considerable emissivity level.[86,185,187,407] However, highly efficient IR emitter alternatives are desired, not only to further boost the radiative cooling performance, but also to be adaptable with flexible, lightweight PV technologies, and in concentrated PV and extraterrestrial environments such as space. To fulfill this aim, various IR emitter structures can be employed such as nanophotonic structure, metamaterials, and polymer layers. Given that solar modules operate typically above ambient temperatures, broadband emitters are more favorable than selective emitters, since thermal emission outside the sky window in the entire wavelength range between 4 and 30 μm can provide additional radiative cooling power.[82]

After their pioneering works in this field,[180] Fan, Raman and co-workers explored the untapped passive daytime radiative cooling of SCs through sky window.[170] They expected that an ideal scheme can passively lower the operating temperature by 18.3 K cooler than bare SC. One of the outstanding representative works on photonic cooler is performed by Li et al. who proposed photonic films with strong heat radiation via thermal emission.[82] For optimal thermal management, tailored transmission and reflection characteristics required strict design considerations in the alternating layers of Al_2O_3/SiN/TiO_2/SiN with aperiodic arrangement of thickness. Upon the integration of such photonic cooler on the top surface, a temperature reduction of 5.7 °C is achieved on underlying encapsulated solar panels without affecting the solar absorption and the generated photocurrent.[82]

Zhao et al. proposed a radiative cooling approach via selective plate composed of photonic structure.[408] The latter was made of 1D stack composed of 30 periodic SiO_2/TiO_2 multilayers and 2D photonic crystal consisting of 500 μm-thick silica with a specific circular lattice array. The achieved nocturnal cooling power of 128.5 W m^{-2} at 303 K outperformed the case of bare cell and glass surface by 6.9% and 30.5%, respectively.[408]

To avoid the burden of designing complex and expensive photonic structures that rely on vacuum deposition equipment and sophisticated patterning techniques, IR emissive polymers present a simple, practical and cost-effective alternative.[409–412] The origin of IR emission from polymers responsible for radiative cooling capabilities is the overlap of the fingerprint region of the intrinsic functional groups such as C—O, C—F, C—N, and Si—O in infrared spectrum with the atmospheric transmittance window.[413] Hence, this offers a promising pathway to control of IR emission region through molecular-level design with appropriate chemical bonding.[414–416] Wang et al. found experimentally that commercial encapsulated c-Si SCs can be cooled down by 2 °C in real environment using a 600 μm-thick pyramid-textured polydimethylsiloxane (PDMS) emitter without convection covering. This is due to a broadband emissivity close to 1 in mid-infrared range and an average transmittance of >90% in the absorption spectrum from 0.3 to 1.1 μm.[417] Visibly clear and flexible radiative cooling metamaterials based on SiO_2 aerogel microparticles randomly distributed in PDMS was developed by Lee et al. to enhance the thermal management of commercial SCs (Figure 11c). Such metamaterials are characterized by an integrated emissivity of >98% in the atmospheric and visible light transmission of >91% at wavelengths of 400–800 nm. According to the outdoor temperature measurement of flexible SC under relative humidity of 30–45%, an average temperature drop of 7.7 °C (5–12 °C) was achieved, with the low-density polyethylene windshield to suppress the convective heat transfer. On the stability aspect, the coverage of Si SCs with this metamaterial allowed a slower thermal degradation by 1.5× after 100 min of light soaking.[403] Recently, Heo et al. compared the performance dependence of micrograting design-based radiative cooler for various PV technologies.[418] It was revealed that multi-junction SC technologies

take the highest benefit of radiative cooling, with a temperature reduction of ≈6 °C compared to conventional glass-mounted baseline in outdoor environment under direct sunlight of ≈900 W m^{-2}.[418] Intriguingly, bandgap tuning plays an importance role in determining the radiative cooling performance and temperature-efficiency sensitivity. It was found that multijunction SCs with low bandgaps were the least vulnerable to sub-bandgap heating and achieved the best enhancement via radiative cooling.[418]

Safi and Munday revealed that the bandgap of the PV absorber affects the temperature reduction and cooling power levels under PRC.[419] The tuning of bandgap to higher values results in lower steady state temperatures due to the minimization of thermalization losses and heat dissipation.

For concentrated PV under elevated heat loads upon exposure to focused sunlight with high solar intensity, heat dissipation through radiation could be a powerful way to passively decrease the operating temperatures of the SCs. Bermel's group has experimentally demonstrated for the first time enhanced radiative cooling for low-bandgap GaSb PV cells under concentrated sunlight.[420] Using a composite radiative cooler consisting of soda-lime glass and an Al reflector, a temperature drop of 10 °C is achieved, corresponding to a relative rise of 5.7% in V_{oc} and an estimated increase of 40% in lifetime at 13 suns. It is expected that this could reduce LCOE by up to 33% for high-activation energy failure modes.[420] By upgrading the passive radiative cooler design, GaSb-based CPV can be cooled down by up to 36 °C, attributed to a 31% increase of open-circuit voltage and 4–15× increase in predicted lifetime (Figure 11d,e).[404] The ultimate capacity of passive radiative cooling is still rising debates in the scientific community, especially for conventionally installed PV panels.[184,185,187] On the one hand, substantial temperature reductions above 10 °C were either predicted or achieved in comparison with surfaces having very low thermal emissivity like bare silicon wafer. On the other hand, the impact of radiative cooling in temperature reduction became less apparent when considering comparisons with coated SCs or glass cover having much higher thermal emissivity. Moreover, very little cooling gain below 2 °C is reached only even with using IR emitters with high emissivity.[185,187] Thus, careful considerations should be taken in the estimation of radiative cooling potential including the specifications of the PV technology and the operation conditions.[185]

3.6.4. Challenges and Prospects

The technological integration of optical-based thermal management approach in PV faces several challenges, such as practical feasibility, cost competitiveness, angular sensitivity and strong dependence on environmental conditions. However, both selective-spectral and radiative cooling approaches have proved a satisfactory performance to overcome these hurdles. In particular, optical-based cooling approaches can fulfill multifunctional purposes, such as tailored sub-bandgap reflection and useful light antireflection, as well as surface self-cleaning.[185]

A noteworthy asset is that the employed structures, such as optical filters with customized wavelength selectivity as well as polymer IR emitters, are readily compatible with large-scale manufacturing and commercially available. The selection of the most suitable cooling pathway can be imposed by the target application. Namely, radiative cooling strategy is very effective in particular for extraterrestrial applications like and space PV.[169,185] Interestingly, the effectiveness of the SBR and PRC is larger when conductive/convective cooling contributions are low.[185] Such operating conditions are favorable in several integrated applications such as BIPV, where the convection at the rear side of the PV modules placed on roof or façade elements is minimal, as well as in space, where the convection is almost null for PV modules positioned in vacuum surrounding.[171] Moreover, the integration of optics-based cooling in PV industry would be a strategic perspective for energy yield control in realistic field operation.[421,422] In respect of long-term reliability, since the degradation mechanism are usually thermally activated, the reduction of operating temperature by cooling approaches is expected to postpone the PV module failure by up to 85% and improve the LCOE.[169]

Another important technological aspect that can open new opportunities for thermal tuning approaches is the integration in mechanically flexible and lightweight PV. Under such conditions, heavy and rigid standard cover glasses are not suitable. Therefore, novel flexible barrier materials and encapsulation strategies are required.[88] In this context, we envision that radiative cooling using polymer-based IR emitters can be concurrently employed with these encapsulation scheme, provided they fulfill other requirements in terms of chemical, thermal and mechanical moisture stability. Overall, tuning strategies for solar PV cooling are very effective approaches not only to reduce the operating temperature and improve the energy yield, but also to promote the versatility of PV applications under different environmental conditions.

4. Versatile Applications of Tunable PV Technologies, Challenges, and Prospects

4.1. Building-Integrated PV

In contrast to the conventional PV technologies used on residential rooftop plants and utility-scale PV power stations, different specifications are desired for BIPV. In this section, we present examples of relevant tunable PV technologies featuring color, transparency and thermal tuning capabilities that can be adapted to façades and windows in buildings.

4.1.1. Façade-Integrated PV

Façade-integrated PV are crucial elements to reduce the global warming, as buildings consume ≈40% of the final energy in Europe and US.[423] Kuhn et al. predicted that an average PV module area of 19 m^2 per building (assuming 200 W_p m^{-2}) is required in the case of Germany to achieve a CO_2-neutral energy system.[424] Also from the perspective of building owners, there are several advantages to BIPV including the on-site generation of clean energy resulting in at least partial independence from energy prices. Furthermore, the attractiveness of the field is promoted owing to the societal awareness of decarbonizing

energy issues, widely accepted perceptions on tackling climate change and the growing interest in improved aesthetics. It follows that BIPV will undoubtedly play a major role for existing and future buildings.[425] In recent years the potential and technical implementation of BIPV has been the subject of several reviews.[423,424,426,427] In this section several examples of BIPV applications are presented with a focus on tunable properties. Due to the techniques allowing to tune the color and transparency of PV modules, there are currently many variations of PV modules that are compatible with full integration on building façades. Such modules with different applied technologies are currently commercially-available from several companies.[428]

A famous example for the application of opaque BIPV with structural color is the Copenhagen International School, which won numerous awards in 2017 (**Figure 12**a).[429] Approximately 12 000 blue-green Kromatix PV modules from SwissINSO were installed at different angles resulting in varied color hues due to the angle dependency of the structural color. The installation has a capacity of 720 kW_p. A more recent example from AVANCIS is a seven-story office building completed in 2020 in Tübingen, Germany. Over 600 bronze colored modules were combined to form a solar façade with a yield of 82 kWp and 50 MWh per year, resulting in an estimated reduction of 30 tons of CO_2 per year.[430] Colored modules of the same type have also been installed on existing buildings. An office building in Oberbipp, Switzerland was renovated in 2018 with a blue façade consisting of 80 blue opaque CIGS modules with a yield of 10 kWp and 7 MWh per year. 84 modules in bronze, green and blue were installed to a residential building in Bern, Switzerland in 2019 with a yield of 12 kWp and 3 MWh per year. (Figure 12b)

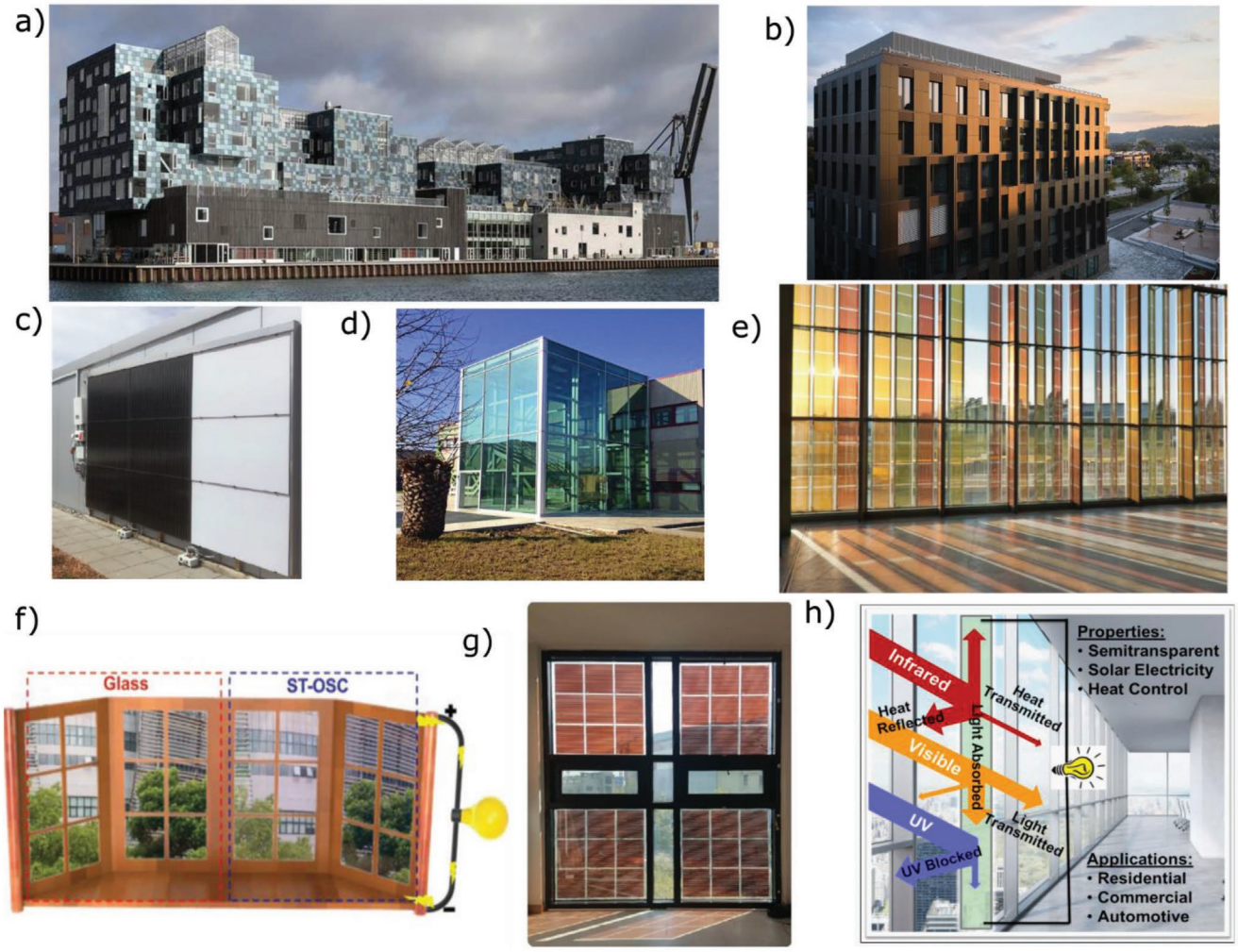

Figure 12. a) Photograph of Copenhagen International School with colored BIPV. Reproduced with permission.[429] Copyright 2021, The Institution of Engineering and Technology. b) Photograph of office building with bronze-colored PV façade. Reproduced with permission[431] Copyright 2022, AVANCIS GmbH; Photographer Albrecht Voss. c) White PV module vertically installed on test field next to black module (supplier: Solaxess SA). Reproduced with permission.[425] Copyright 2018, Springer Nature. d) Transparent solar cell façade at Terina Mediterranean Foundation.[432] Copyright 2022, Onyx Solar Group LLC. e) Solaronix' multicolored transparent PV façade using DSSC technology at the SwissTech Convention Center, Switzerland. Reproduced with permission.[433] Copyright 2022, Solaronix, Source: David Martineau, Solaronix SA. f). Digital photograph of doctor-blade coated ST-OSC applied to the window compared to glass counterpart. Reproduced with permission.[388] Copyright 2019, Wiley. g) View of full-scale dye sensitized PV window for outdoor testing. Reproduced with permission.[434] Copyright 2018, Elsevier. g,h) Illustration of infra-red regulating semi-transparent solar cell for heat control and electricity generation. Reproduced with permission.[23] Copyright 2018, Elsevier.

In particular, elegant and fresh white color is highly-demanded for building architectures. Therefore, white solar panels are considered as exciting and unparalleled product which are currently provided by several BIPV compagnies such as ISSOL,[319] Solaxess. (Figure 12c)[320] Such white PV are expected not only to fulfill power generation and aesthetic functions, but also to play thermal management and energy saving roles. Interestingly, white modules are estimated to operate at lower temperature than standard counterpart. The integration of white panel either on the roof of the façade of buildings can also contribute in the radiative cooling of the interior space. This is in accordance with the universal recommendations for the white painting of buildings to confront global warming.

Furthermore, semitransparent solar panels can find practical applications in the façades of buildings where large exterior walls are made of glass as in modern buildings and skyscrapers. The window surfaces mostly represent an untapped potential for energy generation and in some cases also leads to increased energy consumption by air conditioning systems. Transparent solar panels can replace the inactive window glass while generating electricity, in addition to providing natural lighting for the interior. They can reduce the amount of solar irradiation entering the building and thereby act as additional shading layer. Onyx Solar implemented semi-transparent a-Si modules on the exterior wall of the buildings of the Terina Mediterranean Foundation in Italy (Figure 12d).[435] The modules had an AVT between 10% and 40% and a PCE between 2.8% and 4%.[432] Using CdTe PV technology, semitransparent tinted façade windows were presented by Toledo Solar, with a potentially tunable transmission from ≈20% to ≈50%.[436] Due to a combination of thin organic polymers, fine layers of ink and transparent mesh electrodes, ASCA developed semitransparent organic solar modules with multiple colors as blue, green, grey or red and transparency up to 20% for BIPV applications.[374] A well-known example of DSSC-based semitransparent multicolored façade was showcased by Solaronix at the SwissTech Convention Center. This encompassed around 350 panels over a 200 m^2 active photovoltaic area, arranged in 65 colored columns (Figure 12e). Such semitransparent colored solar façade fulfilled dual functions of electricity generation and overheating prevention by reducing the amount of transmitted light. The transparency of red, green and orange colored-panels was tuned to achieve the overall light transmission target in the building.[433] Until now the application of building integrated photovoltaics has been mostly restricted to emblematic representative projects. For example, in Germany 2019, only 0.3% of the newly installed PV peak power was attributed to the BIPV sector.[424] The increase in complexity for a building with integrated photovoltaics is a challenge which should not be underestimated. Architectural design, scalability, electrical system layout, estimation of energy consumption, yield over the year and the economics of the project are connected complex topics that require cooperation of respective professionals. Though the cost of a BIPV façade remains higher than standard façade claddings, technological studies indicate that if the complete life-cycle is considered, BIPV- façades could return their investment in <10 years.[424,437] We envision a further evolution of the BIPV deployment and related market, owing to spurring policies, coordination of all stakeholders, developed know-how of the involved professionals along with development of highly-efficient modules with exquisite aesthetic quality.[21,438,439] In particular, the latter aspect benefits from the ongoing research and progress in tunability-enabling technologies for PV with respect to color and transparency and thermal management. This also opens new opportunities of applications in BIPV for emerging PV technologies to transform building façades into electric power generators.[440]

4.1.2. Window-Integrated PV

Power Generation: For the natural illumination of buildings through PV windows, both higher AVT and CRI as well as color neutrality and visual comfort are desired features. Windows on buildings typically require an AVT of above 50%. Sun protection glazing can also have values of AVT far below this limit to reduce the heat flux into the building.

It is estimated that a PCE of 5–10% are suitable for power-generating window to achieve a competitive levelized cost of electricity with solar PV windows whereas a lower PCE ≈2–5% may be sufficient for powering smart windows.[17] Especially for applications in office buildings, the CRI, AVT, and window-to-wall ratio (WWR) have to be adapted in such way that enough daylight enters the interior without creating disturbing color effects.[441] For most studied scenarios, the reduced heat income through the lower AVT plays a crucial role.

While there are large numbers of publications about recent developments on transparent SCs,[20,64,344,442] only few of them are ready for larger-scale functionality. Most commercially available devices consist of spatially segmented c-Si technology. However, few exceptions of companies presented innovative solutions for transparency tuning of solar panels integrated in PV windows The company of Ubiquitous Energy offers a UV–NIR selective transparent OSC technology with 38.3% AVT and 9.8% PCE.[443] Zhang et al. studied a semitransparent OSC with AVT of 21% and high PCE of 9.37% (Figure 12f).[388] The noticeable feature of this SC is the high CRI of almost 100. The device in a window application is shown in Figure 12e. Lee and Yoon analyzed the performance of a semi-transparent DSSC module in window scale installed in an outdoor test set-up over a period of two years (Figure 12g).[434] The vertical arranged solar PV window reached an average PCE of 3.4%. They reported an average power yield for a vertically installed PV window was 2.53 kWh kWp^{-1} per day over a two-year period. Bergren et al. presented a QD laminated-glass LSC for a 10 cm × 10 cm PV window with 44% visible transmittance and up to 2.9% PCE.[444] According to performance modeling, over 1 GWh annual electricity production was predicted for a typical urban skyscraper in U.S. cities, which is a great asset for the energy savings budget toward net-zero buildings.

Recently, 3.6%-efficient tinted PV windows based on QD-glass LSC from UbiQD were installed as a pilot project for testing phase on Commercial Buildings in the US.[445]

The necessity to tune the AVT and PCE of a solar PV window depending on the application scenario was shown in a modeling study by Olivieri et al.[446] They analyzed the energy saving potential of solar PV windows with AVT between 10% and 40% and PCE between 3.4% and 2.0%.[446] For small WWRs the best

performing solar PV window solution concerning the energy savings was the device with the highest transparency. The energy savings for this scenario were at such a low level that an implementation in buildings with low WWR seemed to be economic implausible. For larger WWRs, the importance of the AVT relative to the energy savings was reduced. This confirmed that that in scenarios with high window coverage, PV windows are a promising application with high energy saving potential. Vossen et al. analyzed the visual performance depending on the coverage ratio of LSC with clear red coloration in office applications.[447] They found out, that a coverage of 25% of the total window area is accepted and even preferred compared to clear glass, while a 75% coverage was found to be less accepted (Figure 12g). It is noteworthy that beside the direct integration of PV into window for power generation, semitransparent SC devices can be used as an energy source for self-powered electrochromic smart windows ensuring a dynamic control of the optical transmission.[62,402,448,449]

Thermal Management and Heat Insulation of the Interior Spaces: Another advantage of PV window is the regulation of the radiative heat flux through the PV window depending on specific demands of users in interior spaces. This improves the heating and cooling efficiency of buildings, yielding significant energy savings. Solar cells integrated instead of standard see-through windows should allow to tune the IR transmittance, to regulate the heat gain and emissivity and to manipulate the heat loss. In hot weather, to prohibit the transfer of heat from outdoors to indoors, both minimal IR transmission and low emissivity are required.[130,450] In cold weather, high solar transmittance to allow heat entering the building and low MIR emissivity to prevent the heat escaping from indoors to outdoors are desired.[130,450] Several research groups are working on multifunctional TPV which are specifically designed to simultaneously control the electricity generation, visible light transmission and heat insulation. Sun et al. studied a transparent SC based on a polymer absorber coupled with Bragg reflector layers for high IR reflection (Figure 12h).[23] The device reached a PCE of 6%, AVT of 25%, and an IRR of over 80%. The combination of radiative cooling and a semi-transparent SC was also shown by Zhao et al.[451] They presented a device with high emissivity in the IR range and transparency of between 10% and 30% in the visible wavelength range. This shows, that the tuning of spectral response for SC devices is not restricted to visible range, but also extended to IR wavelengths, which is expected to drastically boost the energy savings capabilities of buildings. The thermal behavior of switchable SCs in double glazing configuration under irradiation levels between 100 and 1000 W m^{-2} was studied by Götz-Köhler et al.[24] It was shown that the solar cell layers of the PV window temperature can rise to above 60 °C under full irradiation, but the airgap between the panes works as an effective heat blocking layer.

Needell et al. conducted a market analysis for PV windows in the US.[452] A key finding was that dynamic windows that combine photovoltaics with reversible tunable transmittance in a controllable and intelligent way represent one of the most promising applications for the building sector. Even though there are no available market for PV windows with smart switchable transparency yet, the tuning of the transparency of windows by electrochromic and other switchable technologies is expected to result in a further reduction of the energy consumption of buildings.[118,453–455]

Challenges and Prospects: Several critical challenges remain to be solved and are pointed out in different review articles on transparent PV windows.[20,70,120] This includes techno-economic aspects such as the durability and scalability, the visual comfort inside the building, and payback time. Furthermore, social acceptance has to be guaranteed. In this regard, the desired color neutrality aspect in windows is in favor of UV–NIR wavelength-selective PV and LSC-PV see-through technologies. To achieve competitively-commercialized technologies, the target size should be in the range of 1 m^2, enabling adoptability in PV window applications. Considering the amount of scientific work put into the field of solar PV windows, it seems to be only a matter of time until these problems can be overcome.

In conclusion, PV windows will be a valuable addition to buildings in the near future. Tuning the AVT, PCE, and color appearance can adjust their visual comfort and thermal management on-demand depending on individual situation. The field is growing and market is about to be establish with a lot of emerging new technologies and new demonstrations from different industrial companies. Coupling PV windows to switchable technologies such as thermo-, electro-, or gasochromic layers offers great potential for intelligently regulating the AVT, PCE, color, and SHGC on-demand. This smart optical tuning would be crucial in the reduction of heating, ventilation, and air conditioning (HVAC) energy usage. Benefiting from the accelerated research on smart window technologies, upgraded PV windows might become an efficient way to realize net-zero energy buildings. A possible combination of recently demonstrated radiative cooling and temperature regulation technologies,[415,456,457] with power-generating PV in smart windows could further boost the benefits of energy savings from all-season household thermal regulation.[48]

4.2. Greenhouses in Agrivoltaics

4.2.1. Relevant Tunability Features

In agrivoltaics, besides the traditional spaced opaque PV modules (either on top of agricultural land or greenhouse rooftops with possible implementation of tracking systems), the integration of semitransparent PV into greenhouses is of great interest.[458–460] Proposed concepts allow partial light harvesting by SCs for electricity generation and simultaneous light transmission with adjusted light spectra for crop production.[461] Hence, semitransparent PV integrated into greenhouses requires full spectral tuning from UV to visible to IR to fulfill the multifunctionality in terms of electricity generation, plant growth control and thermal management (**Figure 13**a). Essentially, as the plants need distinct wavebands for photosynthesis, their absorption spectrum shows peaks for blue and red light, where the photoactive pigment chlorophyll is absorbing. Therefore, the absorption of ST-PV can be optically tuned to complement the spectral absorption of chlorophyll. A so-called "green gap" can be defined approximately between 480 and 630 nm.[462] Different photoactive PV materials showcase distinct transmission characteristics over the photosynthetically active radiation

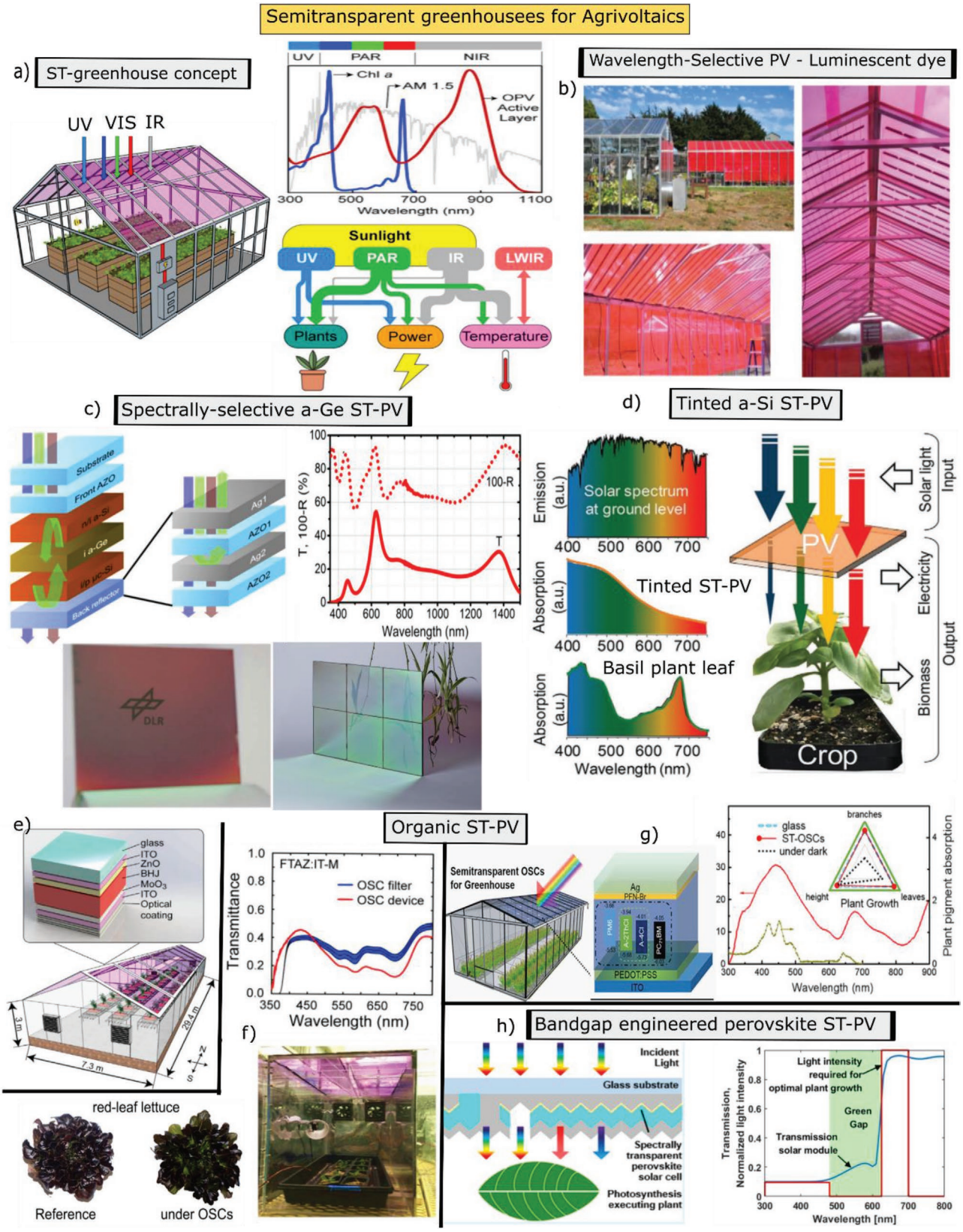

Figure 13. a) Basics of semitransparent greenhouse. Illustration of semitransparent SC-integrated greenhouse indicating spectral use of sunlight (left) Complementary spectral absorption between chlorophyll a (Chl a) and photoactive layer of an organic semitransparent SC (top right) Schematic of sunlight spectrum distribution for plant growth control, power generation, and greenhouse thermal management.(bottom right) Adapted with

(PAR) spectrum.[463] Compared to conventional opaque and neutral semi-transparent solar panels with uniform spectral response, tinted or spectrally-selective PV can offer several advantages with respect to power generation, biomass yields and thermal stabilization.[464,465]

4.2.2. Relevant Research and Development

Loik et al. presented one of the first demonstrations of a spectrally-selective solar-powered greenhouse (Figure 13b).[466] The concept uses a combination of a perylene red dye-based luminescent concentrator with a conventional c-Si PV, allowing partial absorption of blue and green light while transmitting the remaining wavelengths for photosynthesis. An integration in a constructed glasshouse demonstrated the benefits for tomato growth and for powering different electrical operations. Based on an annual power generation monitoring of an LSC-equipped greenhouse, a full coverage of about 22 m^2 was projected to yield 1342 kWh per year.[467]

A spectrally-selective ultrathin a-Ge:H concept was proposed by Osterthun et al. where the spectral transmission and absorption of ST-PV can be easily tuned through a metal/oxide multilayers cavity electrode to meet the plant needs (Figure 13c).[468] Due to the transmission of both blue and red light, a violet color appearance is observed in the optical demonstrator. The assessment of this technology in a lab scale photo-bioreactor has proven significant algae growth.[469] Thompson et al. proposed tinted semitransparent panels based on sufficiently thin a-Si:H absorbers for synergetic crop and electricity production (Figure 13d).[470] These SCs with nominal efficiency of 8% and a power output of 66 W m^{-2}, absorb blue and green light and transmit the red part of the spectrum (transmittance level < 30%), resulting in an orange tint. In small-scale demonstrator greenhouses, selective utilization of different light wavelengths has proven to be beneficial for the growth of basil and spinach in terms of financial gross gain, protein content and biomass. Furthermore, many organic PV technologies have demonstrated their great potential for greenhouse applications due to their tuning capabilities of the absorption characteristics.[463,465] In this context, tinted SCs are not the only promising technologies, but also transparent IR-absorbing organic devices are effective in combining PV and photosynthesis. Liu et al. introduced a 10% efficient transparent organic PV with an AVT ≈ 34% allowing growth of Mung beans underneath in a similar way as under normal sunlight.[461] Considering different photoactive polymers with distinct spectral absorption profiles in the ST-OSC device shown in Figure 13e, Ravishankar et al. predicted energy load, solar power generation, and light entering the greenhouse.[471] A step forward, the evaluation of red leaf lettuce growth in a box covered with ST-OSC confirmed the similar yield and nutrient content compared to the reference. (Figure 13f) Moreover, it was concluded that the selection of the photoactive layer and electrodes, as well as the implementation of DBR optical structures provide a large tunability of spectral control for greenhouse integration. Shi et al. proposed a wavelength-selective ST-PV with a PCE of 7.75% based on a combination of a wide bandgap polymer donor with a near-infrared absorbing non-fullerene acceptor resulting in a crop growth factor of 24.8%.[472] This is enabled by engineering the spectral absorption of the photoactive materials to allow a well-matched transmission with the absorption of chlorophylls. A highly-efficient ST-OSC (PCE = 13.08%) with a good transmittance for plant absorption was developed by Wang et al., yielding a plant growth factor of about 24.7%.[473] (Figure 13g) The evaluation of the plant growth including height, branches, and leaves after 90 h of continuous illumination confirmed a similar performance under SC with filtered light compared to clear glass.

One of the best achievements of DSSC adapted for greenhouse applications was reported by Chalkias et al. using triphenylamine-based dyes and a highly transparent iodine-free electrolyte.[474] A 6%-efficient wavelength-selective semitransparent DSSC was able to deliver almost 85% EQE in the complete blue and green spectral region and 55% transparency in the red part. These performance outputs are expected to yield crop growth factor of almost 35%. The further development of perovskite PV for greenhouse-oriented applications is also stimulating considerable research efforts.[200,462,475] The main reason to choose perovskites is the bandgap tunability aspect which enables a decent transparency with spectral selectivity.[462] Knipp and co-workers suggested spectrally transparent pyramidal textured PSC to combine PV and photosynthesis, as can be seen in Figure 13h.[462] They assumed an optimal plant growth under 10–20% blue light, 0% green light, and 100% red light. The spectral absorption is tailored accordingly. A $MAPb(I_{0.35}\ Br_{0.65})_3$ perovskite with high-band-gap of 1.95 eV and cutoff wavelength of ≈630 nm is engineered allowing red light transmission to the

permission.[37] Copyright 2021, the Authors. Published by Elsevier. b) Constructed glasshouse with wavelength-selective PV panels based on luminescent dyes. Reproduced with permission.[466] Copyright 2017, the Authors. Published by Wiley. c) Schematics of the spectrally selective solar cell with metal/oxide multilayer cavity electrode. (top left) Photograph of optical demonstrators showing violet transmission through the sample (bottom) Reproduced with permission.[468] Copyright 2021, Optical Society. Transmission and (1-R) spectra of PV device. (top right) Reproduced under the terms of the CC BY license.[263] Copyright 2020, the Authors. Published by MDPI. d) Tinted semitransparent a-Si-based solar panel for dual crop and electricity productions. Solar radiation spectrum in the visible range at the ground level and absorption spectrum of ST-PV and basil plant leaf are depicted.(left) Schematic Illustration of the solar energy input and the two relevant outputs of agrivoltaics for electricity and biomass.(right) Adapted under the terms of the CC BY license.[470] Copyright 2020, the authors. Published by Wiley. e) Representation of the considered ST-OSC and greenhouse. Reproduced with permission.[471] Copyright 2020, Elsevier. f) Transmittance spectra of one of the considered ST-OSC. (top) Growth box with plant tray covered with OSC filter. (bottom right) Overhead view of lettuce at final harvest for reference and under ST-OSC. Reproduced with permission.[37] Copyright 2021, Elsevier. g) Illustration of ST-OSCs for greenhouses and corresponding device structure. (left) Transmission of ST-OSC and plant pigment absorption spectra. Inset: Plant growth evaluation under glass, ST-OSC and in dark. Reproduced with permission.[473] Copyright 2021, Elsevier. h) Illustration of spectrally transparent pyramidal textured perovskite SC with blue and red lights transmission. (left) Optimized transmission for the application as a ST-PV featuring spectral selectivity compatible with photosynthesis. Reproduced with permission.[462] Copyright 2021, American Chemical Society.

plants. Blue light can be transmitted through openings within the interconnection scheme. Liu and co-workers proposed a semitransparent flexible $MAPbBr_3$ perovskite-based SC with metal/oxide multilayers transparent electrode for possible utilization on the roof of PV greenhouse.[200] The device reached an average transmittance of 60% in the 540–760 nm wavelength range, which is assumed to be suitable for greenhouse vegetation.

4.2.3. Challenges and Prospects

The application of semitransparent PV in greenhouses is a rather new field of research and encounters several challenges. For instance, the performance and the energy yield of semitransparent-PV technologies should reach competitive levels with respect to spatially-separated opaque PV[476] and tracking-integrated micro-concentrators.[477] Large scale modules have to be realized in order to equip industrial greenhouses, where the microclimate can be different compared to small proof-of-concept greenhouses. This would bring the extrapolation of yield evaluation to commercial level. Also, various plants in different growth states may need different illumination conditions. Further technical and socio-economic studies would provide comprehensive insights and would further extend the farmers acceptance of these emerging technologies. It is also expected that the optimization of the solar power generation and crop productivity would maximize the economic value. According to a global perspective study across diverse climates, the improvement of the net present value for organic solar powered greenhouse with dual crop productivity and energy generation was already estimated in contrast to conventional greenhouse systems.[478]

We envision that the evolution of the learning curve and the succession of effective demonstrations from different ST-PV technologies would bring the blossoming of the greenhouse-integrated PV. As progress steps, first products with thin film a-Si:H[479] and LSC[480] are already available on the market, pointing out the interest in this concept.

Overall, both spectrally selective transparent and tinted emerging PV technologies demonstrated great potential for greenhouse applications with substantial benefit in respect to solar power, plant growth, and thermal management. This is attributed to the tuning features in terms of bandgap and absorption profile of the photoactive materials and spectral engineering capabilities.

4.3. Relevant Tunable SC Technologies for Further Distributed Applications

4.3.1. Indoor PV

Relevant Tunability Features: As illustrated in **Figure 14**a, Indoor PV (IPV) exploits artificial light sources such as fluorescent bulbs or light-emitting diodes (LEDs) with intensity 300–3000× lower than sunlight (0.002–0.003 sun, 300–500 lux) and a narrower spectrum concentrated around the visible range (400–800 nm).[481] Obviously, these conditions imply different optimal design of PV devices compared to conventional solar cells under sunlight.[39,482–485] A wide range of organic and inorganic photoabsorbent materials have been extensively studied for IPV devices in literature.[40,481,486–495] However, the selected photosensitive materials for IPV technologies must satisfy a matching absorption with the emission spectrum of the indoor light source, to avoid the detrimental influence of trap-assisted recombination in the low carrier density regime, as well as minimal voltage losses with low sensitivity to weak illuminance.[39,483,485,494] Considering the light-intensity-sensitive aspect of IPV, bandgap tuning plays a crucial role in defining the device performance in terms of the efficiency limits and the energy losses as well as the adaptability to different light sources.[482,483,494]

Relevant Research and Development: Freunek et al. established the first detailed balance model relevant to IPV, discussing the optimal optoelectronic material properties and efficiency limits under different indoor radiation sources (Figure 14b).[482] The ideal bandgap varies from $E_g = 1.95$ eV in the case of a fluorescent tube reaching an efficiency limit of 46% to $E_g = 2.10$ eV for a sodium discharge lamp with an efficiency limit of 67%. Impressively, matching the material bandgap to the monochromatic source emission, for example, $E_g = 2.25$ eV for $\lambda = 555$ nm, can yield an exceptional efficiency of 72.98%.[482]

Figure 14c depicts the disparity between the standard solar spectrum AM1.5G illumination and indoor artificial light source under 1000 Lux illuminance in terms of theoretical efficiency limits as well as experimentally achieved efficiency levels for different PV technologies as a function of E_g.[40] On a practical level, it has to be noticed that the evolution from standard AM1.5 to indoor conditions is better suited for specific SCs devices such as organic, perovskite and DSSC compared to c-Si and III–V SCs. Commercial indoor PV products can be already provided, such as a-Si SC from Power film and Solem, DSSC from Sharp corporation, 3GSolar and Solaronix, and OPV from infinity PV. In this perspective, IPV is considered as a promising trend for solution-processed SC technologies such OSC, DSSC, PSC, and colloidal QD.[490] In particular, organic and perovskite absorber could greatly benefit from their inherent bandgap tunability in IPV applications.

Another tuning aspect is the absorber thickness adjustment which plays a crucial role in the integration of c-Si technology for indoor applications. Tiedje and co-workers calculated the maximum efficiency as a function of c-Si wafer thickness and found an optimum thickness of about 1.8 µm under white LED indoor conditions reaching an efficiency of 29%, remarkably thinner than the optimum range of outdoor sunlight source (>100 µm).[481] Such thickness level can promote the application of ultrathin lightweight flexible c-Si SCs in indoor applications, albeit the non-optimal bandgap.[58,191,192]

Challenges and Prospects: The main critical difficulties the field of IPV is facing, are the distance from the light source, manufacturing costs to enable competitively-commercialized technologies, the scalability to generate sufficient power from weak-intensity sources, the mechanical flexibility to comply with different applied surfaces, and the environmental reliability to extend the lifetime of PV cells and minimize their harmful ecotoxicity impact.[38,40,487,488,496] Once such obstacles are well tackled on the research and development level and successfully transferred to the industrial level, IPV can be efficiently utilized and widely commercialized in internet of

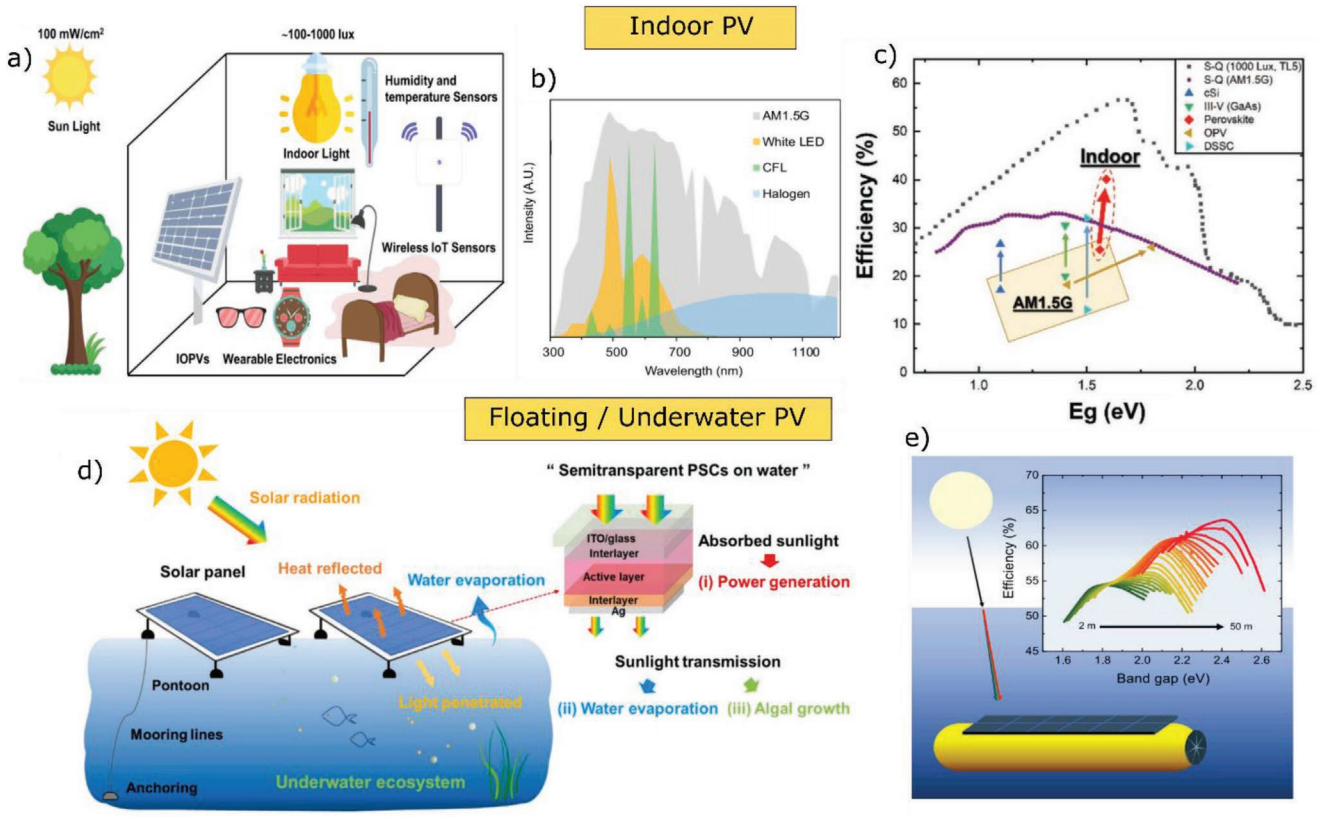

Figure 14. Further distributed applications of tunable PV. a) Illustration of indoor PV applications. Reproduced with permission.[497] Copyright 2020, Wiley-VCH. b) Different spectra of artificial light sources in contrast to standard solar spectrum. Reproduced with permission.[38] Copyright 2019, Elsevier. c) Practical state-of-art efficiencies for different types of PV as a function of the bandgap energy E_g under AM1.5G illumination at 298.15 K and in indoor condition under 1000 Lux illuminance of a TL5. Arrows start from the AM1.5G record efficiencies and point toward the 1000 Lux—illuminated ones. The maximum S-Q efficiency limits are plotted with continuous line for AM1.5G illumination and dashed line for indoor condition under 1000 Lux illuminance. Reproduced with permission.[40] Copyright 2021, Wiley-VCH. g) Illustration of design concept for semitransparent polymer solar cells floating on water: in contrast to conventional opaque system. Reproduced with permission.[498] Copyright 2020. Elsevier. h) Maximum theoretical efficiency as a function of bandgap at different underwater depth levels. Reproduced with permission.[43] Copyright 2020, Elsevier.

things (IoT) applications including wireless sensors and other standalone electronic devices which operate at low illuminance and consume very low power.[38,40] Along with the growth of the indoor IoT/wireless sensors market it is expected that IPV would become one of the fastest growing field among unconventional PV markets with a six-fold increase from $140 million in 2017 to $850 million by 2023 and a 70% compound annual growth reaching 60 million devices per year in 2023.[38] Thereby, established IPV products from different companies will be complemented by potential market entries for different other IPV technologies.[38] This provides a great opportunity for new IPV technologies using new materials with adjusted-bandgap absorbers. Such product diversity of IPV field would be beneficial at startup level, and also, for large PV manufacturer to establish a credibility bridge with customers before launching large-scale conventional facilities.[38]

4.3.2. Floating and Underwater PV

Semitransparent Floating PV: Floating photovoltaics (FPV) consist of solar panels installed on a floating platform on water surfaces and can provide a solution to the issue of land usage and space shortage, especially in land-scarce, and densely populated countries.[499,500] Besides the prevention of land occupation and the power generation potential, FPV can present multiple other benefits. This covers the mitigation of water evaporation by blocking the sunlight heat to conserve fresh potable water, the control of algae growth via the influence of PV array shadows on the photosynthetic processes. Also, the exploitation of the water surrounding in the cooling of the PV devices can boost their performance by up to ≈10%.[42,498] However, the complete blocking of the sunlight by large-area opaque floating panels can be detrimental for the sustainability of the underwater aquatic ecosystem.[42,498] Hence, the usage of semitransparent PV with light transmission capabilities can be advantageous in FPV applications.

Various tunability aspects of SCs are pertinent for FPV to customize the power generation and the transmission window, the visual perception and the thermal management (Figure 14d).[42,498] In this context, Zhang et al. demonstrated for the first time the application of semitransparent OSCs floating on water with conductive heat insulation and water evaporation assessments by means of high-precision electronic balance and

IR cameras.[42] By varying the thickness of an Ag cathode from 80 down to 15 nm, color neutral ST-PV having color coordinates close to (0.33, 0.33) with a PCE of 6.7% and an AVT of 30% was achieved. The mounting of such STPV device on top of fresh water at different tilt angles (0° and 30°) serves as thermal barriers of the heat flux, leading to a drop of the water surface temperature with a reduction by 25–38% and a mitigation of the water evaporation with a reduction by 24–35% compared to bare glass coverage.[42]

Subsequently, the same research group made one step forward in the direction of the evaluation of semitransparent OSC encapsulated by UV-cured resin/glass placed on top of water surface as regulators of underwater algal growth.[498] Using an ultra-thin Ag electrode in a semitransparent OSC with a PCE of 13.0% and AVT over 20%, they demonstrated that a specific transmittance window with controlled light intensity is capable of regulating water evaporation and algal growth and lowering the surface temperature of water by ≈5 °C as compared to uncovered water.[498,501] The analysis of algal growth rates and photosynthetic efficiencies with respect to the light transmittance windows revealed that by tuning the transmittance profile in the wavelength regions of 380–530 nm and 620–700 nm, sufficient feed for aquaculture can be sustained by the algae.[498,501] Additionally, according to an investigation on selected representative microalgea (Cholorella, Carterae, Tricornum, and Synechococcus) relevant to different aquatic environments, that is, offshore, nearshore, and inland waters, it was deduced that the wavelength range of transmitted light and the intensities should be adjusted to suit the growth of specific algae.[501]

Bearing in mind the rapid growth and spread of FPV sector by hundred-fold within 5 years as an extension to ground-mounted and rooftop PV technologies, it is believed that tunable PV featuring customized light transmission and thermal management besides the primary power generation function would promote the sustainability of aquatic ecosystem and the preservation of algae as one of the main producers of oxygen (≈50%) in earth's atmosphere.[498] The technology is still in the early research, modelling, and prototype phase, but the results presented above suggest exciting progress in the near future.

Underwater PV: Another marine application of PV is underwater SCs which can power marine systems such as underwater vehicles, autonomous systems, and sensors at depths as great as 9 m below sea level.[502] Interestingly, the underwater spectrum is altered due to the scattering and absorption effects. For the latter, the absorption of large fraction of red wavelengths (>600 nm) is caused by water medium at shallow depths, while, deep penetration below water surface of the blue to yellow wavelengths portion (400–600 nm) can be allowed.[43] Hence, these conditions impose a restriction on the optimal bandgaps in favor of wide-bandgap photosensitive materials (E_g > 1.8 eV), pointing out the importance of bandgap tuning aspect for underwater PV.[502,503] Previous practical attempts used SC based on a-Si, InGaP, and organic materials.[502,503] Since, the irradiance spectrum gets narrower after light transmission through water, a tremendous change of the efficiency limit is expected for underwater SCs compared to land-based counterparts.[43] In this regard, Röhr, Taylor, and co-workers, established a detailed-balance calculations to estimate the ultimate potential of underwater SCs.[43] They demonstrated that the optimum band gap of photoactive materials in underwater SC shifts by ≈0.6 eV as function of depth from ≈1.8 eV at 2 m (shallow) to ≈2.4 eV at 50 m with a band-gap plateau at ≈2.1 eV between 4 and 20 m (intermediate), irrespective of the water type and the of geographical location (Figure 14e).[43] A sufficient power can be harvested at 50 m depth below sea level, with an efficiency limit of 63%. To this end, along with appropriate encapsulation novel design perspectives relying on bandgap tuning for underwater PV can be envisaged. This paves the route to the more profitable utilization of submerged wide-bandgap-based PV in underwater PV applications. The technological readiness state of underwater PV does not get beyond initial models and therefore still requires a great deal of work to be done to reach first demonstrations.

4.3.3. PV Driven Photoelectrochemical Water Splitting and Solar Hydrogen Generation

In solar-driven water splitting, solar energy can produce green hydrogen within an artificial photosynthesis.[504] Solar-to-hydrogen energy conversion can take place in two different ways. Either indirectly through connecting a PV panel to an electrolyzer through external wiring or directly through submerging the photoactive material into electrolyte to replace the metal electrode.[505]

Relevant Tunability Features: The concept of direct water splitting with SCs relies on voltage biasing of the photoactive material device upon illumination.[506] For this purpose, the bandgap of semiconductor photoelectrode must reach the required level of 1.23 eV for water splitting and the conduction and valence band positions must match the water reduction and oxidation potentials.[507] Due to the required overpotentials to drive simultaneous hydrogen and oxygen reactions as well as possible loss mechanisms in operational devices, a realistic value of PV open circuit voltage V_{oc} must exceed 1.6 eV.[508,509] Therefore, bandgap tuning is crucial in solar water splitting systems.[510] Several concepts of PV-driven water splitting devices have been proposed in literature, including integrated SC technologies such as a-Si multijunction, c-Si, CIGS, perovskite, perovskite/Si tandem, and III–V multijunction.[505,506,511–518]

Relevant Research and Development: One of the representative examples of direct solar-to-hydrogen conversion is the demonstration of independent bandgap tuning in each junction of inverted metamorphic III–V multi-junction architectures (**Figure 15**a).[505] A fabricated photoelectrochemcial/PV tandem device with designed bandgap combination of GaInP (1.8 eV)/GaInAs (1.2 eV) yielded a high maximum solar-to-hydrogen efficiency over 16%, relative to maximum theoretically attainable efficiency of 24%.[505] According to the theoretical calculations, an ideal device with 1.70/1.05 eV bandgaps can achieve a maximum solar to hydrogen efficiency of 27% (Figure 15b).[505,510] One of the highest solar-to-hydrogen efficiencies over 30% under concentrated illumination for indirect photovoltaic-electrolysis was reported by Jia et al.[511] They used triple-junction SC with two series-connected electrolyser system where the three sub-cells of the PV device are made of InGaP (E_g = 1.895 eV), GaAs (E_g = 1.414 eV), and GaInNAs(Sb) (E_g = 0.965 eV).

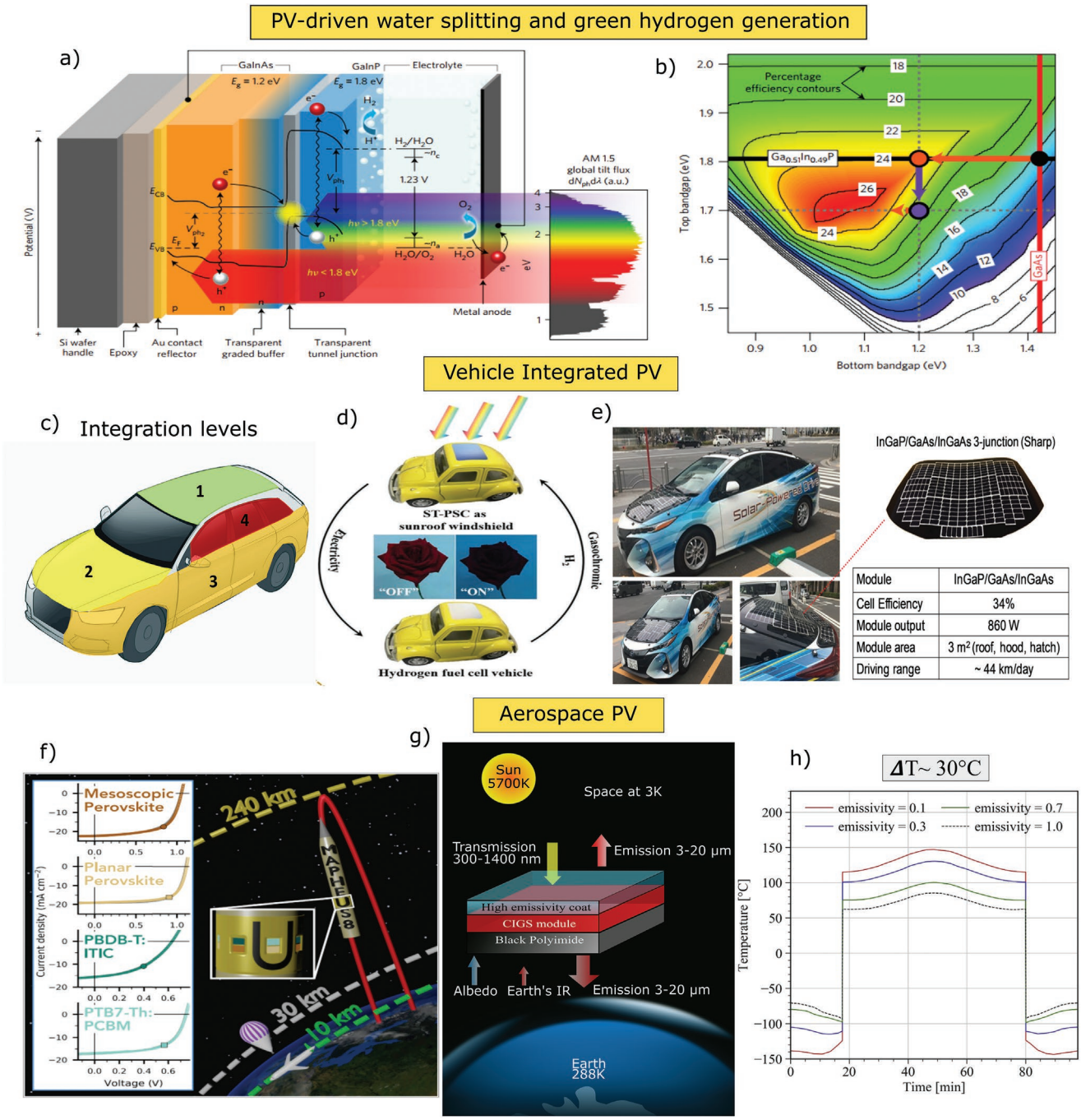

Figure 15. Further distributed applications of tunable PV. a) Structure of inverted metamorphic multi-junction architectures for water splitting. b) Contour plot of maximum theoretically attainable solar-to-hydrogen efficiency. Reproduced with permission.[505] Copyright 2017, Springer Nature. c) Different integration levels for PV in vehicles. Reproduced with permission.[36] Copyright 2020, EUPVSEC. d) Switchable PV integrated on vehicle sky roof. Reproduced with permission.[122] Copyright 2019, Elsevier. e) Toyota Prius PHV demonstration car (left) Reproduced with permission.[521] Copyright 2019, Toyota Motor Corporation. The integrated InGaP/GaAs/InGaAs triple-junction (3-junction) solar cell module and corresponding characteristics. Reproduced with permission.[522] Copyright 2020, Wiley-VCH. f) Schematic overview of the sounding rocket flight with different integrated organic and perovskite PVs. Reproduced with permission.[523] Copyright 2020, Elsevier. g) Illustration of light and heat flow into the PV panel in orbit. h) Calculation of solar cell temperature at 650 km and 0 beta angle orbit with varying emissivity of the front surface coating. Reproduced with permission.[524] Copyright 2020, Elsevier.

Interestingly, the optimal bandgap combination for higher solar-to-hydrogen efficiency could open new opportunities for emerging multijunction technologies, such as perovskite/c-Si, in water splitting applications.

Challenges and Prospects: PV-driven water splitting has to overcome several challenges to become an economically viable technology. This includes large-scale deployment, long-term stability, inexpensive material selection, and device designs, lack

of standardized metric protocols and solar hydrogen cost.[519,520] Overall, the technological readiness of solar water splitting can be seen in technology validation phase at lab-scale achieving high solar to hydrogen efficiency efficiencies. Hence, further progress in upscaling methods is required to reach large-scale demonstrators and to approach the industrial level. Nevertheless, the important achievements and promising technological progress in the field of PV-driven water splitting highlight the great opportunities toward practical solar hydrogen production, especially with the growing interest and future perspectives of the transportation sector.

4.3.4. Vehicle-Integrated PV

In addition to the importance of solar hydrogen in powering vehicles, the exploitation of PV for direct electricity generation in transport sector could enable considerable benefits. This comprises autonomy enhancement, electric vehicle deployment, energy saving, economic gain, and CO_2 emission reduction.[525–528] An extensive overview of the state-of-the-art, recent trends, expected benefits, and perspectives of vehicle-integrated PV (VIPV) is provided in the recent report of the International Energy Agency.[35]As illustrated in Figure 15c, the integration of PV modules in vehicles can be realized on different levels such as 1) roof, 2) engine hood, 3) car sides, and 4) transparent windows. Each of these implementations impose different specifications and requirements in terms of available area, visibility, aesthetic, surface curvature, illumination, and safety.[36]

Relevant Tunability Features: Depending on the integration scenario, different tunability aspects of SCs are relevant to customize the power generation, the color, the transparency, weight, and thermo-mechanical attributes. Similar to the case of building windows, transparent PV technologies can substitute the glass surfaces in vehicles such as windows and sunroofs, providing considerable power, adequate visible light transmission, low haze ratio at different viewing angles, and decent aesthetic functions.[20]

Thermal management is an extra asset that can be provided by the integration of ST-PV on sunroofs. This can be manifested due to the control of the light transmission through ST-PV integrated in glass surfaces.

Another tuning aspect is the need of vivid color in VIPV technologies for premium aesthetical appearance, in a similar way as the case of building facades. This is crucial to vehicle sales. Hence, colored modules with minimal power losses are highly desired as attractive asset for VIPV.[35]

Relevant Research and Development: Traverse et al. estimated that PCE values between 10% and 15% combined with AVT between 65% and 80% (LUE > 6.5%) are desired for the application of transparent PV in electric vehicle windows, to extend its travel distance range by 10–20 miles in a day.[17] Additionally, the integration of TPV or ST-PV could afford cooling solutions to mitigate the internal temperature of the car when parked in hot environments, by powering an electric fan or by activating a tinting state.[17,20] In this context, Yao et al. demonstrated the benefit of the application of a switchable semi-transparent OSC as smart window to the sunroof of hydrogen fuel vehicle. It prevented high temperature in the interior of the car, caused by dazzling sunlight during the summer.[122] This is achieved by a gasochromic dynamic color tuning of the tungsten trioxide/platinum (WO_3/Pt) back reflector layer during hydrogen exposure between colored and bleached states with fast response speed (Figure 15d). The hydrogen can be supplied by high-pressure hydrogen tanks of the vehicle in a sufficient and safe way, since the fuel cells simultaneously use H_2 and atmospheric O_2 to convert into electricity and water via an electrochemical process.[122]

As an example of industrial level, the spin-off Vitsolc presented organic-based ST-PV for the sunroofs of electric vehicles.[529] This was claimed to extend the mileage of electric vehicle due the extra continuous charge process during outdoor use or while parking, without altering of vehicle aesthetics. Another example of integrated PV in vehicle sunroofs was CdTe-based tinted semitransparent technology developed by Toledo Solar, with a tunable transparency from ≈6% to 80% and a matched curvature to automobile sunroofs.[530] This could enable both power generation and solar heat load reduction. It was assumed that such SC device can power a circulating fan for the cooling the interior or can support the charging of the electric vehicle battery. For the integration of opaque colored PV on the vehicle body, several coloring approaches are adopted such as engineered optical coatings or automotive paints.

A prototype of colored solar car roof was manufactured by Fraunhofer ISE using Morpho-Color glass coating as nanophotonic multilayer structure.[36] The spectral engineering of the photonic filter could allow a wide range of colors, while keeping efficiency loss as low as 7%.

Masuda et al. showed colorful CIGS SCs by adding automotive paints based on pigments of glass flakes and mica flakes, which were originally designed for mass-produced cars.[531] Many chromatic colors were obtained such as blue, green, red, and gold, having bright and uniform appearance similar to standard exterior of car bodies. This technology allowed a preservation of about 95% of the initial short-circuit current value. Similarly, blue-colored large-area c-Si module was showed, using diluted automotive paint with around 10% weight concentration of mica pigment. The colored solar module retained around 80% of the output power, compared to the original counterpart.[532]

Since the best place for the integration of PV is the roof of the vehicle, severe space constraints are imposed, hence, higher power-conversion efficiency is demanded.[35] Several curved, flexible and lightweight high-efficiency PV technologies are explored as potential candidates for VIPV such single junction c-Si, III–V, perovskite CIGS, concentrated SCs, and multijunction SCs.[35,522,533]

Considering the vehicle-integrated PV (VIPV) on the roof of passenger cars, Heinrich et al estimated that the currently available c-Si technology with an area of (1.7–2 m^2) and a price below 120 € $piece^{-1}$ can yield a solar driving distance of up to 1900–3400 km $year^{-1}$.[36]

Several manufacturers like SonoMotors and Lightyear are developing PV-powered passenger vehicles equipped with c-Si SCs with a close stage to the market.[35,202]

However, multijunction SC technologies are considered more promising to boost the integration in PV-powered vehicles due to their higher PCE levels (typically over 30%), albeit

elevated prices for commercial use.[35,278] In the same framework of the energy yield estimation applied for c-Si technology, assuming tandem multijunction SC technology with efficiency of 30%, a yearly driving range of ≈15 000 km by means of solar energy can be achieved, with a potential rise under higher solar irradiation levels.[36] Among the representative car models with PV-equipped solar roofs are the Mercedes Vision EQXX, Hyundai Motors Sonata and the Toyota Prius PHV. The latter car model can be seen in Figure 15e, using Sharp's high-efficiency III–V InGaP/GaAs/InGaAs triple-junction solar modules with an efficiency of 32.84% and output power of 860 W, providing a driving range that can reach about 44 km day^{-1}.[522] Intriguingly, bandgap tuning plays a crucial role in solving the spectrum mismatching problem for three-junction multijunction cells through the adjustment of the bandgap in the bottom cell.[534] Recently, modeling studies of electric vehicles in different climatic regions found that the average annual solar range of an electric vehicle with integrated PV with 454 Wp can amount to nearly 35% of the annual mileage of a car in the most favorable climatic conditions.[535]

Challenges and Prospects: In a recent review paper about vehicle-integrated PV, Commault et al. presented the current status of different integration projects from early development to commercialization level in cars, and trucks, but also in drones and planes.[536] The main technological challenges facing VIPV are related to high-efficiency and low-cost requirements, the non-planar curved shape of the vehicle-body, area and weight restrictions, difference of the solar irradiance compared to standard PV, utilization and the storage of the generated power and the transformation losses.[35,36,202,537,538] Given the lack of works on colored solar car roofs, further development and demonstration of prototypes using vehicle-compatible coloration approaches on different relevant PV technologies is required to upgrade the technical maturity closer to the industrialization. Moreover, the rise of temperatures under sunny conditions may induce PV performance losses and then reduce the practical driving ranges of PV-powered vehicles relative to the estimated values. This could be a hint for a possible application of radiative cooling of PV in vehicles. Given the requirements of high-efficiency and low cost, other multijunction technologies, especially, perovskite/c-Si, and all-perovskite tandem can be promising candidate for VIPV. This has attracted the interest of several companies such as Oxford PV and Swift Solar. Hence, bandgap tuning would play a key role in the control of the optimal bandgap combination for high-efficiency tandem devices.

Despite all the challenges, the integration of PV into vehicles proved to be beneficial for all kind of cars from electric to hybrid to conventional, by minimizing the charging time and extending distance range or by reducing the fuel consumption, with supporting activities, respectively.[36] This paves the route toward ambitious objectives to reach a new large PV markets with more than 10 and 50 GW in 2030 and 2040, respectively, owing to the development of PV-powered vehicles.[522]

4.3.5. Aerospace Applications

For the applications in high-altitude satellites, unmanned aerospace aircrafts, orbital, and planetary space stations, PV technologies with high power-to-weight ratio, mechanically flexible and radiation hardness characteristics are typically desired.[19,197] Recently, apart from the standard c-Si and III–V-based SCs, a growing interest was attributed to testing different emerging PV technologies such as perovskite and organic for potential aerospace applications (Figure 15f).[523,539–544] This opens new opportunities for thermal and bandgap tuning in such thin-film PVs to further promote their integration.

Relevant Tunability Features: Bandgap tuning play a crucial role in controlling the performance of multijunction SC oriented for space applications. This is mainly related to high-efficiency III–V tandem technologies which are available in the market of space PV from different companies such as Azur space and Spectrolab. Regarding the bandgap dependence on the surrounding environment, it was reported that the optimum energy bandgap of SC absorber in either single or multijunction configuration can be altered in higher latitudes and under different solar spectrum conditions including extraterrestrial AM0.[545,546] This could be extended as an indicative approach of bandgap tuning to match a particular solar spectrum available at different atmospheres for maximum power generation.[197] Extraterrestrial application scenarios, where SCs could be exposed to high energy degrading UV radiation, could benefit from spectral cooling approaches with UV-reflection features.[197]

On the thermal tuning aspect, in the absence of convective media in space and exposure to extreme temperature fluctuations, thermal radiation is the dominant heat exchange channel for space SCs to cool down under solar irradiance.[170] Therefore, passive radiative cooling approaches present a strategic thermal tuning pathway for excess heat disposal in space. The largest benefits of radiative cooling is assumed for space and extraterrestrial applications.[419] The expected temperature reduction and cooling power level are dependent on the bandgap of the PV absorber. Moreover, for near-sun missions operating at temperatures that can substantially exceed 400 K, more salient cooling benefits are anticipated.[419]

Relevant Research and Development: In the context of radiative cooling for space applications, Banik et al. demonstrated that an efficient IR thermal emitter using organopolysilazane-derived silicon oxycarbonitride (SiCNO) thin polymer coating on ultra-lightweight and flexible CIGS SCs can reduce the operating temperature by up to 30 °C in a lower earth orbit under full solar irradiance, corresponding to an enhancement in maximum power point of 27% (Figure 15g,h).[524] This was achieved by the increase of emissivity by more than 0.4 compared to the bare baseline cell without affecting the power conversion performance. Similar approaches made previously using a dual layer high emissivity coating of Al_2O_3/SiO_2 and silazane/alumina were also reported to have increased the emissivity of flexible CIGS for space applications.[547,548] Sato et al. demonstrated a passive temperature control approach using a spectrally selective multi-layer emitter on GaAs modules that allows emission between 4 and 9 μm and reflects between 9 and 20 μm.[549] This enabled the SCs to passively cool down as they benefit from having high emissivity at high temperature and simultaneously prevented them from plummeting to extreme low temperatures. Recently, photonic structure-based radiative coolers for SCs via orb-shaped membrane energy gathering array concept (SSPS-OMEGA) was proposed.[550] The opto-thermo-electrical

model predicted a temperature reduction of at least 30 °C, indicating a 1.4% increase in PCE of the SCs and corresponding to a 93 MW increase in power output of a 2 GW SSPS-OMEGA system. These cost-effective and scalable PRC approaches can replace the glass cover, thereby reducing power-to-mass ratio of solar modules, which would be very advantageous for space and high-altitude applications.

Challenges and Prospects: Radiative cooling for space application exists until now only in laboratory scale research. Tests and validation in outer space environment have to be conducted to increase the readiness level of this technology. Hereby, further research should be conducted in relevant environments to verify the effectiveness of passive cooling on space PV and the protective nature of the coating materials.

5. Conclusions and Outlooks

The development of PV technologies with customized design capabilities offers widespread integration opportunities in distributed applications beyond power generation. Tunable PVs allow manipulation of their intrinsic properties via adjusted functional materials or tailored retrofit incorporation. Depending on the requirements of the target application, the adaptable features of tunable PV can enable multifunctional characteristics such as aesthetic appearance, visual comfort, and heat insulation.

In this work, we present an overview of tunable SC technologies from fundamental principles of tuning approaches to state-of-the-art SC technologies to relevant PV-integrated applications. The focus is set on spectrum-sensitive aspects related to optoelectronic and thermal tuning capabilities in terms of absorber bandgap, color perception, visible transmission and thermal management. For each of the above-mentioned tuning aspects, the recent progress of representative examples is discussed. Then, we assess the possible integration scenarios of tunable PV into real-world systems for terrestrial, marine and aerospace applications. The evaluation is addressed in the framework of a TRL approach including experimental proof-of-concepts at research level, technology development and validation in relevant environments and systems demonstration and deployment in an operational environment towards commercialization.

Accordingly, in **Figure 16**, we classify the main SC technologies presented along in this review as a function of technical maturity and relevant application. The most advanced TRL levels of different tunable integrated PVs are pointed out with yellow boxes. The technical maturity bars are attributed to the type of relevant tunable PV in orange boxes. Herein, we discuss the specifications of each tuning capability for the adaptation of customized PV technologies to a specific application. It is noteworthy that some categories of tunable PV can involve a combination of different tuning capabilities as illustrated by color bars. The analysis is based on the presented overview throughout the previous sections of this review.

5.1. Façades

Opaque colored PV technologies with color tuning capabilities are suitable for the integration in building skins. Both external (nanophotonic structure and ARC) and internal (intrinsic components of PV devices) modification strategies can be applied. However, complex and expensive approaches must be avoided. For this purpose, external coloration strategies based on multilayer structures or antireflection coatings are widely accepted as the preferred methods. For the majority of colored opaque SCs, the optimal bandgap is around 1.1 eV. For aesthetic purposes, colored modules with saturated colors, angle-insensitive homogeneous appearance, and minimal power losses compared to opaque counterparts are desired. In particular, elegant and fresh white color is highly-demanded for building architectures. Such white PV are expected not only to fulfill power generation and aesthetic functions, but also to provide thermal benefits through radiative cooling of the interior spaces. Given the universal recommendations for the white painting of buildings, white PV module might be a future big trend in BIPV. Owing to the tremendous research and development activities, colorful PV technologies have achieved an advanced TRL. In this regard, standard c-Si with multilayer photonic structures on cover glass is one of the most established opaque colored PV technologies. Using this technology, several building projects with aesthetical façade-integrated PV were demonstrated. On the market, several companies offer high-efficiency PV panels with wide range of colors, such as colored c-Si (Solaxess, ISSOL, and Lof Solar, etc.), CIGS (AVANCIS) and organic solar cells (Heliatek). We envision that establishing standard technological solutions would further promote the widespread of opaque colored PV modules in building façades.

Semitransparent colored PV technologies with predefined static tuning are suitable for glass-based façades in buildings. To fulfill multiple functionalities in terms of power generation, aesthetic appearance, and visual comfort, the integrated PVs should exhibit high and narrow peak transmission (>20%), vivid coloration and a medium PCE between 5% and 15%. Such semitransparent colored solar façade can passively prevent incoming sunlight from overheating the interior spaces. Both external (nanophotonic structure and LSC) and internal (intrinsic component of PV device) modification strategies can be applied. However, simple, cost-effective and fabrication-compatible approaches should be adopted. In this context, color tuning by changing the transparent electrode thickness might be the most straightforward method. Owing to the achieved scientific and technological progress, several semitransparent-colored PV technologies have reached an advanced maturity level. In this context, colored solar façade systems were integrated in representative buildings using DSSC by Solaronix and a-Si PV technology by Onyx. Commercial tinted ST-PV products for the building façade systems are also provided from other different technologies such as CdTe from Toledo Solar and OPV from ASCA. Significant research and development activities have been performed on emerging colored thin-film ST-PVs based on organic and perovskite absorbers. These technologies are validated at lab scale and are considered among the best candidates for colored solar façade, that allow excellent trade-off between efficiency and peak transmission, as well as, wide range of colors with high purity. However, further demonstrations of large-scale prototypes in operational environment are required to reinforce the transition of the corresponding TRL from emerging technology status to a mature industry.

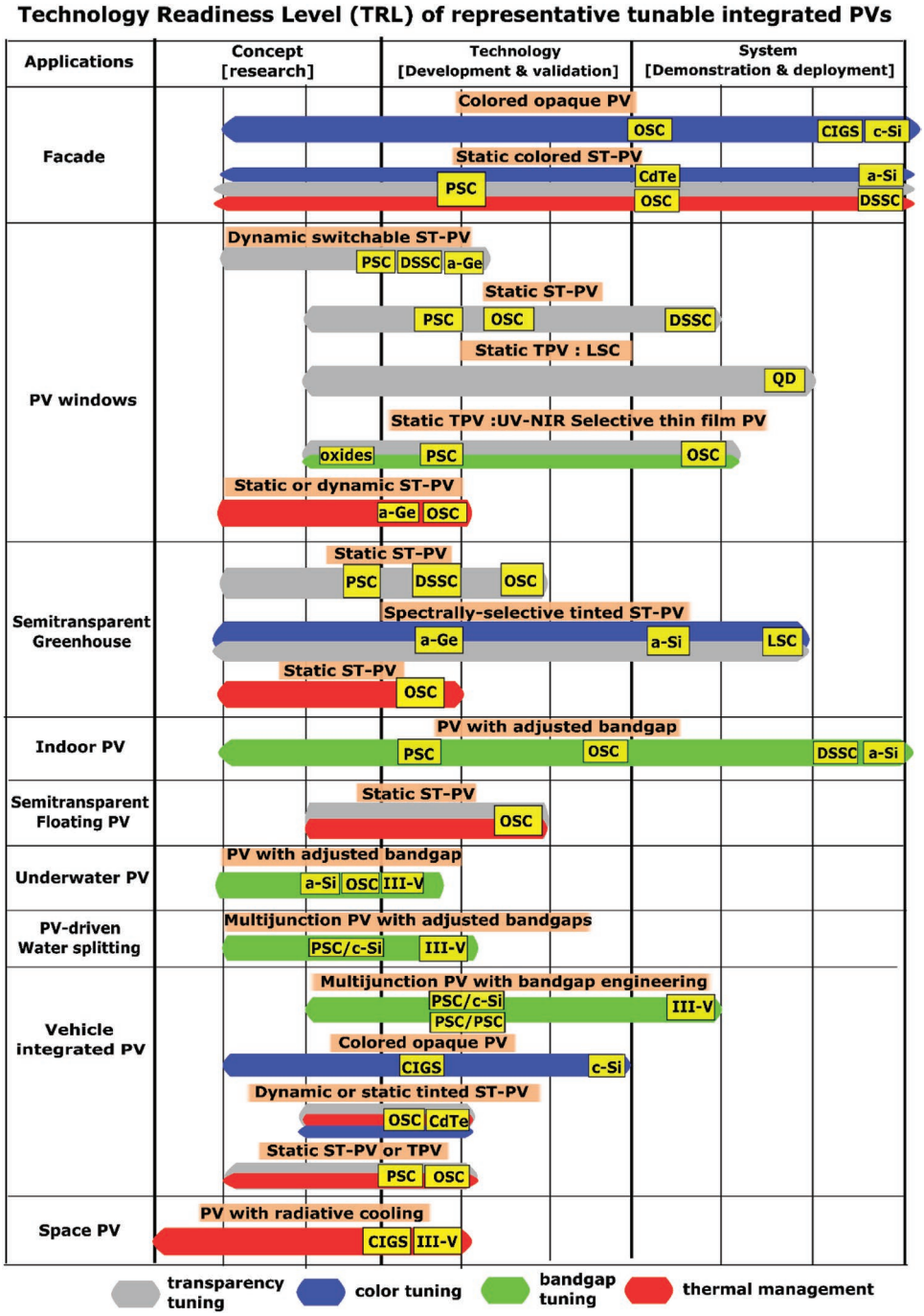

Figure 16. Overview about TRL status of representative tunable PVs with regard to relevant applications.

Furthermore, detailed evaluations of the contribution of colored solar façades in the thermal management of buildings would be insightful for system integration purposes.

5.2. PV Windows

Dynamically switchable ST-PVs with reversible modulation of light transmission or color perception are promising technologies for smart window applications. A suitable trade-off between PCE and AVT is required. The main successful experimental proof-of concepts of relevant PV technologies are thermochromic PSC,[139] gasochromic ultrathin a-Ge SC,[24,123,126] and photochromic DSSC.[128] In order to promote the competitiveness of these technologies validated at lab scale, further enhancement of PCE and AVT output is required. Moreover, dynamically switchable ST-PVs are facing additional technological challenges such as cyclability, switching margin, and degradation issue. Considering switchable SCs as a nascent research field, further optimization efforts and development of novel

responsive materials and concepts are still needed to promote its technical maturity. As a perspective, the stimuli-response must be optimized and selected according to the target functionality. Hence, switchable SC technologies using electrochromic switching mechanism could be a suitable strategy for the integration in PV windows, considering the compatibility with the already-installed smart windows in urban buildings.

Static ST-PVs can be suitable technologies for the integration on glass surfaces of buildings. In order to ensure multifunctional benefits with respect to power generation, light transmission and visual comfort, suitable specifications of PCE (5–10%), AVT (>50%), and CRI (close to 100) must be satisfied. In addition to the direct integration as power-generating PV windows, ST-PV with low efficiency level (PCE ≈ 2–5%) might be a possible solution for powering smart windows. Typically, ST-PV with thinned absorber tend to exhibit a tinted appearance, in contrast to the desired neutral grey, which is considered as the popular choice for architectural aesthetic. One of the important steps toward the integration of ST-PV in windows was the demonstration of full-scale prototype of semitransparent PV window based on DSSC technology in operational environment over a period of two years.[434] Among different thin-film ST-PV, perovskite and organic-based SC technologies demonstrated outstanding trade-off between AVT and PCE at research lab level.[51] Although, the development of ST-PV technologies for PV window is attracting a huge interest from the scientific research community, detailed demonstrations of large-scale prototypes from different ST-PV technologies in operational environment have yet to be achieved. This would be a substantial step for reliable lab-to-fab transfer and for bridging research and industry.

Transparent LSC-PV based on QD or conjugated polymers are one of the most suitable and mature strategies for PV windows. High transparency and color neutrality are the desired features for the integration of LSC windows with unaltered visibility. Despite excellent optical and aesthetic characteristics of LSC-PV, the low efficiency, in particular at large scale, remain a challenging issue for their integration in windows. Further optimization of efficiency at large-scale and prevention of performance losses can be tackled by the development of advanced luminophore materials with high quantum yield and Stokes shift. Nevertheless, taking the benefits of the long development history over the last decades, LSC-PV technologies are well positioned in the TRL level chart and get closer to the commercialization level in the window industry. In this regard, QD-based LSC products are commercially available from UbiQD and ClearVue PV. In this perspective, glass surfaces in buildings should no longer be considered as only construction components, but also as renewable energy resource. To further promote the social acceptance of LSC-PV windows, techno-economic aspects such long-term stability and the analysis of power yield and payback time should be further considered in the future.

UV–NIR selective thin-film TPVs are promising solutions for PV windows toward the fulfillment of the optoelectronic specifications such as PCE (5–10%), AVT (>50%), and CRI (close to 100). The bandgap tuning plays a crucial role for UV-selective harvesting (E_g > 3.2 eV) and NIR-selective harvesting (E_g< 1.6 eV). Although UV-selective PV based on metal oxide or perovskite materials could enable high AVT, they suffer from low PCE and sensitive control of CRI. A combination of UV and NIR-selective perovskite into tandem configuration is considered as a distinguished technological innovation, but, impose manufacturing constraints.[359] Organic-based wavelength selective TPVs can be considered as the most promising technologies for window applications. However, most of the realized concepts at lab-scale level should be further developed and upscaled to push the TRL towards industrialization. The significant progress in organic wavelength-selective TPV realized by Ubiquitous Energy can further promote the PV window industry.

ST-PV integrated into windows can play an important role in the thermal management and the heat insulation. This can be ensured by tuning the IR transmission and the emissivity within ST-PV. The thermal behavior of switchable gasochromic a-Ge ST-PV was demonstrated in double glazing configuration at lab scale.[24] Heat insulation function was also validated in organic ST-PV.[23] However, further demonstrations of large-scale prototypes in operational environment are still lacking to assess the heat management in real interior spaces of buildings. We expect unprecedented possibilities of technology design by combining passive radiative cooling and power generation in smart PV window for all-season household thermal regulation.

5.3. Semitransparent Greenhouses

ST-PV with high transparency at photosynthetic active region are suitable for the integration in semitransparent greenhouses. Different thin-film PV are considered as potential technologies using photoabsorbers such as organic, dye-sensitized and perovskite materials. While the compatibility of semitransparent PSC[462] and DSSC[474] with plant's absorption spectra was experimentally proved, organic ST-PV technology was evaluated in a relevant plant growth environment.[37] Moreover, development activities on organic ST-PV for greenhouse roofs is on-going at the spin-off company Vitsolc. Hence, the integration of ST-PV in greenhouses is still in the testing phase. Further upscaling approaches and technological validation efforts are required to advance the TRL. Hence, the evaluation of crop growth yield in large scale microclimate similar to commercial greenhouses would be insightful. This should be accompanied with relevant economic analysis to accurately estimate the economic value of semitransparent greenhouse compared to conventional counterpart.

Tinted or spectrally-selective ST-PV having a compatible transmission peak with plant growth are considered for semitransparent greenhouses. Spectrally selective ultrathin a-Ge ST-PV using multilayer photonic structures was validated in a lab scale photo-bioreactor.[468,469] Tinted semitransparent a-Si panels was demonstrated on small-scale demonstrator greenhouses.[470] A system of spectrally-selective solar-powered greenhouse using dye-based luminescent concentrator has proven itself in operational environment.[466] Greenhouse-integrated PV systems, using ST-PV technologies such as spectrally-selective LSC from Soliculture and tinted a-Si from Polysolar, are already available in the market.

ST-PV integrated in a greenhouse can play a beneficial role in the thermal management. This is manifested by spectrally controlling the emissivity and the IR transmission. A reduction of the heating load in a plant growth box equipped with organic ST-PV was already validated at a lab scale.[37]

5.4. Indoor PV

The matching of artificial light sources in indoor PV application requires SC with adjusted bandgap (1.9 eV < E_g < 2.1 eV). While conventional IPV technologies such as a-Si and DSSC already exist in the market, perovskite and organic thin-film SC technologies are emerging as contenders for commercialization. These technologies could greatly benefit from their inherent bandgap tunability. To enable competitively-commercialized IPV technologies different challenges such as manufacturing cost, scalability, stability, toxicity concerns, and market dynamics must be tackled. Interestingly, the evolution of the indoor IoT/wireless sensors market is expected to revolutionize IPV field, leading to a fast-growing market.

5.5. Semitransparent Floating PV

Semi-transparent SCs open new opportunity for the application in floating PV. The light transmission should be adjusted to ensure a compatibility with spectral absorption of the algae. In addition, SC should act as thermal barriers of the heat flux to mitigate the water evaporation. Owing to the suitable trade-off between PCE and AVT, organic ST-PV is considered as a fitting technology for semitransparent floating PV application. However, this technology is only partly evaluated in a relevant environment and hence, this integrated PV scheme is still in the testing phase.[42,498,502] In this regard, further detailed analysis and technological optimization are required.

5.6. Underwater PV

SCs with wide-bandgap photoactive materials (E_g > 1.8 eV) are required for underwater PV application. This is due to the alteration of the light spectrum by scattering and absorption effects. The optimum band gap shifts towards higher values with increasing water depth, reaching ≈2.4 eV at 50 m.[43] Therefore, as experimental proof-of-concepts, PV technologies based on a-Si, organic and III–V materials were submerged in water.[43] However, PV integration in underwater application is still in an early technological stage. Further development of SCs with wide-bandgap absorber and detailed evaluation in the relevant underwater environment could be some of the steps to take to advance the TRL.

5.7. PV-Driven Water Splitting

SCs with wide-bandgap photoactive materials (E_g > 1.8 eV) are also required for PV-driven water splitting due to the required energy and the overpotentials. In two-junction SCs with tandem configuration, the ideal bandgap combination is (1.7 eV/1.05 eV) to achieve a maximum solar to hydrogen efficiency. Among different SC types, III–V multijunction technology have demonstrated the best performance and have reached the most advanced TRL.[505,511] However, large-scale system with long-term stability and cost-effective fabrication has to be realized to enable the progress toward more practical solar hydrogen production. Emerging multijunction technologies, such as perovskite/c-Si tandem can be promising candidate for water splitting applications,[516] considering their high efficiency and their suitable bandgap combination.

5.8. Vehicle-Integrated PV

Depending on the integration scenario, different tunability aspects of SCs are desired for vehicle-integrated PV.

Since the roof is the preferred place for installation, high-efficiency SC are required due to the limited surface. Multijunction PV modules based on III–V materials are considered as one of the promising candidates. The band tuning in these devices is not only beneficial for the boost of performance, but also for preventing the spectrum mismatching problem. The implementation of III–V multijunction modules on car roofs has reached an advanced TRL close to full commercialization. Given the requirements of high-efficiency and low cost, other multijunction technologies, especially, perovskite/c-Si and all-perovskite tandem can be promising contenders for VIPV. Such technologies are currently under intensive development by several companies such as Oxford PV and Swift Solar, respectively. This would be a promising future direction for the field of VIPV. In this framework, bandgap tuning would play a key role in the control of the optimal bandgap combination (1.6 eV < E_g < 1.9 eV [top]/0.9 eV < E_g < 1.2 eV) [bottom]) for high performance two-junction PV devices. In particular, all perovskite tandem would be a good option for flexible and lightweight PV application.

Colored opaque modules with vivid colors, angle-invariant homogeneous appearance and minimal power losses are also desired for aesthetic purposes. The main colored PV technologies that have been already integrated on car roof are CIGS[531] and c-Si PV[532] using automotive painting and c-Si modules with nanophotonic structures.[36] As the color of the vehicle is a crucial attribute for the market penetration, further progress in the research and development for colorful VIPV is strongly recommended.

On the glass surfaces such as windows and sunroofs, semi-transparent PV can satisfy the specifications of power generation, light transmission, and visual comfort. To date, there is only one single lab-scale example of switchable ST-PV as a smart window in the sunroof.[122] This is also expected to reject IR radiation and lower the interior temperature. Development activities on organic ST-PV for sunroofs is on-going at the spin-off Vitsolc. Considering the lack of examples for the technological integration of ST-PV into vehicle windows, further research and development activities are recommended to obtain a detailed assessment and to advance the corresponding TRL.

5.9. Space PV

High-efficiency SC technologies are mandatory for aerospace PV applications due to the limited available area and weight constraints. Given the absence of convective media in space, passive radiative cooling of PV module is considered as promising thermal management strategy. Significant temperature reduction was demonstrated on III–V[549] and CIGS-based PV[524] modules with high-emissivity. Bandgap tuning can be beneficial in multijunction configuration and also under extraterrestrial spectrum conditions. Further advances in the technological maturity of tunable PV would necessitate more testing missions in the outer space environment. In addition, beyond spectrum-related aspects, further customization attributes need to be considered such as high power-to-weight ratio, mechanical flexibility, and radiation hardness. Thus, passive radiative cooling approaches can be an appropriate alternative for standard heavy and rigid standard cover glasses in the integration of flexible and lightweight space PV.

To push forward the technical maturity, there are general requirements that are valid for all the mentioned integration scenarios of tunable PV. These include, but are not limited to the long-term stability, scalability with minimal cell-to-module efficiency gap, cost-effective fabrication. Different aspects such as social acceptance, extensive collaboration of all stakeholders and policy should be also considered. For instance, this implies a more effective cooperation with architects for BIPV, farmers for agrivoltaics and engineers for vehicle-integrated PV.

It is also important to consider further tuning capabilities beyond spectrum-sensitive aspects, mainly, flexible, and lightweight attributes. Nowadays, flexible PV are considered more promising than rigid counterparts in terms of cost and productivity. Hence, it is expected that flexible lightweight solar panels will be the foremost option to achieve industrialization and commercialization by PV manufacturers. This would also expand the customized integration solutions for extra applications such as wearable PV for self-powered electronics.[41]

It is noteworthy that the presented TRL chart of tunable PVs adapted to versatile applications is only a simplified overview attempt. This might trigger an establishment of a relevant consensus statement for technical maturity assessment of TRL status related to different integrated PV. Such initiative would enable timely tracking of the technical progress and would offer a perfect bridge between research and industry.

To this end, considering the achieved progress and the exceptional adaptability to versatile applications, we envision a bright future for tunable integrated PV technologies.

Supporting Information

Supporting Information is available from the Wiley Online Library or from the author.

Acknowledgements

The authors acknowledge funding from the Energy branch of the German Aerospace Center (DLR).

Open access funding enabled and organized by Projekt DEAL.

Conflict of Interest

The authors declare no conflict of interest.

Keywords

band gap engineering, colored solar cells tunable photovoltaics, dynamic optical switching, optoelectronic properties, photonic engineering, solar energy distributed applications, spectral engineering, transparent solar cells

Received: March 1, 2022
Revised: April 19, 2022
Published online:

[1] D. Bogdanov, J. Farfan, K. Sadovskaia, A. Aghahosseini, M. Child, A. Gulagi, A. S. Oyewo, L. de Souza Noel Simas Barbosa, C. Breyer, *Nat. Commun.* **2019**, *10*, 1077.
[2] D. Gielen, F. Boshell, D. Saygin, M. D. Bazilian, N. Wagner, R. Gorini, *Energy Strategy Rev.* **2019**, *24*, 38.
[3] N. Haegel, S. Kurtz, *IEEE J. Photovoltaics* **2021**, *11*, 1335.
[4] IEA, International Energy Agency, Global Energy Review, https://www.iea.org/reports/global-energy-review-2021 (accessed: January 2022).
[5] P. A. Owusu, S. Asumadu-Sarkodie, *Cogent Eng.* **2016**, *3*, 1167990.
[6] M. Victoria, N. Haegel, I. M. Peters, R. Sinton, A. Jäger-Waldau, C. Del Cañizo, C. Breyer, M. Stocks, A. Blakers, I. Kaizuka, K. Komoto, A. Smets, *Joule* **2021**, *5*, 1041.
[7] R. R. Hernandez, A. Armstrong, J. Burney, G. Ryan, K. Moore-O'Leary, I. Diédhiou, S. M. Grodsky, L. Saul-Gershenz, R. Davis, J. Macknick, D. Mulvaney, G. A. Heath, S. B. Easter, M. K. Hoffacker, M. F. Allen, D. M. Kammen, *Nat. Sustain.* **2019**, *2*, 560.
[8] C. Breyer, D. Bogdanov, A. Aghahosseini, A. Gulagi, M. Child, A. S. Oyewo, J. Farfan, K. Sadovskaia, P. Vainikka, *Prog. Photovoltaics Res. Appl.* **2018**, *26*, 505.
[9] C. Breyer, D. Bogdanov, A. Gulagi, A. Aghahosseini, L. S. Barbosa, O. Koskinen, M. Barasa, U. Caldera, S. Afanasyeva, M. Child, J. Farfan, P. Vainikka, *Prog. Photovoltaics Res. Appl.* **2017**, *25*, 727.
[10] T. W. Brown, T. Bischof-Niemz, K. Blok, C. Breyer, H. Lund, B. V. Mathiesen, *Renewable Sustainable Energy Rev.* **2018**, *92*, 834.
[11] A. Blakers, M. Stocks, B. Lu, C. Cheng, R. Stocks, *IEEE J. Photovoltaics* **2019**, *9*, 1828.
[12] M. Victoria, K. Zhu, T. Brown, G. B. Andresen, M. Greiner, *Prog. Photovoltaic Res. Appl.* **2020**, *28*, 483.
[13] NREL's Best Research-Cell Efficiency Chart, https://www.nrel.gov/pv/assets/pdfs/best-research-cell-efficiencies-rev210726.pdf (accessed: January 2022).
[14] M. A. Green, *Joule* **2019**, *3*, 631.
[15] J. Jean, M. Woodhouse, V. Bulović, *Joule* **2019**, *3*, 2824.
[16] N. M. Haegel, H. Atwater, T. Barnes, C. Breyer, A. Burrell, Y.-M. Chiang, S. de Wolf, B. Dimmler, D. Feldman, S. Glunz, J. C. Goldschmidt, D. Hochschild, R. Inzunza, I. Kaizuka, B. Kroposki, S. Kurtz, S. Leu, R. Margolis, K. Matsubara, A. Metz, W. K. Metzger, M. Morjaria, S. Niki, S. Nowak, I. M. Peters, S. Philipps, T. Reindl, A. Richter, D. Rose, K. Sakurai, et al, *Science* **2019**, *364*, 836.
[17] C. J. Traverse, R. Pandey, M. C. Barr, R. R. Lunt, *Nat. Energy* **2017**, *2*, 849.
[18] G. P. Kini, S. J. Jeon, D. K. Moon, *Adv. Funct. Mater.* **2021**, *31*, 2007931.

[19] Y. Hu, T. Niu, Y. Liu, Y. Zhou, Y. Xia, C. Ran, Z. Wu, L. Song, P. Müller-Buschbaum, Y. Chen, W. Huang, *ACS Energy Lett.* **2021**, *6*, 2917.
[20] K. Lee, H.-D. Um, D. Choi, J. Park, N. Kim, H. Kim, K. Seo, *Cell Rep. Phys. Sci.* **2020**, *1*, 100143.
[21] Z. Li, T. Ma, H. Yang, L. Lu, R. Wang, *Sol. RRL* **2021**, *5*, 2000614.
[22] A. K. Jena, A. Kulkarni, T. Miyasaka, *Chem. Rev.* **2019**, *119*, 3036.
[23] C. Sun, R. Xia, H. Shi, H. Yao, X. Liu, J. Hou, F. Huang, H.-L. Yip, Y. Cao, *Joule* **2018**, *2*, 1816.
[24] M. Götz-Köhler, U. Banik, H. Meddeb, N. Neugebohrn, D. Berends, K. Gehrke, M. Vehse, C. Agert, *Sol. Energy* **2022**, *232*, 433.
[25] Di Wang, R. Qin, G. Zhou, X. Li, R. Xia, Y. Li, L. Zhan, H. Zhu, X. Lu, H.-L. Yip, H. Chen, C.-Z. Li, *Adv. Mater.* **2020**, *32*, 2001621.
[26] E. Dauzon, X. Sallenave, C. Plesse, F. Goubard, A. Amassian, T. D. Anthopoulos, *Adv. Mater.* **2021**, *33*, 2101469.
[27] S. Kim, H. van Quy, C. W. Bark, *Mater. Today Energy* **2021**, *19*, 100583.
[28] X. Li, P. Li, Z. Wu, D. Luo, H.-Y. Yu, Z.-H. Lu, *Mater. Rep. Energy* **2021**, *1*, 100001.
[29] M. O. Reese, S. Glynn, M. D. Kempe, D. L. McGott, M. S. Dabney, T. M. Barnes, S. Booth, D. Feldman, N. M. Haegel, *Nat. Energy* **2018**, *3*, 1002.
[30] M. Zhu, F. Zhu, O. G. Schmidt, *Nano Mater. Sci.* **2021**, *3*, 107.
[31] P. Albert, A. Jaouad, G. Hamon, M. Volatier, C. E. Valdivia, Y. Deshayes, K. Hinzer, L. Béchou, V. Aimez, M. Darnon, *Prog, Photovoltaics Res. Appl.* **2021**, *29*, 990.
[32] Y. Hu, Y. Chu, Q. Wang, Z. Zhang, Y. Ming, A. Mei, Y. Rong, H. Han, *Joule* **2019**, *3*, 2076.
[33] D. H. Kim, J. B. Whitaker, Z. Li, M. F. van Hest, K. Zhu, *Joule* **2018**, *2*, 1437.
[34] M. Batmunkh, Y. L. Zhong, H. Zhao, *Adv. Mater.* **2020**, *32*, 2000631.
[35] International Energy Agency, Photovoltaic Power Systems Programme, https://iea-pvps.org/ (accessed: January 2022).
[36] M. Heinrich, C. Kutter, F. Basler, M. Mittag, L. Alanis, D. Eberlein, A. Schmid, C. Reise, T. Kroyer, D. Holger Neuhaus, H. Wirth, *37th European PV Solar Energy Conference and Exhibition*, EUPVSEC, Online **2020**, p. 1695.
[37] E. Ravishankar, M. Charles, Y. Xiong, R. Henry, J. Swift, J. Rech, J. Calero, S. Cho, R. E. Booth, T. Kim, A. H. Balzer, Y. Qin, C. Hoi Yi Ho, F. So, N. Stingelin, A. Amassian, C. Saravitz, W. You, H. Ade, H. Sederoff, B. T. O'Connor, *Cell Rep. Phys. Sci.* **2021**, *2*, 100381.
[38] I. Mathews, S. N. Kantareddy, T. Buonassisi, I. M. Peters, *Joule* **2019**, *3*, 1415.
[39] V. Pecunia, L. G. Occhipinti, R. L. Z. Hoye, *Adv. Energy Mater.* **2021**, *11*, 2100698.
[40] C. Polyzoidis, K. Rogdakis, E. Kymakis, *Adv. Energy Mater.* **2021**, *11*, 2101854.
[41] S. A. Hashemi, S. Ramakrishna, A. G. Aberle, *Energy Environ. Sci.* **2020**, *13*, 685.
[42] N. Zhang, G. Chen, Y. Xu, X. Xu, L. Yu, *ACS Appl. Energy Mater.* **2019**, *2*, 6060.
[43] J. A. Röhr, J. Lipton, J. Kong, S. A. Maclean, A. D. Taylor, *Joule* **2020**, *4*, 840.
[44] I. Burgués-Ceballos, L. Lucera, P. Tiwana, K. Ocytko, L. W. Tan, S. Kowalski, J. Snow, A. Pron, H. Bürckstümmer, N. Blouin, G. Morse, *Joule* **2021**, *5*, 2261.
[45] F. M. van der Staaij, I. M. van Keulen, E. von Hauff, *Sol. RRL* **2021**, *5*, 2100167.
[46] Perovskites take steps to industrialization, Editorial, *Nat. Energy* **2020**, *5*, 1.
[47] J. Guillemoles, T. Kirchartz, D. Cahen, U. Rau, *Nat. Photonics* **2019**, *13*, 501.
[48] M. Patel, J. H. Seo, T. T. Nguyen, J. Kim, *Cell Rep. Phys. Sci* **2021**, *2*, 100591.
[49] R. Zhou, J. Xu, P. Luo, L. Hu, X. Pan, J. Xu, Y. Jiang, L. Wang, *Adv. Energy Mater.* **2021**, *11*, 2101923.
[50] P. K. Nayak, S. Mahesh, H. J. Snaith, D. Cahen, *Nat. Rev. Mater.* **2019**, *4*, 269.
[51] O. Almora, D. Baran, G. C. Bazan, C. Berger, C. I. Cabrera, K. R. Catchpole, S. Erten-Ela, F. Guo, J. Hauch, A. W. Y. Ho-Baillie, T. J. Jacobsson, R. A. J. Janssen, T. Kirchartz, N. Kopidakis, Y. Li, M. A. Loi, R. R. Lunt, X. Mathew, M. D. McGehee, J. Min, D. B. Mitzi, M. K. Nazeeruddin, J. Nelson, A. F. Nogueira, U. W. Paetzold, N.-G. Park, B. P. Rand, U. Rau, H. J. Snaith, E. Unger, et al, *Adv. Energy Mater.* **2021**, *11*, 2102526.
[52] O. Almora, C. I. Cabrera, J. Garcia-Cerrillo, T. Kirchartz, U. Rau, C. J. Brabec, *Adv. Energy Mater.* **2021**, *11*, 2100022.
[53] H. Wang, J. Li, H. A. Dewi, N. Mathews, S. Mhaisalkar, A. Bruno, *J. Phys. Chem. Lett.* **2021**, *12*, 1321.
[54] A. Polman, M. Knight, E. C. Garnett, B. Ehrler, W. C. Sinke, *Science* **2016**, *352*, aad4424.
[55] L. M. Wheeler, V. M. Wheeler, *ACS Energy Lett.* **2019**, *4*, 2130.
[56] A. A. Husain, W. Z. W. Hasan, S. Shafie, M. N. Hamidon, S. S. Pandey, *Renewable Sustainable Energy Rev.* **2018**, *94*, 779.
[57] K. Lee, N. Kim, K. Kim, H.-D. Um, W. Jin, D. Choi, J. Park, K. J. Park, S. Lee, K. Seo, *Joule* **2020**, *4*, 235.
[58] S. Wang, B. D. Weil, Y. Li, K. X. Wang, E. Garnett, S. Fan, Y. Cui, *Nano Lett.* **2013**, *13*, 4393.
[59] D. Liu, C. Yang, R. R. Lunt, *Joule* **2018**, *2*, 1827.
[60] R. Karsthof, P. Räcke, H. von Wenckstern, M. Grundmann, *Phys. Status Solidi A* **2016**, *213*, 30.
[61] A. J. Lopez-Garcia, A. Bauer, R. Fonoll Rubio, D. Payno, Z. Jehl Li-Kao, S. Kazim, D. Hariskos, V. Izquierdo-Roca, E. Saucedo, A. Pérez-Rodríguez, *Sol. RRL* **2020**, *4*, 2000470.
[62] N. C. Davy, M. Sezen-Edmonds, J. Gao, X. Lin, A. Liu, N. Yao, A. Kahn, Y.-L. Loo, *Nat. Energy* **2017**, *2*, 17104.
[63] P. Huang, S. Xu, M. Zhang, W. Zhong, Z. Xiao, Y. Luo, *Int. J. Energy Res.* **2021**, *45*, 17709.
[64] S.-Y. Chang, P. Cheng, G. Li, Y. Yang, *Joule* **2018**, *2*, 1039.
[65] D.-H. Lim, J.-W. Ha, H. Choi, S. C. Yoon, B. R. Lee, S.-J. Ko, *Nanoscale Adv.* **2021**, *3*, 4306.
[66] W. Zhang, M. Anaya, G. Lozano, M. E. Calvo, M. B. Johnston, H. Míguez, H. J. Snaith, *Nano Lett.* **2015**, *15*, 1698.
[67] I. Massiot, A. Cattoni, S. Collin, *Nat. Energy* **2020**, *5*, 959.
[68] K.-S. Chen, J.-F. Salinas, H.-L. Yip, L. Huo, J. Hou, A. K.-Y. Jen, *Energy Environ. Sci.* **2012**, *5*, 9551.
[69] A. Anand, M. M. Islam, R. Meitzner, U. S. Schubert, H. Hoppe, *Adv. Energy Mater.* **2021**, *11*, 2100875.
[70] Z. Hu, J. Wang, X. Ma, J. Gao, C. Xu, K. Yang, Z. Wang, J. Zhang, F. Zhang, *Nano Energy* **2020**, *78*, 105376.
[71] L. Duan, B. Hoex, A. Uddin, *Sol. RRL* **2021**.
[72] Y. Li, G. Xu, C. Cui, Y. Li, *Adv. Energy Mater.* **2018**, *8*, 1701791.
[73] J. Yun, *Adv. Funct. Mater.* **2017**, *27*, 1606641.
[74] K. Ellmer, *Nat. Photonics* **2012**, *6*, 809.
[75] C. Guillén, J. Herrero, *Thin Solid Films* **2011**, *520*, 1.
[76] Y. Sun, M. Chang, L. Meng, X. Wan, H. Gao, Y. Zhang, K. Zhao, Z. Sun, C. Li, S. Liu, H. Wang, J. Liang, Y. Chen, *Nat. Electron.* **2019**, *2*, 513.
[77] P. M. Rajanna, H. Meddeb, O. Sergeev, A. P. Tsapenko, S. Bereznev, M. Vehse, O. Volobujeva, M. Danilson, P. D. Lund, A. G. Nasibulin, *Nano Energy* **2020**, *67*, 104183.
[78] L. Wieland, H. Li, C. Rust, J. Chen, B. S. Flavel, *Adv. Energy Mater.* **2021**, *11*, 2002880.
[79] C.-Y. Chen, G.-H. Tan, H.-L. Hsu, C.-P. Chen, H.-W. Lin, *Adv. Energy Sustainable Res.* **2020**, *1*, 2000035.
[80] M. A. Kats, F. Capasso, *Laser Photonics Rev.* **2016**, *10*, 735.
[81] Y. Wang, P. Shen, J. Liu, Y. Xue, Y. Wang, M. Yao, L. Shen, *Sol. RRL* **2019**, *3*, 1900181.
[82] W. Li, Y. Shi, K. Chen, L. Zhu, S. Fan, *ACS Photonics* **2017**, *4*, 774.
[83] H. S. Jung, G. S. Han, N.-G. Park, M. J. Ko, *Joule* **2019**, *3*, 1850.

[84] P. D. Lund, J. Halme, G. Hashmi, I. Asghar, K. Miettunen, *Flex. Print. Electron.* **2018**, *3*, 13002.
[85] J. Qin, L. Lan, S. Chen, F. Huang, H. Shi, W. Chen, H. Xia, K. Sun, C. Yang, *Adv. Funct. Mater.* **2020**, *30*, 2002529.
[86] I. Subedi, T. J. Silverman, M. G. Deceglie, N. J. Podraza, *Sol. Energy Mater. Sol. Cells* **2019**, *190*, 98.
[87] T. J. Silverman, M. G. Deceglie, I. Subedi, N. J. Podraza, I. M. Slauch, V. E. Ferry, I. Repins, *IEEE J. Photovoltaics* **2018**, *8*, 532.
[88] L. J. Sutherland, H. C. Weerasinghe, G. P. Simon, *Adv. Energy Mater.* **2021**, *11*, 2101383.
[89] W. Wang, L. Qi, *Adv. Funct. Mater.* **2019**, *29*, 1807275.
[90] J.-H. Chai, B. T. Wong, S. Juodkazis, *Mater. Today Energy* **2020**, *18*, 100539.
[91] H. Lee, H.-J. Song, *WIREs Energy Environ.* **2021**, *10*, e403.
[92] S. Schlisske, F. Mathies, D. Busko, N. Strobel, T. Rödlmeier, B. S. Richards, U. Lemmer, U. W. Paetzold, G. Hernandez-Sosa, E. Klampaftis, *ACS Appl. Energy Mater.* **2019**, *2*, 764.
[93] Y. Guo, K. Shoyama, W. Sato, E. Nakamura, *Adv. Energy Mater.* **2016**, *6*, 1502317.
[94] K.-T. Lee, J.-Y. Jang, J. Zhang, S.-M. Yang, S. Park, H. J. Park, *Sci. Rep.* **2017**, *7*, 10640.
[95] Y. Gu, L. Zhang, J. K. W. Yang, S. P. Yeo, C.-W. Qiu, *Nanoscale* **2015**, *7*, 6409.
[96] C. Ji, K.-T. Lee, T. Xu, J. Zhou, H. J. Park, L. J. Guo, *Adv.Opt. Mater.* **2017**, *5*, 1700368.
[97] K.-T. Lee, J.-Y. Jang, S. J. Park, S. A. Ok, H. J. Park, *Nanoscale* **2017**, *9*, 13983.
[98] A. Soman, A. Antony, *Sol. Energy* **2019**, *181*, 1.
[99] R. Schregle, M. Krehel, S. Wittkopf, *Buildings* **2017**, *7*, 72.
[100] N. Jolissaint, R. Hanbali, J.-C. Hadorn, A. Schüler, *Energy Procedia* **2017**, *122*, 175.
[101] M. B. Upama, M. A. Mahmud, H. Yi, N. K. Elumalai, G. Conibeer, D. Wang, C. Xu, A. Uddin, *Org. Electron.* **2019**, *65*, 401.
[102] J. H. Noh, S. H. Im, J. H. Heo, T. N. Mandal, S. I. Seok, *Nano Lett.* **2013**, *13*, 1764.
[103] G. E. Eperon, S. D. Stranks, C. Menelaou, M. B. Johnston, L. M. Herz, H. J. Snaith, *Energy Environ. Sci.* **2014**, *7*, 982.
[104] L. Yuan, Z. Wang, R. Duan, P. Huang, K. Zhang, Q. Chen, N. K. Allam, Y. Zhou, B. Song, Y. Li, *J. Mater. Chem. A* **2018**, *6*, 19696.
[105] M. Chen, M.-G. Ju, H. F. Garces, A. D. Carl, L. K. Ono, Z. Hawash, Y. Zhang, T. Shen, Y. Qi, R. L. Grimm, D. Pacifici, X. C. Zeng, Y. Zhou, N. P. Padture, *Nat. Commun.* **2019**, *10*, 16.
[106] Y. Deng, Q. Wang, Y. Yuan, J. Huang, *Mater. Horiz.* **2015**, *2*, 578.
[107] G. E. Eperon, V. M. Burlakov, A. Goriely, H. J. Snaith, *ACS Nano* **2014**, *8*, 591.
[108] Z. Liu, L. Wu, X. Wang, Q. Xu, Y. Hu, K. Meng, G. Chen, *Nanoscale* **2020**, *12*, 8425.
[109] K.-T. Lee, M. Fukuda, S. Joglekar, L. J. Guo, *J. Mater. Chem. C* **2015**, *3*, 5377.
[110] J. Li, H. Wang, X. Y. Chin, H. A. Dewi, K. Vergeer, T. W. Goh, J. W. M. Lim, J. H. Lew, K. P. Loh, C. Soci, T. C. Sum, H. J. Bolink, N. Mathews, S. Mhaisalkar, A. Bruno, *Joule* **2020**, *4*, 1035.
[111] H. Wang, H. A. Dewi, T. M. Koh, A. Bruno, S. Mhaisalkar, N. Mathews, *ACS App. Mat. Interfaces* **2020**, *12*, 484.
[112] F. Meinardi, S. Ehrenberg, L. Dhamo, F. Carulli, M. Mauri, F. Bruni, R. Simonutti, U. Kortshagen, S. Brovelli, *Nat. Photonics* **2017**, *11*, 177.
[113] J. Heo, I. Jung, H. Park, J. H. Han, H. Kim, H. Park, J.-S. Park, H. Jeon, K.-T. Lee, H. J. Park, *Adv. Opt. Mater.* **2021**, *10*, 2101696.
[114] T. S. Liang, M. Pravettoni, C. Deline, J. S. Stein, R. Kopecek, J. P. Singh, W. Luo, Y. Wang, A. G. Aberle, Y. S. Khoo, *Energy Environ. Sci.* **2019**, *12*, 116.
[115] C. D. Rodríguez-Gallegos, H. Liu, O. Gandhi, J. P. Singh, V. Krishnamurthy, A. Kumar, J. S. Stein, S. Wang, L. Li, T. Reindl, I. M. Peters, *Joule* **2020**, *4*, 1514.
[116] C. G. Granqvist, *Thin Solid Films* **2014**, *564*, 1.
[117] G. Cai, J. Wang, P. S. Lee, *Acc. Chem. Res.* **2016**, *49*, 1469.
[118] A. Cannavale, U. Ayr, F. Fiorito, F. Martellotta, *Energies* **2020**, *13*, 1449.
[119] A. Cannavale, G. E. Eperon, P. Cossari, A. Abate, H. J. Snaith, G. Gigli, *Energy Environ. Sci.* **2015**, *8*, 1578.
[120] A. Cannavale, F. Martellotta, F. Fiorito, U. Ayr, *Energies* **2020**, *13*, 1929.
[121] A. Cannavale, P. Cossari, G. E. Eperon, S. Colella, F. Fiorito, G. Gigli, H. J. Snaith, A. Listorti, *Energy Environ. Sci.* **2016**, *9*, 2682.
[122] M. Yao, T. Li, Y. Long, P. Shen, G. Wang, C. Li, J. Liu, W. Guo, Y. Wang, L. Shen, X. Zhan, *Sci. Bull.* **2020**, *65*, 217.
[123] M. Götz-Köhler, H. Meddeb, K. Gehrke, M. Vehse, C. Agert, *IEEE J. Photovoltaics* **2021**, *11*, 1388.
[124] J. Karst, M. Hentschel, F. Sterl, H. Linnenbank, M. Ubl, H. Giessen, *Opt. Mater. Express* **2020**, *10*, 1346.
[125] K. J. Palm, J. B. Murray, T. C. Narayan, J. N. Munday, *ACS Photonics* **2018**, *5*, 4677.
[126] M. Götz, M. Lengert, N. Osterthun, K. Gehrke, M. Vehse, C. Agert, *ACS Photonics* **2020**, *7*, 1022.
[127] Y. Ke, J. Chen, G. Lin, S. Wang, Y. Zhou, J. Yin, P. S. Lee, Y. Long, *Adv. Energy Mater.* **2019**, *9*, 1902066.
[128] Q. Huaulmé, V. M. Mwalukuku, D. Joly, J. Liotier, Y. Kervella, P. Maldivi, S. Narbey, F. Oswald, A. J. Riquelme, J. A. Anta, R. Demadrille, *Nat. Energy* **2020**, *5*, 468.
[129] H.-K. Kwon, K.-T. Lee, K. Hur, S. H. Moon, M. M. Quasim, T. D. Wilkinson, J.-Y. Han, H. Ko, I.-K. Han, B. Park, B. K. Min, B.-K. Ju, S. M. Morris, R. H. Friend, D.-H. Ko, *Adv. Energy Mater.* **2015**, *5*, 1401347.
[130] Y. Cui, Y. Ke, C. Liu, Z. Chen, N. Wang, L. Zhang, Y. Zhou, S. Wang, Y. Gao, Y. Long, *Joule* **2018**, *2*, 1707.
[131] F. Guo, S. Chen, Z. Chen, H. Luo, Y. Gao, T. Przybilla, E. Spiecker, A. Osvet, K. Forberich, C. J. Brabec, *Adv. Opt. Mater.* **2015**, *3*, 1524.
[132] Y. Ke, Y. Yin, Q. Zhang, Y. Tan, P. Hu, S. Wang, Y. Tang, Y. Zhou, X. Wen, S. Wu, T. J. White, J. Yin, J. Peng, Q. Xiong, D. Zhao, Y. Long, *Joule* **2019**, *3*, 858.
[133] J. Lin, M. Lai, L. Dou, C. S. Kley, H. Chen, F. Peng, J. Sun, D. Lu, S. A. Hawks, C. Xie, F. Cui, A. P. Alivisatos, D. T. Limmer, P. Yang, *Nat. Mater.* **2018**, *17*, 261.
[134] A. A. Zhumekenov, M. I. Saidaminov, O. F. Mohammed, O. M. Bakr, *Joule* **2021**, *5*, 2027.
[135] J. Zhou, Y. Gao, Z. Zhang, H. Luo, C. Cao, Z. Chen, L. Dai, X. Liu, *Sci. Rep.* **2013**, *3*, 3029.
[136] B. A. Rosales, L. E. Mundt, T. G. Allen, D. T. Moore, K. J. Prince, C. A. Wolden, G. Rumbles, L. T. Schelhas, L. M. Wheeler, *Nat. Commun.* **2020**, *11*, 5234.
[137] M. de Bastiani, M. I. Saidaminov, I. Dursun, L. Sinatra, W. Peng, U. Buttner, O. F. Mohammed, O. M. Bakr, *Chem. Mater.* **2017**, *29*, 3367.
[138] C. Bechinger, S. Ferrere, A. Zaban, J. Sprague, B. Gregg, *Nature* **1996**, *383*, 608.
[139] L. M. Wheeler, D. T. Moore, R. Ihly, N. J. Stanton, E. M. Miller, R. C. Tenent, J. L. Blackburn, N. R. Neale, *Nat. Commun.* **2017**, *8*, 1722.
[140] J. Murray, D. Ma, J. N. Munday, *ACS Photonics* **2017**, *4*, 1.
[141] S. Tao, I. Schmidt, G. Brocks, J. Jiang, I. Tranca, K. Meerholz, S. Olthof, *Nat. Commun.* **2019**, *10*, 2560.
[142] G. E. Eperon, M. T. Hörantner, H. J. Snaith, *Nat. Rev. Chem.* **2017**, *1*, 0095.
[143] T. Feurer, P. Reinhard, E. Avancini, B. Bissig, J. Löckinger, P. Fuchs, R. Carron, T. P. Weiss, J. Perrenoud, S. Stutterheim, S. Buecheler, A. N. Tiwari, *Prog. Photovoltaics Res. Appl.* **2017**, *25*, 645.

[144] N. Mufti, T. Amrillah, A. Taufiq, Sunaryono, Aripriharta, M. Diantoro, Zulhadjri, H. Nur, *Sol. Energy* **2020**, *207*, 1146.
[145] C.-Z. Ning, L. Dou, P. Yang, *Nat. Rev. Mater.* **2017**, *2*, 17070.
[146] J. F. Geisz, R. M. France, K. L. Schulte, M. A. Steiner, A. G. Norman, H. L. Guthrey, M. R. Young, T. Song, T. Moriarty, *Nat. Energy* **2020**, *5*, 326.
[147] E. G. Barbagiovanni, D. J. Lockwood, P. J. Simpson, L. V. Goncharova, *App. Phys. Rev.* **2014**, *1*, 11302.
[148] M. C. Beard, J. M. Luther, O. E. Semonin, A. J. Nozik, *Acc. Chem. Res.* **2013**, *46*, 1252.
[149] A. Chaves, J. G. Azadani, H. Alsalman, D. R. Da Costa, R. Frisenda, A. J. Chaves, S. H. Song, Y. D. Kim, D. He, J. Zhou, A. Castellanos-Gomez, F. M. Peeters, Z. Liu, C. L. Hinkle, S.-H. Oh, P. D. Ye, S. J. Koester, Y. H. Lee, P. Avouris, X. Wang, T. Low, *npj 2D Mater. Appl.* **2020**, *4*, 29.
[150] R. Prasanna, A. Gold-Parker, T. Leijtens, B. Conings, A. Babayigit, H.-G. Boyen, M. F. Toney, M. D. McGehee, *J. Am. Chem. Soc.* **2017**, *139*, 11117.
[151] M. R. Filip, G. E. Eperon, H. J. Snaith, F. Giustino, *Nat. Commun.* **2014**, *5*, 5757.
[152] A. Shah, *Thin-Film Silicon Solar Cells*, EPFL Press; Taylor & Francis, Lausanne **2010**.
[153] R. Woods-Robinson, Y. Han, H. Zhang, T. Ablekim, I. Khan, K. A. Persson, A. Zakutayev, *Chem. Rev.* **2020**, *120*, 4007.
[154] I. Sayed, S. M. Bedair, *IEEE J. Photovoltaics* **2019**, *9*, 402.
[155] M. C. Scharber, N. S. Sariciftci, *Prog. Polym. Sci.* **2013**, *38*, 1929.
[156] B. Xie, Z. Chen, L. Ying, F. Huang, Y. Cao, *InfoMat* **2020**, *2*, 57.
[157] Y.-J. Cheng, S.-H. Yang, C.-S. Hsu, *Chem. Rev.* **2009**, *109*, 5868.
[158] A. Armin, W. Li, O. J. Sandberg, Z. Xiao, L. Ding, J. Nelson, D. Neher, K. Vandewal, S. Shoaee, T. Wang, H. Ade, T. Heumüller, C. Brabec, P. Meredith, *Adv. Energy Mater.* **2021**, *11*, 2003570.
[159] M. Anaya, G. Lozano, M. E. Calvo, H. Míguez, *Joule* **2017**, *1*, 769.
[160] Z. Hu, Z. Lin, J. Su, J. Zhang, J. Chang, Y. Hao, *Sol. RRL* **2019**, *3*, 1900304.
[161] A. D. Yoffe, *Adv. Phys* **1993**, *42*, 173.
[162] A. P. Alivisatos, *Science* **1996**, *271*, 933.
[163] T. Edvinsson, *R. Soc. Open Sci.* **2018**, *5*, 180387.
[164] H. Zhao, F. Rosei, *Chem* **2017**, *3*, 229.
[165] S. Karuthedath, J. Gorenflot, Y. Firdaus, N. Chaturvedi, C. S. P. de Castro, G. T. Harrison, J. I. Khan, A. Markina, A. H. Balawi, T. A. D. Peña, W. Liu, R.-Z. Liang, A. Sharma, S. H. K. Paleti, W. Zhang, Y. Lin, E. Alarousu, S. Lopatin, D. H. Anjum, P. M. Beaujuge, S. de Wolf, I. McCulloch, T. D. Anthopoulos, D. Baran, D. Andrienko, F. Laquai, *Nat. Mater.* **2021**, *20*, 378.
[166] L. Lu, T. Zheng, Q. Wu, A. M. Schneider, D. Zhao, L. Yu, *Chem. Rev.* **2015**, *115*, 12666.
[167] O. E. Semonin, J. M. Luther, M. C. Beard, *Mater. Today* **2012**, *15*, 508.
[168] O. Dupré, R. Vaillon, M. A. Green, *Thermal Behavior of Photovoltaic Devices*, Springer International Publishing, Cham **2017**.
[169] X. Sun, T. J. Silverman, Z. Zhou, M. R. Khan, P. Bermel, M. A. Alam, *IEEE J. Photovoltaics* **2017**, *7*, 566.
[170] L. Zhu, A. Raman, K. X. Wang, M. A. Anoma, S. Fan, *Optica* **2014**, *1*, 32.
[171] R. Vaillon, O. Dupré, R. B. Cal, M. Calaf, *Sci. Rep.* **2018**, *8*, 13163.
[172] L. C. Hirst, N. J. Ekins-Daukes, *Prog. Photovoltaics Res. Appl.* **2011**, *19*, 286.
[173] I. M. Slauch, M. G. Deceglie, T. J. Silverman, V. E. Ferry, *ACS Photonics* **2018**, *5*, 1528.
[174] I. M. Slauch, M. G. Deceglie, T. J. Silverman, V. E. Ferry, *ACS Appl. Energy Mater.* **2019**, *2*, 3614.
[175] I. M. Slauch, M. G. Deceglie, T. J. Silverman, V. E. Ferry, *Cell Rep. Phys. Sci* **2021**, *2*, 100430.
[176] M. Ryyan Khan, M. A. Alam, *Appl. Phys. Lett.* **2015**, *107*, 223502.
[177] D. Sato, N. Yamada, *Renewable Sustainable Energy Rev.* **2019**, *104*, 151.
[178] J. Siecker, K. Kusakana, B. P. Numbi, *Renewable Sustainable Energy Rev.* **2017**, *79*, 192.
[179] X. Yin, R. Yang, G. Tan, S. Fan, *Science* **2020**, *370*, 786.
[180] A. P. Raman, M. A. Anoma, L. Zhu, E. Rephaeli, S. Fan, *Nature* **2014**, *515*, 540.
[181] S. Ahmed, Z. Li, M. S. Javed, T. Ma, *Mater. Today Energy* **2021**, *21*, 100776.
[182] Y. An, C. Sheng, X. Li, *Nanoscale* **2019**, *11*, 17073.
[183] J. Dumoulin, E. Drouard, M. Amara, *Sustainable Energy Fuels* **2021**, *5*, 2085.
[184] A. R. Gentle, G. B. Smith, *Sol. Energy Mater. Sol. Cells* **2016**, *150*, 39.
[185] Z. Li, S. Ahmed, T. Ma, *Sol. RRL* **2021**, *5*, 2000735.
[186] L. Xu, W. Liu, H. Liu, C. Ke, M. Wang, C. Zhang, E. Aydin, M. Al-Aswad, K. Kotsovos, I. Gereige, A. Al-Saggaf, A. Jamal, X. Yang, P. Wang, F. Laquai, T. G. Allen, S. de Wolf, *Joule* **2021**, *5*, 631.
[187] B. Zhao, M. Hu, X. Ao, G. Pei, *Sol. Energy* **2018**, *176*, 248.
[188] S. E. Root, S. Savagatrup, A. D. Printz, D. Rodriquez, D. J. Lipomi, *Chem. Rev.* **2017**, *117*, 6467.
[189] N. El-Atab, M. M. Hussain, *MRS Energy Sustainability* **2020**, *7*, 1.
[190] J. Ramanujam, D. M. Bishop, T. K. Todorov, O. Gunawan, J. Rath, R. Nekovei, E. Artegiani, A. Romeo, *Prog. Mater. Sci.* **2020**, *110*, 100619.
[191] H.-D. Um, I. Hwang, D. Choi, K. Seo, *Acc. Mater. Res.* **2021**, *2*, 701.
[192] M. Xue, K. N. Nazif, Z. Lyu, J. Jiang, C.-Y. Lu, N. Lee, K. Zang, Y. Chen, T. Zheng, T. I. Kamins, M. L. Brongersma, K. C. Saraswat, J. S. Harris, *Nano Energy* **2020**, *70*, 104466.
[193] K. J. Yu, L. Gao, J. S. Park, Y. R. Lee, C. J. Corcoran, R. G. Nuzzo, D. Chanda, J. A. Rogers, *Adv. Energy Mater.* **2013**, *3*, 1401.
[194] J. Jean, A. Wang, V. Bulović, *Org. Electron.* **2016**, *31*, 120.
[195] S. Zhang, T. Zhang, Z. Liu, J. Wang, L. Yu, J. Xu, K. Chen, P. Roca i Cabarrocas, *Nano Energy* **2021**, *86*, 106121.
[196] T. S. Kim, H. J. Kim, D.-M. Geum, J.-H. Han, I. S. Kim, N. Hong, G. H. Ryu, J. Kang, W. J. Choi, K. J. Yu, *ACS App. Mat. Interfaces* **2021**, *13*, 13248.
[197] F. Lang, G. E. Eperon, K. Frohna, E. M. Tennyson, A. Al-Ashouri, G. Kourkafas, J. Bundesmann, A. Denker, K. G. West, L. C. Hirst, H.-C. Neitzert, S. D. Stranks, *Adv. Energy Mater.* **2021**, *11*, 2102246.
[198] D. Sato, T. Masuda, K. Araki, M. Yamaguchi, K. Okumura, A. Sato, R. Tomizawa, N. Yamada, *Commun. Mater.* **2021**, *2*, 7.
[199] W. Song, Y. Liu, B. Fanady, Y. Han, L. Xie, Z. Chen, K. Yu, X. Peng, X. Zhang, Z. Ge, *Nano Energy* **2021**, *86*, 106044.
[200] Z. Wang, X. Zhu, J. Feng, D. Yang, S. Liu, *Sol. RRL* **2021**, *5*, 2100264.
[201] J. Zhao, J. Zha, Z. Zeng, C. Tan, *J. Mater. Chem. A* **2021**, *9*, 18887.
[202] S. Kim, M. Holz, S. Park, Y. Yoon, E. Cho, J. Yi, *Sustainability* **2021**, *13*, 2532.
[203] D. J. Lipomi, B. C.-K. Tee, M. Vosgueritchian, Z. Bao, *Adv. Mater.* **2011**, *23*, 1771.
[204] N. Zhang, J. Chen, Y. Huang, W. Guo, J. Yang, J. Du, X. Fan, C. Tao, *Adv. Mater.* **2016**, *28*, 263.
[205] A. Satharasinghe, T. Hughes-Riley, T. Dias, *Sensors* **2020**, *20*, 5938.
[206] M. M. Potter, M. E. Phelan, P. Balaji, P. Jahelka, H. C. Bauser, R. D. Glaudell, C. M. Went, M. J. Enright, D. R. Needell, A. Augusto, H. A. Atwater, R. G. Nuzzo, *ACS Appl. Mater. Interfaces* **2021**, *13*, 45600.
[207] A. Satharasinghe, T. Hughes-Riley, T. Dias, *Prog Photovolt Res Appl* **2020**, *28*, 578.
[208] B. Svetozarevic, M. Begle, P. Jayathissa, S. Caranovic, R. F. Shepherd, Z. Nagy, I. Hischier, J. Hofer, A. Schlueter, *Nat. Energy* **2019**, *4*, 671.
[209] Y. Gao, J. Dong, O. Isabella, R. Santbergen, H. Tan, M. Zeman, G. Zhang, *App. Energy* **2018**, *228*, 1454.
[210] Y. Gao, J. Dong, O. Isabella, R. Santbergen, H. Tan, M. Zeman, G. Zhang, *App. Energy* **2019**, *233–234*, 424.

[211] W. Shockley, H. J. Queisser, *J. App. Phys.* **1961**, *32*, 510.
[212] P. Kaienburg, L. Krückemeier, D. Lübke, J. Nelson, U. Rau, T. Kirchartz, *Phys. Rev. Res.* **2020**, *2*, 023109.
[213] T. Kirchartz, U. Rau, *Adv. Energy Mater.* **2018**, *8*, 1703385.
[214] B. Ehrler, E. Alarcón-Lladó, S. W. Tabernig, T. Veeken, E. C. Garnett, A. Polman, *ACS Energy Lett.* **2020**, *5*, 3029.
[215] M. A. Green, E. D. Dunlop, J. Hohl-Ebinger, M. Yoshita, N. Kopidakis, X. Hao, *Prog. Photovoltaics Res. Appl.* **2021**, *29*, 657.
[216] O. Almora, D. Baran, G. C. Bazan, C. Berger, C. I. Cabrera, K. R. Catchpole, S. Erten-Ela, F. Guo, J. Hauch, A. W. Y. Ho-Baillie, T. J. Jacobsson, R. A. J. Janssen, T. Kirchartz, N. Kopidakis, Y. Li, M. A. Loi, R. R. Lunt, X. Mathew, M. D. McGehee, J. Min, D. B. Mitzi, M. K. Nazeeruddin, J. Nelson, A. F. Nogueira, U. W. Paetzold, N.-G. Park, B. P. Rand, U. Rau, H. J. Snaith, E. Unger, et al, *Adv. Energy Mater.* **2021**, *11*, 2002774.
[217] A. Zakutayev, J. D. Major, X. Hao, A. Walsh, J. Tang, T. K. Todorov, L. H. Wong, E. Saucedo, *J. Phys. Energy* **2021**, *3*, 32003.
[218] R. R. Lunt, *Appl. Phys. Lett.* **2012**, *101*, 43902.
[219] J. Halme, P. Mäkinen, *Energy Environ. Sci.* **2019**, *12*, 1274.
[220] C. Yang, R. R. Lunt, *Adv. Opt. Mater.* **2017**, *5*, 1600851.
[221] C. Yang, W. Sheng, M. Moemeni, M. Bates, C. K. Herrera, B. Borhan, R. R. Lunt, *Adv. Energy Mater.* **2021**, *11*, 2003581.
[222] A. Røyset, T. Kolås, B. P. Jelle, *Energy Build.* **2020**, *208*, 109623.
[223] K. Forberich, F. Guo, C. Bronnbauer, C. J. Brabec, *Energy Technol.* **2015**, *3*, 1051.
[224] C. Yang, D. Liu, M. Bates, M. C. Barr, R. R. Lunt, *Joule* **2019**, *3*, 1803.
[225] J. Y. Kim, J.-W. Lee, H. S. Jung, H. Shin, N.-G. Park, *Chem. Rev.* **2020**, *120*, 7867.
[226] A. Kojima, K. Teshima, Y. Shirai, T. Miyasaka, *J. Am. Chem. Soc.* **2009**, *131*, 6050.
[227] T. J. Jacobsson, A. Hultqvist, A. García-Fernández, A. Anand, A. Al-Ashouri, A. Hagfeldt, A. Crovetto, A. Abate, A. G. Ricciardulli, A. Vijayan, A. Kulkarni, A. Y. Anderson, B. P. Darwich, B. Yang, B. L. Coles, C. A. R. Perini, C. Rehermann, D. Ramirez, D. Fairen-Jimenez, D. Di Girolamo, D. Jia, E. Avila, E. J. Juarez-Perez, F. Baumann, F. Mathies, G. S. A. González, G. Boschloo, G. Nasti, G. Paramasivam, G. Martínez-Denegri, et al, *Nat. Energy* **2022**, *7*, 107.
[228] J. Jeong, M. Kim, J. Seo, H. Lu, P. Ahlawat, A. Mishra, Y. Yang, M. A. Hope, F. T. Eickemeyer, M. Kim, Y. J. Yoon, I. W. Choi, B. P. Darwich, S. J. Choi, Y. Jo, J. H. Lee, B. Walker, S. M. Zakeeruddin, L. Emsley, U. Rothlisberger, A. Hagfeldt, D. S. Kim, M. Grätzel, J. Y. Kim, *Nature* **2021**, *592*, 381.
[229] J. J. Yoo, G. Seo, M. R. Chua, T. G. Park, Y. Lu, F. Rotermund, Y.-K. Kim, C. S. Moon, N. J. Jeon, J.-P. Correa-Baena, V. Bulović, S. S. Shin, M. G. Bawendi, J. Seo, *Nature* **2021**, *590*, 587.
[230] R. Swartwout, M. T. Hoerantner, V. Bulović, *Energy Environ. Mater.* **2019**, *2*, 119.
[231] F. Yang, D. Jang, L. Dong, S. Qiu, A. Distler, N. Li, C. J. Brabec, H.-J. Egelhaaf, *Adv. Energy Mater.* **2021**, *11*, 2101973.
[232] T.-Y. Yang, Y. Y. Kim, J. Seo, *APL Mater.* **2021**, *9*, 110901.
[233] J. Zhang, H. S. Tan, X. Guo, A. Facchetti, H. Yan, *Nat. Energy* **2018**, *3*, 720.
[234] J. Gong, Y. Kong, J. Li, K. Wang, X. Wang, Z. Zhang, Z. Ding, X. Xiao, *Nano Energy* **2019**, *62*, 205.
[235] H. Meddeb, N. Osterthun, M. Götz, O. Sergeev, K. Gehrke, M. Vehse, C. Agert, *Nano Energy* **2020**, *76*, 105048.
[236] H. Meddeb, N. Osterthun, M. Götz, O. Sergeev, K. Gehrke, M. Vehse, C. Agert, in *2020 IEEE 47th Photovoltaic Specialists Conference*, IEEE, Virtual conference **2020**, p. 1149.
[237] A. G. Pattantyus-Abraham, I. J. Kramer, A. R. Barkhouse, X. Wang, G. Konstantatos, R. Debnath, L. Levina, I. Raabe, M. K. Nazeeruddin, M. Grätzel, E. H. Sargent, *ACS Nano* **2010**, *4*, 3374.
[238] G. Dennler, M. C. Scharber, C. J. Brabec, *Adv. Mater.* **2009**, *21*, 1323.
[239] C. J. Brabec, S. Gowrisanker, J. J. M. Halls, D. Laird, S. Jia, S. P. Williams, *Adv. Mater.* **2010**, *22*, 3839.
[240] J. Nelson, *Mater. Today* **2011**, *14*, 462.
[241] C. J. Brabec, M. Heeney, I. McCulloch, J. Nelson, *Chem. Soc. Rev.* **2011**, *40*, 1185.
[242] P. Cheng, G. Li, X. Zhan, Y. Yang, *Nat. Photonics* **2018**, *12*, 131.
[243] C. Yan, S. Barlow, Z. Wang, H. Yan, A. K.-Y. Jen, S. R. Marder, X. Zhan, *Nat. Rev. Mater.* **2018**, *3*, 18003.
[244] N. Gasparini, A. Salleo, I. McCulloch, D. Baran, *Nat. Rev. Mater.* **2019**, *4*, 229.
[245] L. Chang, M. Sheng, L. Duan, A. Uddin, *Org. Electron.* **2021**, *90*, 106063.
[246] C. Yang, J. Zhang, N. Liang, H. Yao, Z. Wei, C. He, X. Yuan, J. Hou, *J. Mater. Chem. A* **2019**, *7*, 18889.
[247] A. Classen, C. L. Chochos, L. Lüer, V. G. Gregoriou, J. Wortmann, A. Osvet, K. Forberich, I. McCulloch, T. Heumüller, C. J. Brabec, *Nat. Energy* **2020**, *5*, 711.
[248] M. C. Scharber, D. Mühlbacher, M. Koppe, P. Denk, C. Waldauf, A. J. Heeger, C. J. Brabec, *Adv. Mater.* **2006**, *18*, 789.
[249] M. Zhang, L. Zhu, G. Zhou, T. Hao, C. Qiu, Z. Zhao, Q. Hu, B. W. Larson, H. Zhu, Z. Ma, Z. Tang, W. Feng, Y. Zhang, T. P. Russell, F. Liu, *Nat. Commun.* **2021**, *12*, 309.
[250] L. W. T. NG, S. W. Lee, D. W. Chang, J. M. Hodgkiss, D. Vak, *Adv. Mater. Technol.* **2022**, 2101556.
[251] J. Ramanujam, U. P. Singh, *Energy Environ. Sci.* **2017**, *10*, 1306.
[252] M. Contreras, J. Tuttle, D. Du, Y. Qi, A. Swartzlander, A. Tennant, R. Noufi, *Appl. Phys. Lett.* **1993**, *63*, 1824.
[253] A. M. Gabor, J. R. Tuttle, D. S. Albin, M. A. Contreras, R. Noufi, A. M. Hermann, *Appl. Phys. Lett.* **1994**, *65*, 198.
[254] A. Chirilă, S. Buecheler, F. Pianezzi, P. Bloesch, C. Gretener, A. R. Uhl, C. Fella, L. Kranz, J. Perrenoud, S. Seyrling, R. Verma, S. Nishiwaki, Y. E. Romanyuk, G. Bilger, A. N. Tiwari, *Nat. Mater.* **2011**, *10*, 857.
[255] M. A. Green, E. D. Dunlop, J. Hohl-Ebinger, M. Yoshita, N. Kopidakis, X. Hao, *Prog. Photovoltaics Res. Appl.* **2022**, *30*, 3.
[256] K. W. J. Barnham, G. Duggan, *J. App. Phys.* **1990**, *67*, 3490.
[257] K. Toprasertpong, T. Inoue, Y. Nakano, M. Sugiyama, *Sol. Energy Mater. Sol. Cells* **2018**, *174*, 146.
[258] R. E. Welser, S. J. Polly, M. Kacharia, A. Fedorenko, A. K. Sood, S. M. Hubbard, *Sci. Rep.* **2019**, *9*, 13955.
[259] J. Liang, Z. Zhang, Q. Xue, Y. Zheng, X. Wu, Y. Huang, X. Wang, C. Qin, Z. Chen, C.-C. Chen, *Energy Environ. Sci.* **2022**, *15*, 296.
[260] H. Chen, S. Teale, B. Chen, Y. Hou, L. Grater, T. Zhu, K. Bertens, S. M. Park, H. R. Atapattu, Y. Gao, M. Wei, A. K. Johnston, Q. Zhou, K. Xu, D. Yu, C. Han, T. Cui, E. H. Jung, C. Zhou, W. Zhou, A. H. Proppe, S. Hoogland, F. Laquai, T. Filleter, K. R. Graham, Z. Ning, E. H. Sargent, *Nat. Photonics* **2022**, *16*, 352.
[261] H. Meddeb, M. Gotz-Kohler, N. Osterthun, O. Sergeev, K. Gehrke, M. Vehse, C. Agert, *IEEE 48th Photovoltaic Specialists Conference*, IEEE, Virtual conference **2021**, p. 975.
[262] H. Meddeb, M. Götz-Köhler, N. Osterthun, O. Sergeev, K. Gehrke, M. Vehse, C. Agert, *IEEE J. Photovoltaics* **2022**, *12*, 760.
[263] M. Götz, N. Osterthun, K. Gehrke, M. Vehse, C. Agert, *Coatings* **2020**, *10*, 218.
[264] N. Osterthun, H. Meddeb, N. Neugebohrn, O. Sergeev, K. Gehrke, M. Vehse, C. Agert, *App. Surf. Sci. Adv.* **2022**, *7*, 100206.
[265] A. J. Nozik, *Nat. Energy* **2018**, *3*, 170.
[266] D.-T. Nguyen, L. Lombez, F. Gibelli, S. Boyer-Richard, A. Le Corre, O. Durand, J.-F. Guillemoles, *Nat. Energy* **2018**, *3*, 236.
[267] M. R. Kim, D. Ma, *J. Phys. Chem. Lett.* **2015**, *6*, 85.
[268] E. H. Sargent, *Nat. Photonics* **2012**, *6*, 133.
[269] H. Lee, H.-J. Song, M. Shim, C. Lee, *Energy Environ. Sci.* **2020**, *13*, 404.

[270] Q. Zhao, R. Han, A. R. Marshall, S. Wang, B. M. Wieliczka, J. Ni, J. Zhang, J. Yuan, J. M. Luther, A. Hazarika, G.-R. Li, *Adv. Mater.* **2022**, *34*, 2107888.
[271] I. M. Peters, T. Buonassisi, *Joule* **2018**, *2*, 1160.
[272] M. P. Lumb, S. Mack, K. J. Schmieder, M. González, M. F. Bennett, D. Scheiman, M. Meitl, B. Fisher, S. Burroughs, K.-T. Lee, J. A. Rogers, R. J. Walters, *Adv. Energy Mater.* **2017**, *7*, 1700345.
[273] S. P. Bremner, C. Yi, I. Almansouri, A. Ho-Baillie, M. A. Green, *Sol. Energy* **2016**, *135*, 750.
[274] M. T. Hörantner, T. Leijtens, M. E. Ziffer, G. E. Eperon, M. G. Christoforo, M. D. McGehee, H. J. Snaith, *ACS Energy Lett.* **2017**, *2*, 2506.
[275] Z. Yu, M. Leilaeioun, Z. Holman, *Nat. Energy* **2016**, *1*, 16137.
[276] T. Leijtens, K. A. Bush, R. Prasanna, M. D. McGehee, *Nat. Energy* **2018**, *3*, 828.
[277] J. Zeitouny, E. A. Katz, A. Dollet, A. Vossier, *Sci. Rep.* **2017**, *7*, 1766.
[278] M. Yamaguchi, F. Dimroth, J. F. Geisz, N. J. Ekins-Daukes, *J. App. Phys.* **2021**, *129*, 240901.
[279] R. Cariou, J. Benick, F. Feldmann, O. Höhn, H. Hauser, P. Beutel, N. Razek, M. Wimplinger, B. Bläsi, D. Lackner, M. Hermle, G. Siefer, S. W. Glunz, A. W. Bett, F. Dimroth, *Nat. Energy* **2018**, *3*, 326.
[280] P. Schygulla, R. Müller, D. Lackner, O. Höhn, H. Hauser, B. Bläsi, F. Predan, J. Benick, M. Hermle, S. W. Glunz, F. Dimroth, *Prog. Photovoltaics Res. Appl.* **2021**, 3503.
[281] K. T. VanSant, A. C. Tamboli, E. L. Warren, *Joule* **2021**, *5*, 514.
[282] A. Al-Ashouri, E. Köhnen, B. Li, A. Magomedov, H. Hempel, P. Caprioglio, J. Márquez, A. Morales Vilches, E. Kasparavicius, J. Smith, N. Phung, D. Menzel, M. Grischek, L. Kegelmann, D. Skroblin, C. Gollwitzer, T. Malinauskas, M. Jošt, G. Matic, B. Rech, R. Schlatmann, M. Topic, L. Korte, Abate, Antonio, B. Stannowski, D. Neher, M. Stolterfoht, T. Unold, V. Getautis, et al, *Science* **2020**, *370*, 1300.
[283] F. Sahli, J. Werner, B. A. Kamino, M. Bräuninger, R. Monnard, B. Paviet-Salomon, L. Barraud, L. Ding, J. J. Diaz Leon, D. Sacchetto, G. Cattaneo, M. Despeisse, M. Boccard, S. Nicolay, Q. Jeangros, B. Niesen, C. Ballif, *Nat. Mater.* **2018**, *17*, 820.
[284] B. Chen, Z. Yu, K. Liu, X. Zheng, Y. Liu, J. Shi, D. Spronk, P. N. Rudd, Z. Holman, J. Huang, *Joule* **2019**, *3*, 177.
[285] G. E. Eperon, T. Leijtens, K. A. Bush, R. Prasanna, T. Green, J. T.-W. Wang, D. P. McMeekin, G. Volonakis, R. L. Milot, R. May, A. Palmstrom, D. J. Slotcavage, R. A. Belisle, J. B. Patel, E. S. Parrott, R. J. Sutton, W. Ma, F. Moghadam, B. Conings, A. Babayigit, H.-G. Boyen, S. Bent, F. Giustino, L. M. Herz, M. B. Johnston, M. D. McGehee, H. J. Snaith, *Science* **2016**, *354*, 861.
[286] X. Zheng, A. Y. Alsalloum, Y. Hou, E. H. Sargent, O. M. Bakr, *Acc. Mater. Res.* **2020**, *1*, 63.
[287] C. Li, Z. Song, C. Chen, C. Xiao, B. Subedi, S. P. Harvey, N. Shrestha, K. K. Subedi, L. Chen, D. Liu, Y. Li, Y.-W. Kim, C. Jiang, M. J. Heben, D. Zhao, R. J. Ellingson, N. J. Podraza, M. Al-Jassim, Y. Yan, *Nat. Energy* **2020**, *5*, 768.
[288] R. Lin, J. Xu, M. Wei, Y. Wang, Z. Qin, Z. Liu, J. Wu, K. Xiao, B. Chen, S. M. Park, G. Chen, H. R. Atapattu, K. R. Graham, J. Xu, J. Zhu, L. Li, C. Zhang, E. H. Sargent, H. Tan, *Nature* **2022**, *603*, 73.
[289] H. Shen, T. Duong, J. Peng, D. Jacobs, N. Wu, J. Gong, Y. Wu, S. K. Karuturi, X. Fu, K. Weber, X. Xiao, T. P. White, K. Catchpole, *Energy Environ. Sci.* **2018**, *11*, 394.
[290] S. Gharibzadeh, I. M. Hossain, P. Fassl, B. A. Nejand, T. Abzieher, M. Schultes, E. Ahlswede, P. Jackson, M. Powalla, S. Schäfer, M. Rienäcker, T. Wietler, R. Peibst, U. Lemmer, B. S. Richards, U. W. Paetzold, *Adv. Funct. Mater.* **2020**, *30*, 1909919.
[291] M. Jošt, L. Kegelmann, L. Korte, S. Albrecht, *Adv. Energy Mater.* **2020**, *10*, 1904102.
[292] X. Chen, Z. Jia, Z. Chen, T. Jiang, L. Bai, F. Tao, J. Chen, X. Chen, T. Liu, X. Xu, C. Yang, W. Shen, W. E. Sha, H. Zhu, Y. Yang, *Joule* **2020**, *4*, 1594.
[293] W. Chen, Y. Zhu, J. Xiu, G. Chen, H. Liang, S. Liu, H. Xue, E. Birgersson, J. W. Ho, X. Qin, J. Lin, R. Ma, T. Liu, Y. He, A. M.-C. Ng, X. Guo, Z. He, H. Yan, A. B. Djurišić, Y. Hou, *Nat. Energy* **2022**, *7*, 229.
[294] K. O. Brinkmann, T. Becker, F. Zimmermann, C. Kreusel, T. Gahlmann, M. Theisen, T. Haeger, S. Olthof, C. Tückmantel, M. Günster, T. Maschwitz, F. Göbelsmann, C. Koch, D. Hertel, P. Caprioglio, F. Peña-Camargo, L. Perdigón-Toro, A. Al-Ashouri, L. Merten, A. Hinderhofer, L. Gomell, S. Zhang, F. Schreiber, S. Albrecht, K. Meerholz, D. Neher, M. Stolterfoht, T. Riedl, *Nature* **2022**, *604*, 280.
[295] P. Cheng, Y. Liu, S.-Y. Chang, T. Li, P. Sun, R. Wang, H.-W. Cheng, T. Huang, L. Meng, S. Nuryyeva, C. Zhu, K.-H. Wei, B. Sun, X. Zhan, Y. Yang, *Joule* **2019**, *3*, 432.
[296] Z. Jia, S. Qin, L. Meng, Q. Ma, I. Angunawela, J. Zhang, X. Li, Y. He, W. Lai, N. Li, H. Ade, C. J. Brabec, Y. Li, *Nat. Commun.* **2021**, *12*, 178.
[297] Z. Zheng, J. Wang, P. Bi, J. Ren, Y. Wang, Y. Yang, X. Liu, S. Zhang, J. Hou, *Joule* **2022**, *6*, 171.
[298] J. Troughton, S. Neubert, N. Gasparini, D. R. Villalva, J. Bertrandie, A. Seitkhan, S. H. K. Paleti, A. Sharma, M. de Bastiani, E. Aydin, T. D. Anthopoulos, S. de Wolf, R. Schlatmann, D. Baran, *Adv. Energy Mater.* **2021**, *11*, 2100166.
[299] T. Moot, J. Werner, G. E. Eperon, K. Zhu, J. J. Berry, M. D. McGehee, J. M. Luther, *Adv. Mater.* **2020**, *32*, 2003312.
[300] Z. Wang, Z. Song, Y. Yan, S. F. Liu, D. Yang, *Adv. Sci.* **2019**, *6*, 1801704.
[301] A. F. Palmstrom, G. E. Eperon, T. Leijtens, R. Prasanna, S. N. Habisreutinger, W. Nemeth, E. A. Gaulding, S. P. Dunfield, M. Reese, S. Nanayakkara, T. Moot, J. Werner, J. Liu, B. To, S. T. Christensen, M. D. McGehee, M. F. van Hest, J. M. Luther, J. J. Berry, D. T. Moore, *Joule* **2019**, *3*, 2193.
[302] G. M. Wilson, M. Al-Jassim, W. K. Metzger, S. W. Glunz, P. Verlinden, G. Xiong, L. M. Mansfield, B. J. Stanbery, K. Zhu, Y. Yan, J. J. Berry, A. J. Ptak, F. Dimroth, B. M. Kayes, A. C. Tamboli, R. Peibst, K. Catchpole, M. O. Reese, C. S. Klinga, P. Denholm, M. Morjaria, M. G. Deceglie, J. M. Freeman, M. A. Mikofski, D. C. Jordan, G. TamizhMani, D. B. Sulas-Kern, *J. Phys. D: Appl. Phys.* **2020**, *53*, 493001.
[303] M. Yamaguchi, K.-H. Lee, K. Araki, N. Kojima, *J. Phys. D: Appl. Phys.* **2018**, *51*, 133002.
[304] M. A. Green, S. P. Bremner, *Nat. Mater.* **2016**, *16*, 23.
[305] M. T. Hörantner, H. J. Snaith, *Energy Environ. Sci.* **2017**, *10*, 1983.
[306] D. McMeekin, G. Sadoughi, W. Rehman, G. E. Eperon, M. Saliba, M. T. Hörantner, A. Haghighirad, N. Sakai, L. Korte, B. Rech, M. B. Johnston, L. M. Herz, H. J. Snaith, *Science* **2016**, *351*, 151.
[307] D. Kim, H. J. Jung, I. J. Park, B. W. Larson, S. P. Dunfield, C. Xiao, J. Kim, J. Tong, P. Boonmongkolras, S. G. Ji, F. Zhang, S. R. Pae, M. Kim, S. B. Kang, V. Dravid, J. J. Berry, J. Y. Kim, K. Zhu, D. H. Kim, B. Shin, *Science* **2020**, *368*, 155.
[308] E. Köhnen, P. Wagner, F. Lang, A. Cruz, B. Li, M. Roß, M. Jošt, A. B. Morales-Vilches, M. Topič, M. Stolterfoht, D. Neher, L. Korte, B. Rech, R. Schlatmann, B. Stannowski, S. Albrecht, *Sol. RRL* **2021**, *5*, 2100244.
[309] F. Martinho, *Energy Environ. Sci.* **2021**, *14*, 3840.
[310] L. A. Zafoschnig, S. Nold, J. C. Goldschmidt, *IEEE J. Photovoltaics* **2020**, *10*, 1632.
[311] C. Messmer, B. S. Goraya, S. Nold, P. S. Schulze, V. Sittinger, J. Schön, J. C. Goldschmidt, M. Bivour, S. W. Glunz, M. Hermle, *Prog. Photovoltaics Res. Appl.* **2021**, *29*, 744.
[312] B. Chen, N. Ren, Y. Li, L. Yan, S. Mazumdar, Y. Zhao, X. Zhang, *Adv. Energy Mater.* **2022**, *12*, 2003628.

[313] J. Qian, M. Ernst, N. Wu, A. Blakers, *Sustainable Energy Fuels* **2019**, *3*, 1439.
[314] L. Schmidt-Mende, V. Dyakonov, S. Olthof, F. Ünlü, K. M. T. Lê, S. Mathur, A. D. Karabanov, D. C. Lupascu, L. M. Herz, A. Hinderhofer, F. Schreiber, A. Chernikov, D. A. Egger, O. Shargaieva, C. Cocchi, E. Unger, M. Saliba, M. M. Byranvand, M. Kroll, F. Nehm, K. Leo, A. Redinger, J. Höcker, T. Kirchartz, J. Warby, E. Gutierrez-Partida, D. Neher, M. Stolterfoht, U. Würfel, M. Unmüssig, et al, *APL Mater.* **2021**, *9*, 109202.
[315] E. Aydin, T. G. Allen, M. de Bastiani, L. Xu, J. Ávila, M. Salvador, E. van Kerschaver, S. de Wolf, *Nat. Energy* **2020**, *5*, 851.
[316] B. Blasi, T. Kroyer, T. Kuhn, O. Hohn, *IEEE J. Photovoltaics* **2021**, *11*, 1305.
[317] C. Ji, Z. Zhang, T. Masuda, Y. Kudo, L. J. Guo, *Nanoscale Horiz.* **2019**, *4*, 874.
[318] J. Escarre, H.-Y. Li, L. Sansonnens, F. Galliano, G. Cattaneo, P. Heinstein, S. Nicolay, J. Bailat, S. Eberhard, C. Ballif, L.-E. Perret-Aebi, in *2015 IEEE 42nd Photovoltaic Specialist Conference (PVSC)*, IEEE, New Orleans, LA, USA **2015**.
[319] ISSOL | Architecture – BIPV, http://www.issol.eu/, (accessed: January 2022).
[320] SOLAXESS, https://www.solaxess.ch/, (accessed: January 2022).
[321] SwissINSO, https://www.swissinso.com/, (accessed: January 2022).
[322] G. Y. Yoo, R. Azmi, C. Kim, W. Kim, B. K. Min, S.-Y. Jang, Y. R. Do, *ACS Nano* **2019**, *13*, 10129.
[323] AVANCIS, https://www.avancis.de/en/, (accessed: January **2022**).
[324] T. Gewohn, S. Blankemeyer, M. R. Vogt, H. Schulte-Huxel, M. Kntges, B. Lim, C. Schinke, R. Brendel, *35th European Photovoltaic Solar Energy Conference and Exhibition*, EUPVSEC, Brussels, Belgium **2018**, p. 1842.
[325] L. H. Slooff-Hoek, J. A. M. van Roosmalen, L. A. G. Okel, T. de Vries, T. Minderhoud, G. Gijzen, T. Sepers, A. Versluis, F. Frumau, M. Rietbergen, L. Polinder, E. M. B. Heller, F. de Vries, *33rd European Photovoltaic Solar Energy Conference and Exhibition*, EUPVSEC, Amsterdam, The Netherlands **2016**, p. 2110.
[326] M. Mittag, M. Ebert, H. Wilson, T. Fellmeth, *35th European Photovoltaic Solar Energy Conference and Exhibition*, EUPVSEC, Brussels, Belgium **2018**, p. 1458.
[327] Kameleon Solar | Home, https://kameleonsolar.com/, (accessed: January 2022).
[328] S. Bae, Y. W. Noh, D.-S. Park, M. H. Song, S.-W. Choi, *Nano Energy* **2022**, *93*, 106801.
[329] Onyx Solar – Photovoltaic Glass for Buildings, https://www.onyx-solar.com/, (accessed: January 2022).
[330] K. Ding, X. Zhang, L. Ning, Z. Shao, P. Xiao, A. Ho-Baillie, X. Zhang, J. Jie, *Nano Energy* **2018**, *46*, 257.
[331] N. Neugebohrn, K. Gehrke, K. Brucke, M. Götz, M. Vehse, *Thin Solid Films* **2019**, *685*, 131.
[332] K.-T. Lee, J. Y. Lee, S. Seo, L. J. Guo, *Light Sci. Appl.* **2014**, *3*, e215.
[333] C. Kutter, B. Blsi, H. R. Wilson, T. Kroyer, M. Mittag, O. Hhn, M. Heinrich, *35th European Photovoltaic Solar Energy Conference and Exhibition*, EUPVSEC, Brussels, Belgium **2018**, p. 1488.
[334] L. Zeng, M. Li, Y. Chen, H. Shen, *Sol. Energy* **2014**, *103*, 343.
[335] J. H. Selj, T. T. Mongstad, R. Søndenå, E. S. Marstein, *Sol. Energy Mater. Sol. Cells* **2011**, *95*, 2576.
[336] Lof Solar – Color Solar Cell, http://www.lofsolar.com/, (accessed: January 2022).
[337] D. Cui, Z. Yang, D. Yang, X. Ren, Y. Liu, Q. Wei, H. Fan, J. Zeng, S. Liu, *J. Phys. Chem. C* **2016**, *120*, 42.
[338] K. Deng, Z. Liu, M. Wang, L. Li, *Adv. Funct. Mater.* **2019**, *29*, 1900830.
[339] N. Neugebohrn, N. Osterthun, M. Götz-Köhler, K. Gehrke, C. Agert, *Nanoscale Res. Lett.* **2021**, *16*, 50.
[340] M. A. Kats, R. Blanchard, P. Genevet, F. Capasso, *Nat. Mater.* **2013**, *12*, 20.
[341] C. O. Ramírez Quiroz, C. Bronnbauer, I. Levchuk, Y. Hou, C. J. Brabec, K. Forberich, *ACS Nano* **2016**, *10*, 5104.
[342] M. G. Debije, P. P. C. Verbunt, *Adv. Energy Mater.* **2012**, *2*, 12.
[343] I. Papakonstantinou, M. Portnoi, M. G. Debije, *Adv. Energy Mater.* **2021**, *11*, 2002883.
[344] F. Meinardi, F. Bruni, S. Brovelli, *Nat. Rev. Mater.* **2017**, *2*, 17072.
[345] Y. Li, Y. Sun, Y. Zhang, Y. Li, R. Verduzco, *Polym. Int.* **2021**, *70*, 475.
[346] M. Nam, H.-K. Kwon, S. J. Kwon, S.-H. Kwon, M. Cha, S.-H. Lee, S. Park, D. Jeong, K.-T. Lee, H. Rhee, Y. R. Do, S. Kim, K. Kim, R. H. Friend, J. S. Han, I. K. Han, D.-H. Ko, *Adv. Energy Mater.* **2016**, *6*, 1502404.
[347] L. ZdraŽil, S. Kalytchuk, K. Holá, M. Petr, O. Zmeškal, Š. Kment, A. L. Rogach, R. Zbořil, *Nanoscale* **2020**, *12*, 6664.
[348] H. Zhao, D. Benetti, X. Tong, H. Zhang, Y. Zhou, G. Liu, D. Ma, S. Sun, Z. M. Wang, Y. Wang, F. Rosei, *Nano Energy* **2018**, *50*, 756.
[349] S.-J. Ha, J.-H. Kang, D. H. Choi, S. K. Nam, E. Reichmanis, J. H. Moon, *ACS Photonics* **2018**, *5*, 3621.
[350] Y. Jiang, B. Luo, F. Jiang, F. Jiang, C. Fuentes-Hernandez, T. Liu, L. Mao, S. Xiong, Z. Li, T. Wang, B. Kippelen, Y. Zhou, *Nano Lett.* **2016**, *16*, 7829.
[351] S. Wang, J. Chen, L. Li, L. Zuo, T.-Y. Qu, H. Ren, Y. Li, A. K.-Y. Jen, J.-X. Tang, *ACS Nano* **2020**, *14*, 5998.
[352] J.-H. Lu, Y.-H. Lin, B.-H. Jiang, C.-H. Yeh, J.-C. Kao, C.-P. Chen, *Adv. Funct. Mater.* **2018**, *28*, 1703398.
[353] Y. Cui, C. Yang, H. Yao, J. Zhu, Y. Wang, G. Jia, F. Gao, J. Hou, *Adv. Mater.* **2017**, *29*, 1703080.
[354] J. Y. Lee, K.-T. Lee, S. Seo, L. J. Guo, *Sci. Rep.* **2014**, *4*, 4192.
[355] S. B. Kang, B. Salimzhanov, W. J. Park, M. H. Jeong, J.-Y. Kim, K. J. Choi, *Adv. Funct. Mater.* **2021**, *32*, 2110435.
[356] E. S. Arinze, B. Qiu, N. Palmquist, Y. Cheng, Y. Lin, G. Nyirjesy, G. Qian, S. M. Thon, *Opt. Express* **2017**, *25*, A101.
[357] Y. Zhao, G. A. Meek, B. G. Levine, R. R. Lunt, *Adv. Opt. Mater.* **2014**, *2*, 606.
[358] N. Chaturvedi, N. Gasparini, D. Corzo, J. Bertrandie, N. Wehbe, J. Troughton, D. Baran, *Adv. Funct. Mater.* **2021**, *31*, 2009996.
[359] L. Zuo, X. Shi, W. Fu, A. K.-Y. Jen, *Adv. Mater.* **2019**, *31*, 1901683.
[360] H. in Jeong, S. Biswas, S. C. Yoon, S.-J. Ko, H. Kim, H. Choi, *Adv. Energy Mater.* **2021**, *11*, 2102397.
[361] J. Wook Lim, M. Shin, J. Da Lee, S. Hyun Lee, S. Jin Yun, *Sol. Energy Mater. Sol. Cells* **2014**, *128*, 301.
[362] M. J. Shin, J. H. Jo, A. Cho, J. Gwak, J. H. Yun, K. Kim, S. K. Ahn, J. H. Park, J. Yoo, I. Jeong, B.-H. Choi, J.-S. Cho, *Sol. Energy* **2019**, *181*, 276.
[363] X. Zhang, C. Hägglund, M. B. Johansson, K. Sveinbjörnsson, E. M. J. Johansson, *Adv. Funct. Mater.* **2016**, *26*, 1921.
[364] X. Zhang, C. Hägglund, E. M. J. Johansson, *Energy Environ. Sci.* **2017**, *10*, 216.
[365] H.-J. Lee, S.-P. Cho, S. Na, S.-S. Kim, *J. Alloys Compd.* **2019**, *797*, 65.
[366] A. Roy, A. Ghosh, S. Bhandari, P. Selvaraj, S. Sundaram, T. K. Mallick, *J. Phys. Chem. C* **2019**, *123*, 23834.
[367] W. Yang, W. Wang, Y. Wang, R. Sun, J. Guo, H. Li, M. Shi, J. Guo, Y. Wu, T. Wang, G. Lu, C. J. Brabec, Y. Li, J. Min, *Joule* **2021**, *5*, 1209.
[368] H.-W. Cheng, Y. Zhao, Y. Yang, *Adv. Energy Mater.* **2022**, *12*, 2102908.
[369] G. Bernardo, T. Lopes, D. G. Lidzey, A. Mendes, *Adv. Energy Mater.* **2021**, *11*, 2100342.
[370] B. Lee, L. Lahann, Y. Li, S. R. Forrest, *Sustainable Energy Fuels* **2020**, *4*, 5765.
[371] L. Duan, A. Uddin, *Adv. Sci.* **2020**, *7*, 1903259.
[372] L. A. Castriotta, M. Zendehdel, N. Yaghoobi Nia, E. Leonardi, M. Löffler, B. Paci, A. Generosi, B. Rellinghaus, A. Di Carlo, *Adv. Energy Mater.* **2022**, *12*, 2103420.
[373] M. V. Khenkin, E. A. Katz, A. Abate, G. Bardizza, J. J. Berry, C. Brabec, F. Brunetti, V. Bulović, Q. Burlingame, A. Di Carlo,

R. Cheacharoen, Y.-B. Cheng, A. Colsmann, S. Cros, K. Domanski, M. Dusza, C. J. Fell, S. R. Forrest, Y. Galagan, D. Di Girolamo, M. Grätzel, A. Hagfeldt, E. von Hauff, H. Hoppe, J. Kettle, H. Köbler, M. S. Leite, S. Liu, Y.-L. Loo, J. M. Luther, et al, *Nat. Energy* **2020**, *5*, 35.
[374] *ASCA |Organic solar film (OPV) – Transparent and flexible*, https://en.asca.com/ (accessed: February 2022).
[375] Saule Technologies, *Saule Technologies – Inkjet-Printed Perovskite Solar Cells*, https://sauletech.com/.
[376] N. Kumar, M. Patel, T. T. Nguyen, S. Kim, J. Kim, *Prog. Photovoltaics Res. Appl.* **2021**, *29*, 943.
[377] D. Liu, C. Yang, P. Chen, M. Bates, S. Han, P. Askeland, R. R. Lunt, *ACS Appl. Energy Mater.* **2019**, *2*, 3972.
[378] Q. Liu, L. G. Gerling, F. Bernal-Texca, J. Toudert, T. Li, X. Zhan, J. Martorell, *Adv. Energy Mater.* **2020**, *10*, 1904196.
[379] S. Kim, M. Patel, T. T. Nguyen, J. Yi, C.-P. Wong, J. Kim, *Nano Energy* **2020**, *77*, 105090.
[380] S. Kim, M. Patel, T. T. Nguyen, N. Kumar, P. Bhatnagar, J. Kim, *ACS Appl. Mater. Interfaces* **2022**, *14*, 706.
[381] D. Chen, Y. Ba, M. Deng, W. Zhu, W. Chai, H. Xi, D. Chen, J. Zhang, C. Zhang, Y. Hao, *ACS Appl. Energy Mater.* **2021**, *4*, 12121.
[382] R. R. Lunt, V. Bulovic, *Appl. Phys. Lett.* **2011**, *98*, 113305.
[383] C.-C. Chen, L. Dou, R. Zhu, C.-H. Chung, T.-B. Song, Y. B. Zheng, S. Hawks, G. Li, P. S. Weiss, Y. Yang, *ACS Nano* **2012**, *6*, 7185.
[384] C.-C. Chen, L. Dou, J. Gao, W.-H. Chang, G. Li, Y. Yang, *Energy Environ. Sci.* **2013**, *6*, 2714.
[385] Y. Li, J.-D. Lin, X. Che, Y. Qu, F. Liu, L.-S. Liao, S. R. Forrest, *J. Am. Chem. Soc.* **2017**, *139*, 17114.
[386] Y. Li, X. Guo, Z. Peng, B. Qu, H. Yan, H. Ade, M. Zhang, S. R. Forrest, *Proc. Natl. Acad. Sci. U. S. A.* **2020**, *117*, 21147.
[387] W. Naim, V. Novelli, I. Nikolinakos, N. Barbero, I. Dzeba, F. Grifoni, Y. Ren, T. Alnasser, A. Velardo, R. Borrelli, S. Haacke, S. M. Zakeeruddin, M. Graetzel, C. Barolo, F. Sauvage, *JACS Au* **2021**, *1*, 409.
[388] J. Zhang, G. Xu, F. Tao, G. Zeng, M. Zhang, Y. M. Yang, Y. Li, Y. Li, *Adv. Mater.* **2019**, *31*, 1807159.
[389] K. M. Boopathi, C. Hanmandlu, A. Singh, Y.-F. Chen, C. S. Lai, C. W. Chu, *ACS Appl. Energy Mater.* **2018**, *1*, 632.
[390] C. Yang, M. Moemeni, M. Bates, W. Sheng, B. Borhan, R. R. Lunt, *Adv. Optical Mater.* **2020**, *8*, 1901536.
[391] K. Wu, H. Li, V. I. Klimov, *Nat. Photonics* **2018**, *12*, 105.
[392] R. Mazzaro, A. Vomiero, *Adv. Energy Mater.* **2018**, *8*, 1801903.
[393] H. Li, K. Wu, J. Lim, H.-J. Song, V. I. Klimov, *Nat. Energy* **2016**, *1*, 16157.
[394] C. Yang, H. A. Atwater, M. A. Baldo, D. Baran, C. J. Barile, M. C. Barr, M. Bates, M. G. Bawendi, M. R. Bergren, B. Borhan, C. J. Brabec, S. Brovelli, V. Bulović, P. Ceroni, M. G. Debije, J.-M. Delgado-Sanchez, W.-J. Dong, P. M. Duxbury, R. C. Evans, S. R. Forrest, D. R. Gamelin, N. C. Giebink, X. Gong, G. Griffini, F. Guo, C. K. Herrera, A. W. Ho-Baillie, R. J. Holmes, S.-K. Hong, T. Kirchartz, et al, *Joule* **2022**, *6*, 8.
[395] G. E. Eperon, D. Bryant, J. Troughton, S. D. Stranks, M. B. Johnston, T. Watson, D. A. Worsley, H. J. Snaith, *J. Phys. Chem. Lett.* **2015**, *6*, 129.
[396] Z. Liu, S. E. Sofia, H. S. Laine, M. Woodhouse, S. Wieghold, I. M. Peters, T. Buonassisi, *Energy Environ. Sci.* **2020**, *13*, 12.
[397] C. Bechinger, S. Ferrere, A. Zaban, J. Sprague, B. A. Gregg, *Nature* **1996**, *383*, 608.
[398] J.-J. Wu, M.-D. Hsieh, W.-P. Liao, W.-T. Wu, J.-S. Chen, *ACS Nano* **2009**, *3*, 2297.
[399] A. L. Dyer, R. H. Bulloch, Y. Zhou, B. Kippelen, J. R. Reynolds, F. Zhang, *Adv. Mater.* **2014**, *26*, 4895.
[400] Y. Xia, X. Liang, Y. Jiang, S. Wang, Y. Qi, Y. Liu, L. Yu, H. Yang, X.-Z. Zhao, *Adv. Energy Mater.* **2019**, *9*, 1900720.
[401] M. Götz-Köhler, H. Meddeb, K. Gehrke, M. Vehse, C. Agert, in *2021 IEEE 48th Photovoltaic Specialists Conference*, IEEE, Virtual conference **2021**, p. 774.
[402] H. Ling, J. Wu, F. Su, Y. Tian, Y. J. Liu, *Nat. Commun.* **2021**, *12*, 1010.
[403] K. W. Lee, W. Lim, M. S. Jeon, H. Jang, J. Hwang, C. H. Lee, D. R. Kim, *Adv. Funct. Mater.* **2021**, *32*, 2105882.
[404] Z. Wang, D. Kortge, J. Zhu, Z. Zhou, H. Torsina, C. Lee, P. Bermel, *Joule* **2020**, *4*, 2702.
[405] D. Zhao, A. Aili, Y. Zhai, S. Xu, G. Tan, X. Yin, R. Yang, *App. Phys. Rev.* **2019**, *6*, 21306.
[406] B. Zhao, M. Hu, X. Ao, Q. Xuan, G. Pei, *App. Energy* **2020**, *262*, 114548.
[407] A. Kumar, A. Chowdhury, *Sol. Energy* **2019**, *183*, 410.
[408] B. Zhao, M. Hu, X. Ao, Q. Xuan, G. Pei, *Sol. Energy Mater. Sol. Cells* **2018**, *178*, 266.
[409] J. Mandal, Y. Fu, A. C. Overvig, M. Jia, K. Sun, N. N. Shi, H. Zhou, X. Xiao, N. Yu, Y. Yang, *Science* **2018**, *362*, 315.
[410] Y. Zhai, Y. Ma, S. N. David, D. Zhao, R. Lou, G. Tan, R. Yang, X. Yin, *Science* **2017**, *355*, 1062.
[411] X. Yu, J. Chan, C. Chen, *Nano Energy* **2021**, *88*, 106259.
[412] Y. Yang, Y. Zhang, *MRS Energy Sustainability* **2020**, *7*, 1.
[413] A. Aili, Z. Y. Wei, Y. Z. Chen, D. L. Zhao, R. G. Yang, X. B. Yin, *Mater. Today Phys.* **2019**, *10*, 100127.
[414] D. Li, X. Liu, W. Li, Z. Lin, B. Zhu, Z. Li, J. Li, B. Li, S. Fan, J. Xie, J. Zhu, *Nat. Nanotechnol.* **2021**, *16*, 153.
[415] Z. Zhou, X. Wang, Y. Ma, B. Hu, J. Zhou, *Cell Rep. Phys. Sci.* **2020**, *1*, 100231.
[416] U. Banik, A. Agrawal, H. Meddeb, O. Sergeev, N. Reininghaus, M. Götz-Köhler, K. Gehrke, J. Stührenberg, M. Vehse, M. Sznajder, C. Agert, *ACS App. Mat. Interfaces* **2021**, *13*, 24130.
[417] K. Wang, G. Luo, X. Guo, S. Li, Z. Liu, C. Yang, *Sol. Energy* **2021**, *225*, 245.
[418] S.-Y. Heo, D. H. Kim, Y. M. Song, G. J. Lee, *Adv. Energy Mater.* **2021**, *12*, 2103258.
[419] T. S. Safi, J. N. Munday, *Opt. Express* **2015**, *23*, A1120.
[420] Z. Zhou, Z. Wang, P. Bermel, *Opt. Express* **2019**, *27*, A404.
[421] M. Jošt, B. Lipovšek, B. Glažar, A. Al-Ashouri, K. Brecl, G. Matič, A. Magomedov, V. Getautis, M. Topič, S. Albrecht, *Adv. Energy Mater.* **2020**, *10*, 2000454.
[422] O. Dupré, B. Niesen, S. de Wolf, C. Ballif, *J. Phys. Chem. Lett.* **2018**, *9*, 446.
[423] L. Belussi, B. Barozzi, A. Bellazzi, L. Danza, A. Devitofrancesco, C. Fanciulli, M. Ghellere, G. Guazzi, I. Meroni, F. Salamone, F. Scamoni, C. Scrosati, *J. Build. Eng.* **2019**, *25*, 100772.
[424] T. E. Kuhn, C. Erban, M. Heinrich, J. Eisenlohr, F. Ensslen, D. H. Neuhaus, *Energy Build.* **2021**, *231*, 110381.
[425] C. Ballif, L.-E. Perret-Aebi, S. Lufkin, E. Rey, *Nat. Energy* **2018**, *3*, 438.
[426] A. Ghosh, *J. Cleaner Prod.* **2020**, *276*, 123343.
[427] D. E. Attoye, A. Hassan, *Sustainability* **2017**, *9*, 2287.
[428] P. Heinstein, C. Ballif, L.-E. Perret-Aebi, *Green* **2013**, *3*, 125.
[429] P. Nørgaard, S. H. Poder, *J. Eng.* **2019**, *2019*, 5134.
[430] S. |. https://www.skalafacade.com, *Avancis Skala: Solarmodule für individuelle Solarfassaden*, https://www.skalafacade.com/#startseite-downloads (accessed: January 2022).
[431] S. |. https://www.skalafacade.com, *Avancis Skala: Solarmodule für individuelle Solarfassaden*, https://www.skalafacade.com/ (accessed: January 2022).
[432] ONYX Solar Group LLC, *Technical Specifications*, https://www.onyxsolar.com/product-services/technical-specifications (accessed: January 2022).
[433] *Solaronix – Solar Cells*, https://www.solaronix.com/solarcells/ (accessed: January 2022).

[434] H. M. Lee, J. H. Yoon, *App. Energy* **2018**, *225*, 1013.
[435] *TERINA MEDITERRANEAN FOUNDATION* **2022**, https://www.onyxsolar.com/terina-mediterranean-foundation (accessed: January 2022).
[436] *Solar Windows for Buildings (BIPV) – Toledo Solar*, https://toledo-solar.com/building-integrated-photovoltaics/ (accessed: January 2022).
[437] H. Gholami, H. N. Røstvik, *Energy* **2020**, *204*, 117931.
[438] M. Economidou, V. Todeschi, P. Bertoldi, D. D'Agostino, P. Zangheri, L. Castellazzi, *Energy Build.* **2020**, *225*, 110322.
[439] D. Ürge-Vorsatz, R. Khosla, R. Bernhardt, Y. C. Chan, D. Vérez, S. Hu, L. F. Cabeza, *Annu. Rev. Environ. Resour.* **2020**, *45*, 227.
[440] T. M. Koh, H. Wang, Y. F. Ng, A. Bruno, S. Mhaisalkar, N. Mathews, *Adv. Mater.* **2021**, 2104661.
[441] D. Liu, Y. Sun, R. Wilson, Y. Wu, *Renewable Energy* **2020**, *145*, 1399.
[442] B. Shi, L. Duan, Y. Zhao, J. Luo, X. Zhang, *Adv. Mater.* **2020**, *32*, 1806474.
[443] Ubiquitous Energy Inc., *Product*https://ubiquitous.energy/ (accessed: February 2022).
[444] M. R. Bergren, N. S. Makarov, K. Ramasamy, A. Jackson, R. Guglielmetti, H. McDaniel, *ACS Energy Lett.* **2018**, *3*, 520.
[445] UbiQD, *Home – UbiQD*, https://ubiqd.com/ (accessed: February 2022).
[446] L. Olivieri, E. Caamaño-Martín, F. J. Moralejo-Vázquez, N. Martín-Chivelet, F. Olivieri, F. J. Neila-Gonzalez, *Energy* **2014**, *76*, 572.
[447] F. M. Vossen, M. P. Aarts, M. G. Debije, *Energy Build.* **2016**, *113*, 123.
[448] K.-S. Ahn, S. J. Yoo, M.-S. Kang, J.-W. Lee, Y.-E. Sung, *J. Power Sources* **2007**, *168*, 533.
[449] J. Sun, Y. Li, J. Sun, Z. Zhu, Y. Zhai, S. Dong, *Chem. Comm.* **2019**, *55*, 12060.
[450] J. Xu, A. P. Raman, *iScience* **2021**, *24*, 102825.
[451] B. Zhao, C. Wang, M. Hu, X. Ao, J. Liu, Q. Xuan, G. Pei, *Energy* **2022**, *238*, 121761.
[452] D. R. Needell, M. E. Phelan, J. T. Hartlove, H. A. Atwater, *Energy* **2021**, *219*, 119567.
[453] S. Tak, S. Woo, J. Park, S. Park, *Sustainability* **2017**, *9*, 950.
[454] R. Tällberg, B. P. Jelle, R. Loonen, T. Gao, M. Hamdy, *Sol. Energy Mater. Sol. Cells* **2019**, *200*, 109828.
[455] Y. Sun, X. Liu, Y. Ming, X. Liu, D. Mahon, R. Wilson, H. Liu, P. Eames, Y. Wu, *Appl. Energy* **2021**, *293*, 116826.
[456] S. Wang, T. Jiang, Y. Meng, R. Yang, G. Tan, Y. Long, *Science* **2021**, *374*, 1501.
[457] K. Tang, K. Dong, J. Li, M. Gordon, F. Reichertz, H. Kim, Y. Rho, Q. Wang, C.-Y. Lin, C. Grigoropoulos, A. Javey, J. Urban, J. Yao, R. Levinson, J. Wu, *Science* **2021**, *374*, 1504.
[458] A. Weselek, A. Ehmann, S. Zikeli, I. Lewandowski, S. Schindele, P. Högy, *Agron. Sustainable Dev.* **2019**, *39*.
[459] C. Toledo, A. Scognamiglio, *Sustainability* **2021**, *13*, 6871.
[460] M. A. Zainol Abidin, M. N. Mahyuddin, M. A. A. Mohd Zainuri, *Sustainability* **2021**, *13*, 7846.
[461] Y. Liu, P. Cheng, T. Li, R. Wang, Y. Li, S.-Y. Chang, Y. Zhu, H.-W. Cheng, K.-H. Wei, X. Zhan, B. Sun, Y. Yang, *ACS Nano* **2019**, *13*, 1071.
[462] S. Weng, A. Tamang, A. Salleo, H. Fujiwara, M. Nakamura, Y. Zhang, D. Knipp, *ACS Appl. Mat. Interfaces* **2021**, *13*, 39230.
[463] R. Meitzner, U. S. Schubert, H. Hoppe, *Adv. Energy Mater.* **2021**, *11*, 2002551.
[464] C. S. Allardyce, C. Fankhauser, S. M. Zakeeruddin, M. Grätzel, P. J. Dyson, *Sol. Energy* **2017**, *155*, 517.
[465] C. J. M. Emmott, J. A. Röhr, M. Campoy-Quiles, T. Kirchartz, A. Urbina, N. J. Ekins-Daukes, J. Nelson, *Energy Environ. Sci.* **2015**, *8*, 1317.
[466] M. E. Loik, S. A. Carter, G. Alers, C. E. Wade, D. Shugar, C. Corrado, D. Jokerst, C. Kitayama, *Earth's Future* **2017**, *5*, 1044.
[467] C. Corrado, S. W. Leow, M. Osborn, I. Carbone, K. Hellier, M. Short, G. Alers, S. A. Carter, *J. Renewable Sustainable Energy* **2016**, *8*, 43502.
[468] N. Osterthun, N. Neugebohrn, K. Gehrke, M. Vehse, C. Agert, *Opt. Express* **2021**, *29*, 938.
[469] N. Osterthun, M. Helamieh, D. Berends, N. Neugebohrn, K. Gehrke, M. Vehse, M. Kerner, C. Agert, *AIP Conf. Proc.* **2021**, *2361*, 70001.
[470] E. P. Thompson, E. L. Bombelli, S. Shubham, H. Watson, A. Everard, V. D'Ardes, A. Schievano, S. Bocchi, N. Zand, C. J. Howe, P. Bombelli, *Adv. Energy Mater.* **2020**, *10*, 2001189.
[471] E. Ravishankar, R. E. Booth, C. Saravitz, H. Sederoff, H. W. Ade, B. T. O'Connor, *Joule* **2020**, *4*, 490.
[472] H. Shi, R. Xia, G. Zhang, H.-L. Yip, Y. Cao, *Adv. Energy Mater.* **2019**, *9*, 1803438.
[473] Di Wang, H. Liu, Y. Li, G. Zhou, L. Zhan, H. Zhu, X. Lu, H. Chen, C.-Z. Li, *Joule* **2021**, *5*, 945.
[474] D. A. Chalkias, C. Charalampopoulos, A. K. Andreopoulou, A. Karavioti, E. Stathatos, *J. Power Sources* **2021**, *496*, 229842.
[475] W. S. Subhani, K. Wang, M. Du, X. Wang, N. Yuan, J. Ding, S. Liu, *J. Energy Chem.* **2019**, *34*, 12.
[476] A. Yano, M. Cossu, *Renewable Sustainable Energy Rev.* **2019**, *109*, 116.
[477] G. Nardin, C. Domínguez, Á. F. Aguilar, L. Anglade, M. Duchemin, D. Schuppisser, F. Gerlich, M. Ackermann, L. Coulot, B. Cuénod, D. Petri, X. Niquille, N. Badel, A. Lachowicz, M. Despeisse, J. Levrat, C. Ballif, S. Askins, R. Núñez, N. Jost, G. Vallerotto, I. Antón, *Prog. Photovoltaics Res. Appl.* **2021**, *29*, 819.
[478] E. Ravishankar, R. E. Booth, J. A. Hollingsworth, H. Ade, H. Sederoff, J. F. DeCarolis, B. T. O'Connor, *Energy Environ. Sci.* **2022**, *15*, 1659.
[479] *Solar PV Greenhouses*, https://www.polysolar.co.uk/domestic/greenhouses (accessed: February 2022).
[480] *Soliculture – Greenhouse Integrated Solar Photovoltaics*, http://www.soliculture.com/ (accessed: February 2022).
[481] V. Bahrami-Yekta, T. Tiedje, *Opt. Express* **2018**, *26*, 28238.
[482] M. Freunek, M. Freunek, L. M. Reindl, *IEEE J. Photovoltaics* **2013**, *3*, 59.
[483] D. Lübke, P. Hartnagel, J. Angona, T. Kirchartz, *Adv. Energy Mater.* **2021**, *11*, 2101474.
[484] M. Mainville, M. Leclerc, *ACS Energy Lett.* **2020**, *5*, 1186.
[485] M. A. Saeed, S. H. Kim, H. Kim, J. Liang, H. Y. Woo, T. G. Kim, H. Yan, J. W. Shim, *Adv. Energy Mater.* **2021**, *11*, 2003103.
[486] F. Bai, J. Zhang, A. Zeng, H. Zhao, K. Duan, H. Yu, K. Cheng, G. Chai, Y. Chen, J. Liang, W. Ma, H. Yan, *Joule* **2021**, *5*, 1231.
[487] S. Biswas, H. Kim, *Polymers* **2020**, *12*, 1338.
[488] X. Hou, Y. Wang, H. K. H. Lee, R. Datt, N. Uslar Miano, D. Yan, M. Li, F. Zhu, B. Hou, W. C. Tsoi, Z. Li, *J. Mater. Chem. A* **2020**, *8*, 21503.
[489] L. K. Jagadamma, S. Wang, *Front. Chem.* **2021**, *9*, 632021.
[490] B. Li, B. Hou, G. A. J. Amaratunga, *InfoMat* **2021**, *3*, 445.
[491] L.-K. Ma, Y. Chen, P. C. Chow, G. Zhang, J. Huang, C. Ma, J. Zhang, H. Yin, A. M. Hong Cheung, K. S. Wong, S. K. So, H. Yan, *Joule* **2020**, *4*, 1486.
[492] Y. Peng, T. N. Huq, J. Mei, L. Portilla, R. A. Jagt, L. G. Occhipinti, J. L. MacManus-Driscoll, R. L. Z. Hoye, V. Pecunia, *Adv. Energy Mater.* **2021**, *11*, 2002761.
[493] H. S. Ryu, S. Y. Park, T. H. Lee, J. Y. Kim, H. Y. Woo, *Nanoscale* **2020**, *12*, 5792.
[494] L. Xie, W. Song, J. Ge, B. Tang, X. Zhang, T. Wu, Z. Ge, *Nano Energy* **2021**, *82*, 105770.
[495] Y. Cui, Y. Wang, J. Bergqvist, H. Yao, Y. Xu, B. Gao, C. Yang, S. Zhang, O. Inganäs, F. Gao, J. Hou, *Nat. Energy* **2019**, *4*, 768.

[496] J. Luke, L. Corrêa, J. Rodrigues, J. Martins, M. Daboczi, D. Bagnis, J.-S. Kim, *Adv. Energy Mater.* **2021**, *11*, 2003405.
[497] X. Xu, W. Liu, X. Luo, H. Chen, Q. Wei, J. Yuan, Y. Zou, *ChemSusChem* **2021**, *14*, 3428.
[498] N. Zhang, T. Jiang, C. Guo, L. Qiao, Q. Ji, L. Yin, L. Yu, P. Murto, X. Xu, *Nano Energy* **2020**, *77*, 105111.
[499] A. Sahu, N. Yadav, K. Sudhakar, *Renewable Sustainable Energy Rev.* **2016**, *66*, 815.
[500] P. Ranjbaran, H. Yousefi, G. B. Gharehpetian, F. R. Astaraei, *Renewable Sustainable Energy Rev.* **2019**, *110*, 332.
[501] L. Yin, Y. Zhou, T. Jiang, Y. Xu, T. Liu, N. Li, K. Zhou, L. Yu, C. Guo, P. Murto, X. Xu, *J. Mater. Chem. C* **2021**, *9*, 13132.
[502] P. P. Jenkins, S. Messenger, K. M. Trautz, S. I. Maximenko, D. Goldstein, D. Scheiman, R. Hoheisel, R. J. Walters, *IEEE J. Photovoltaics* **2014**, *4*, 202.
[503] J. Kong, D. Nordlund, J. S. Jin, S. Y. Kim, S.-M. Jin, Di Huang, Y. Zheng, C. Karpovich, G. Sertic, H. Wang, J. Li, G. Weng, F. Antonio, M. Mariano, S. Maclean, T. Goh, J. Y. Kim, A. D. Taylor, *ACS Energy Lett.* **2019**, *4*, 1034.
[504] J. Qi, W. Zhang, R. Cao, *Adv. Energy Mater.* **2018**, *8*, 1701620.
[505] J. L. Young, M. A. Steiner, H. Döscher, R. M. France, J. A. Turner, T. G. Deutsch, *Nat. Energy* **2017**, *2*, 17028.
[506] O. Khaselev, J. Turner, *Science* **1998**, *280*, 425.
[507] K. Sivula, R. van de Krol, *Nat. Rev. Mater.* **2016**, *1*, 15010.
[508] C. Jiang, S. J. A. Moniz, A. Wang, T. Zhang, J. Tang, *Chem. Soc. Rev.* **2017**, *46*, 4645.
[509] F. F. Abdi, L. Han, A. H. M. Smets, M. Zeman, B. Dam, R. van de Krol, *Nat. Commun.* **2013**, *4*, 2195.
[510] S. Hu, C. Xiang, S. Haussener, A. Berger, N. S. Lewis, *Energy Environ. Sci.* **2013**, *6*, 2984.
[511] J. Jia, L. C. Seitz, J. D. Benck, Y. Huo, Y. Chen, J. W. D. Ng, T. Bilir, J. S. Harris, T. F. Jaramillo, *Nat. Commun.* **2016**, *7*, 13237.
[512] A. Alfano, A. Mezzetti, F. Fumagalli, C. Tao, E. Rovera, A. Petrozza, F. Di Fonzo, *iScience* **2021**, *24*, 102463.
[513] İ. Bayrak Pehlivan, U. Malm, P. Neretnieks, A. Glüsen, M. Müller, K. Welter, S. Haas, S. Calnan, A. Canino, R. G. Milazzo, S. M. S. Privitera, S. A. Lombardo, L. Stolt, M. Edoff, T. Edvinsson, *Sustainable Energy Fuels* **2020**, *4*, 6011.
[514] S. Calnan, R. Bagacki, F. Bao, I. Dorbandt, E. Kemppainen, C. Schary, R. Schlatmann, M. Leonardi, S. A. Lombardo, R. G. Milazzo, S. M. S. Privitera, F. Bizzarri, C. Connelli, D. Consoli, C. Gerardi, P. Zani, M. Carmo, S. Haas, M. Lee, M. Mueller, W. Zwaygardt, J. Oscarsson, L. Stolt, M. Edoff, T. Edvinsson, I. B. Pehlivan, *Sol. RRL* **2021**, *6*, 2100479.
[515] J. Chen, C. Dong, H. Idriss, O. F. Mohammed, O. M. Bakr, *Adv. Energy Mater.* **2020**, *10*, 1902433.
[516] J. Gao, F. Sahli, C. Liu, D. Ren, X. Guo, J. Werner, Q. Jeangros, S. M. Zakeeruddin, C. Ballif, M. Grätzel, J. Luo, *Joule* **2019**, *3*, 2930.
[517] M. Lee, X. Ding, S. Banerjee, F. Krause, V. Smirnov, O. Astakhov, T. Merdzhanova, B. Klingebiel, T. Kirchartz, F. Finger, U. Rau, S. Haas, *Adv. Mater. Technol.* **2020**, *5*, 2000592.
[518] G. Segev, J. W. Beeman, J. B. Greenblatt, I. D. Sharp, *Nat. Mater.* **2018**, *17*, 1115.
[519] I. R. Hamdani, A. N. Bhaskarwar, *Renewable Sustainable Energy Rev.* **2021**, *138*, 110503.
[520] J. H. Kim, D. Hansora, P. Sharma, J.-W. Jang, J. S. Lee, *Chem. Soc. Rev.* **2019**, *48*, 1908.
[521] *Toyota Motor Corporation*, https://global.toyota/en/newsroom/corporate/28787347.html (accessed: February 2022).
[522] M. Yamaguchi, T. Masuda, K. Araki, D. Sato, K.-H. Lee, N. Kojima, T. Takamoto, K. Okumura, A. Satou, K. Yamada, T. Nakado, Y. Zushi, Y. Ohshita, M. Yamazaki, *Prog. Photovoltaics Res. Appl.* **2021**, *29*, 684.
[523] L. K. Reb, M. Böhmer, B. Predeschly, S. Grott, C. L. Weindl, G. I. Ivandekic, R. Guo, C. Dreißigacker, R. Gernhäuser, A. Meyer, P. Müller-Buschbaum, *Joule* **2020**, *4*, 1880.
[524] U. Banik, K. Sasaki, N. Reininghaus, K. Gehrke, M. Vehse, M. Sznajder, T. Sproewitz, C. Agert, *Sol. Energy Mater. Sol. Cells* **2020**, *209*, 110456.
[525] M. Yamaguchi, T. Masuda, K. Araki, D. Sato, K.-H. Lee, N. Kojima, T. Takamoto, K. Okumura, A. Satou, K. Yamada, T. Nakado, Y. Zushi, M. Yamazaki, H. Yamada, *EPE* **2020**, *12*, 375.
[526] M. Yamaguchi, T. Masuda, T. Nakado, Y. Zushi, K. Araki, T. Takamoto, K. Okumura, A. Satou, K. Yamada, Y. Ota, K. Nishioka, T. Tanimoto, K. Nakamura, R. Ozaki, N. Kojima, Y. Ohshita, *EPE* **2021**, *13*, 147.
[527] T. Kobashi, K. Say, J. Wang, M. Yarime, D. Wang, T. Yoshida, Y. Yamagata, *J. Cleaner Prod.* **2020**, *253*, 119933.
[528] R. K. Kaufmann, D. Newberry, C. Xin, S. Gopal, *Nat. Energy* **2021**, *6*, 143.
[529] Vitsolc, *Unique transparent photovoltaic cell technology – Vitsolc*, https://www.vitsolc.com/ (accessed: February 2022).
[530] *Automotive Solar Windows – Toledo Solar*, https://toledo-solar.com/automotive-integrated-photovoltaics-aipv/ (accessed: February 2022).
[531] T. Masuda, S. Hirai, M. Inoue, J. Chantana, Y. Kudo, T. Minemoto, *IEEE J. Photovoltaics* **2018**, *8*, 1326.
[532] T. Masuda, Y. Kudo, D. Banerjee, *Coatings* **2018**, *8*, 282.
[533] M. Yamaguchi, R. Ozaki, K. Nakamura, K.-H. Lee, N. Kojima, Y. Ohshita, T. Masuda, K. Okumura, A. Satou, T. Nakado, K. Yamada, K. Araki, Y. Ota, K. Nishioka, T. Takamoto, Y. Zushi, T. Tanimoto, C. Thiel, A. Tsakalidis, A. Jäger-Waldau, *Sol. RRL* **2021**, *6*, 2100429.
[534] K. Araki, D. Sato, T. Masuda, K.-H. Lee, N. Yamada, M. Yamaguchi, *15th International Conference on Concentrator Photovoltaic Systems (CPV-15)*, AIP Publishing, Fes, Morocco **2019**, p. 50003.
[535] C. Thiel, A. Gracia Amillo, A. Tansini, A. Tsakalidis, G. Fontaras, E. Dunlop, N. Taylor, A. Jäger-Waldau, K. Araki, K. Nishioka, Y. Ota, M. Yamaguchi, *Renewable Sustainable Energy Rev.* **2022**, *158*, 112109.
[536] B. Commault, T. Duigou, V. Maneval, J. Gaume, F. Chabuel, E. Voroshazi, *Appl. Sci.* **2021**, *11*, 11598.
[537] K. Araki, Y. Ota, M. Yamaguchi, *Appl. Sci.* **2020**, *10*, 872.
[538] T. Tayagaki, K. Araki, M. Yamaguchi, T. Sugaya, *IEEE J. Photovoltaics* **2019**, *9*, 1721.
[539] J. Barbé, A. Pockett, V. Stoichkov, D. Hughes, H. K. H. Lee, M. Carnie, T. Watson, W. C. Tsoi, *J. Mater. Chem. C* **2020**, *8*, 1715.
[540] I. Cardinaletti, T. Vangerven, S. Nagels, R. Cornelissen, D. Schreurs, J. Hruby, J. Vodnik, D. Devisscher, J. Kesters, J. D'Haen, A. Franquet, V. Spampinato, T. Conard, W. Maes, W. Deferme, J. V. Manca, *Sol. Energy Mater. Sol. Cells* **2018**, *182*, 121.
[541] S. Guo, C. Brandt, T. Andreev, E. Metwalli, W. Wang, J. Perlich, P. Müller-Buschbaum, *ACS Appl. Mat. Interfaces* **2014**, *6*, 17902.
[542] D. A. Lamb, S. J. C. Irvine, M. A. Baker, C. I. Underwood, S. Mardhani, *Prog. Photovoltaics Res. Appl.* **2021**, *29*, 1000.
[543] F. Lang, M. Jošt, K. Frohna, E. Köhnen, A. Al-Ashouri, A. R. Bowman, T. Bertram, A. B. Morales-Vilches, D. Koushik, E. M. Tennyson, K. Galkowski, G. Landi, M. Creatore, B. Stannowski, C. A. Kaufmann, J. Bundesmann, J. Rappich, B. Rech, A. Denker, S. Albrecht, H.-C. Neitzert, N. H. Nickel, S. D. Stranks, *Joule* **2020**, *4*, 1054.
[544] Y. Tu, J. Wu, G. Xu, X. Yang, R. Cai, Q. Gong, R. Zhu, W. Huang, *Adv. Mater.* **2021**, *33*, 2006545.
[545] T. Zdanowicz, T. Rodziewicz, M. Zabkowska-Waclawek, *Sol. Energy Mater. Sol. Cells* **2005**, *87*, 757.
[546] T. Rodziewicz, M. Rajfur, J. Teneta, P. Świsłowski, M. Wacławek, *Energy Rep.* **2021**, *7*, 565.
[547] K. Shimazaki, M. Imaizumi, K. Kibe, *Thin Solid Films* **2008**, *516*, 2218.
[548] M. Pscherer, M. Günthner, C. A. Kaufmann, A. Rahm, G. Motz, *Sol. Energy Mater. Sol. Cells* **2015**, *132*, 296.
[549] D. Sato, N. Yamada, K. Tanaka, *IEEE J. Photovoltaics* **2017**, *7*, 374.
[550] G. Fan, B. Duan, Y. Zhang, X. Li, X. Ji, *Acta Astronaut.* **2021**, *180*, 196.

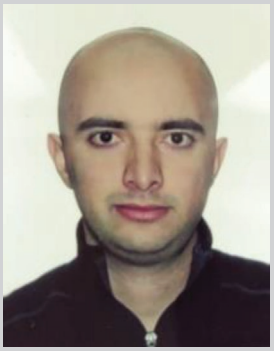

Hosni Meddeb was a recipient of the international scholarship from INTEL-KACST Consortium Center of Excellence in Nano-manufacturing Applications CENA in 2012 to conduct his doctoral research at IMEC in Belgium. In 2015, he received his Ph.D. degree in Physics, on the development of silicon heterojunction solar cells. He joined the 3IT institute in Sherbrooke-Canada, developing TFET transistors for CMOS technology. Since 2017, he is working as research scientist in the department of Urban and Residential Technologies at the German Aerospace Center, DLR Institute of Networked Energy Systems, involved in the development and integration of innovative optoelectronic devices for energy applications and thermal management.

Maximilian Götz-Köhler studied physics at the Friedrich-Alexander University Erlangen-Nuremberg, Germany. After finishing his master's thesis about nano-optical structures at the Helmholtz-Zentrum Berlin in 2017, he joined the department of Urban and Residential technologies at the DLR Institute of Networked Energy Systems in Oldenburg. In the framework of his Ph.D. studies, he investigates the combination of ultra-thin absorber layers with switchable mirror systems to create switchable photovoltaic windows.

Kai Gehrke is a Team Leader in the department Urban and Residential Technologies at the DLR Institute of Networked Energy Systems. He studied Physics at the Georg-August-University of Göttingen and finished his Ph.D. in 2009 working on Interface modification in magnetic multilayer thin film systems. In 2010 he joined OSRAM Opto Semiconductors in Regensburg as a Process Engineer in the PVD coating group. Since 2017, he has been working at the German Aerospace Center.

Martin Vehse is the head of the department Urban and Residential Technologies at DLR Institute of Networked Energy Systems. He studied physics at the University of Bremen, finished his Ph.D. study with the doctoral level in 2001. Afterward, he spent a post-doctoral period at the University of California, Santa Barbara at the Institute for Polymers and Organic Solids, working on conducting polymers. In 2004, he started his professional career as project manager on OLED technology at the company Novaled GmbH, and joined the photovoltaics activities at the research institute NEXT ENERGY in 2010. Since 2017, he has been working at the German Aerospace Center.